Dissertation
submitted to the
Combined Faculty of Natural Sciences and Mathematics
of the Ruperto Carola University Heidelberg, Germany
for the degree of
Doctor of Natural Sciences

presented by
M.Sc. Tinatini Tavhelidse
born in: Heidelberg
Oral examination: 22.03.2019

The role of *rx* genes in establishment and maintenance of the medaka ciliary marginal zone

Referees: Prof. Dr. Joachim Wittbrodt
Jun.-Prof. Dr. Steffen Lemke

Für meine Familie

Abstract

Postembryonic growth is a highly coordinated and delicate process, during which shape and function of complex organs have to be maintained. Anamniotes, such as fish and amphibia, grow lifelong. This property is mediated by stem cells, which must ensure full organ functionality along with proper scaling with the increasing body size. In the anamniote retina, postembryonic neurogenesis and growth is mediated by retinal stem cells in the ciliary marginal zone (CMZ).

The family of Rx transcription factors is highly conserved among vertebrates and plays a key role in early eye development. In the teleost medaka (*Oryzias latipes*), the retina-specific homeobox transcription factor 2 (Rx2) has been shown to be a marker for multipotent retinal stem cells. Its closely related paralogue Rx1 has not been studied in detail so far.

I hypothesise a role for *rx1* and *rx2* genes in establishment of the retinal stem cell domain and therefore in mediating postembryonic growth and shape of the eye.

I used novel CRISPR/Cas9-mediated gene tagging approaches, developed in the framework of this thesis, to visualise endogenous medaka *rx2* and, for the first time, *rx1* expression. I carried out clonal loss-of-function studies of medaka *rx1* and *rx2*, indicating a role in balancing stem cell fate decisions. Systemic loss-of-function studies of $rx1^{-/-}/rx2^{-/-}$ double mutants revealed a role in early retinal morphogenesis, as well as in establishment and maintenance of the CMZ by conferring retinal stem cell identity.

Furthermore, I established tools necessary to generate a labelled allelic series of *rx1* and *rx2* mutants.

Eventually, I characterised an *rx2 conditional* allele, which will be instrumental to address late function of *rx2* in the CMZ, thereby deciphering whether the retinal stem cell niche is dynamic or rather deterministic.

Taken together, my results reveal a function for *rx1* and *rx2* in establishment and maintenance of the medaka CMZ and indicate a role in regulation of growth and scaling of eye size.

Zusammenfassung

Postembryonales Wachstum ist ein höchst koordinierter und sensibler Vorgang, bei dem Gestalt und Funktion komplexer Organe erhalten bleiben müssen. Anamnioten wie Fische und Amphibien wachsen ihr Leben lang. Diese Eigenschaft wird von Stammzellen vermittelt, die sowohl volle Organfunktionalität als auch -skalierung bei gleichzeitig zunehmender Körpergröße gewährleisten müssen. Postembryonale Neurogenese in der Retina von Anamnioten wird durch retinale Stammzellen in der ziliären Randzone vermittelt.

Die Familie der Rx-Transkriptionsfaktoren ist innerhalb der Vertebraten stark konserviert und spielt eine Schlüsselrolle bei der frühen Augenentwicklung. Der retinaspezifische Homeobox-Transkriptionsfaktor 2 (Rx2) ist im Teleosten Medaka (*Oryzias latipes*) ein Marker für multipotente retinale Stammzellen. Das mit Rx2 eng verwandte Paralog Rx1 wurde bisher noch nicht im Detail untersucht.

Ich stelle die Hypothese auf, dass die *rx1*-und *rx2*-Gene eine Rolle bei der Etablierung der retinalen Stammzelldomäne und daher bei der Vermittlung postembryonalen Wachstums und der Formgebung des Auges spielen.

Zur Anwendung kamen neue CRISPR/Cas9-vermittelte Gen-Tagging-Methoden, die im Rahmen dieser Doktorarbeit entwickelt wurden, um die endogene Expression der Medaka-Gene *rx2*, und erstmals auch *rx1*, zu visualisieren. Ich führte klonale Funktionsverluststudien der Medaka-Gene *rx1* und *rx2* durch, die auf eine Rolle bei der Ausbalancierung von Schicksalsentscheidungen der Stammzellen hindeuten. Die systemischen Funktionsverluststudien an den $rx1^{-/-}/rx2^{-/-}$-Doppelmutanten zeigten eine Rolle sowohl bei der frühen retinalen Morphogenese als auch bei der Etablierung und Aufrechterhaltung der ziliären Randzone durch Festlegung der retinalen Stammzellidentität auf.

Des weiteren etablierte ich die erforderlichen Tools, um eine fluoreszenzmarkierte Allel-Serie von *rx1*- und *rx2*-Mutanten zu generieren.

Schließlich charakterisierte ich ein *rx2*-konditionales Allel, das von entscheidender Bedeutung sein wird, um die späte Funktion von *rx2* in der ziliären Randzone zu adressieren und dabei zu entschlüsseln, ob die retinale Stammzellnische dynamisch oder doch eher deterministisch ist.

Zusammenfassend zeigen meine Ergebnisse eine Funktion für *rx1* und *rx2* in der Etablierung und Aufrechterhaltung der Medaka-ziliären Randzone auf und deuten auf eine wesentliche Rolle bei der Regulierung von Wachstum und Skalierung der Augengröße hin.

Contents

Abbreviations

ArCoS	arched continuous stripe
BMP	bone morphogenetic protein
BrdU	bromodeoxyuridine
Cas	CRISPR-associated system
CMZ	ciliary marginal zone
condi	conditional
CRISPR	clustered regularly interspaced short palindromic repeats
Crx	Cone-rod homeobox
DamID	DNA adenine methyltransferase identification
DAPI	4',6-diamidino-2-phenyindole
DNA	deoxyribonucleic acid
dNTP	deoxynucleoside triphosphate
dpf	days post fertilisation
DSB	double-strand break
eGFP	enhanced green fluorescent protein
ERM	embryo rearing medium
EV	Entry vector
FGF	fibroblast growth factor
FGFR	fibroblast growth factor receptor
FL	flexible linker
FP	fluorescent protein
FRT	flippase recognition target
fwd	forward
GCL	ganglion cell layer
GFP	green fluorescent protein
Gli3	glioma-associated oncogene family zinc finger 3
GSK3	glycogen synthase kinase 3
HDR	homology-directed repair
her9	hairy-related 9
hes4	hairy and enhancer of split 4
HF	homology flank
Hh	Hedgehog
hpf	hours post fertilisation
IGF	insulin like growth factor
INL	inner nuclear layer
IPL	inner plexiform layer
IRBP	interphotoreceptor retinoid-binding protein
Isl-1	Islet-1
kb	kilo base pair
LB	lysogeny broth
NHEJ	non-homologous end joining
Nlcam	neurolin-like cell adhesion molecule

NR	neural retina
ON	optic nerve
ONL	outer nuclear layer
OPL	outer plexiform layer
OPT	ocean pout transcriptional terminator
ORF	open reading frame
Otx2	orthodenticle homeobox 2
PAM	protospacer adjacent motif
Pax6	paired box 6
PCE-1	photoreceptor conserved element 1
PCNA	proliferating cell nuclear antigen
PCR	Polymerase chain reaction
pGGDest	Golden GATEway destination vector
PH3	phosphorylated histone H3
Pvalb	Parvalbumin
rax	retinal and anterior neural fold homeobox
rev	reverse
RNA	ribonucleic acid
RNASeq	RNA sequencing
rNTP	ribonucleoside triphosphate
RPC	retinal progenitor cell
RPE	retinal pigmented epithelium
RSC	retinal stem cell
RT-PCR	reverse transcription PCR
Rx	Retinal homeobox transcription factor
SDS-PAGE	sodium dodecyl sulfate polyacrylamide gel electrophoresis
sgRNA	single guide RNA
Shh	Sonic hedgehog
Six3	sine oculis homeobox 3
Sox2	sex determining region Y-box 2
st.	developmental stage
TALEN	transcription activator-like effector nuclease
TGF	transforming growth factor
TLE2	transducin like enhancer of split 2
Tlx	Tailless
UTR	Untranslated region
WISH	whole mount *in situ* hybridisation
wpf	weeks post fertilisation
wt	wild-type
Xhmgb3	Xenopus high mobility group box 3
Xrx1	Xenopus rx1
ZFN	zinc finger nuclease
Zic2	Zinc finger protein of the cerebellum 2
Zpr-1	Zinc finger protein 1

Contributions

In the following, people that contributed to the experimental data described in this thesis are listed:

Beate Wittbrodt helped with genotyping, phenotyping, cDNA preparation and analysis, *in situ* hybridisation, cloning and fish work.

Thomas Thumberger (TT) designed the sgRNAs for the *rx1* and *rx2* loci, as well as the ocean pout knock-in cassettes, analysed the DamID dataset and, together with **Arturo Gutierrez (AG)** worked on the *rx1* and *rx2* tagging.

Robert Reinhardt established the *rx1* and *rx2* TALEN single mutant lines.

Lázaro Centanin helped with the *rx2* transplantations.

Erika Tsingos wrote the Fiji macro for the analysis of angular width of ArCoSs.

Kerim Anlas helped with the analysis of the *rx1* transplantation data, cloned the eGFP-FL-rx1 and H2B-eGFPwCR13-OPT-rx1 constructs and injected the *H2B-eGFPwCR13-OPT-rx1* and *H2B-mRFP-OPT-rx2* transgenic lines.

Natalia Sokolova (NS) helped with the cloning of the mCherry-FL-rx2 construct and dissected the *rx1*$^{-/-}$/*rx2*$^{-/-}$ double mutant optic vesicles for RNA sequencing.

David Ibberson (DI) prepared the samples for RNA sequencing.

Juan Luis Mateo Cerdán (JM) analysed the RNA sequencing data.

Isabelle Thomas helped with the characterisation of the *rx1* and *rx2* tagged lines, helped with the cloning of the mCherry-FL-rx2 construct and injected the *H2B-eGFPwCR13-OPT-rx1* and *H2B-mRFP-OPT-rx2* transgenic lines.

Dustin Herrmann helped with Western and Southern Blots.

Manuel Stemmer (MS) established the *rx2 conditional* line.

Tanja Kellner helped with RT-PCR analysis of the *rx2 conditional* line.

Furthermore, **Colin Lischik** helped with the LaTeX layout of this thesis.

"Whom has belonged first sight
First sound
First fear
First breath
First feeling
wrap in the thoughts ...
After that you're sunk
To sleep"

Noshrevani

1 Introduction

Anamniotes such as fish and amphibia grow lifelong, a capacity mediated by stem cells in every organ. Lifelong growth imposes remarkable challenges to the organism, since all organs have to grow proportionally with increasing body size, while at the same time constantly maintaining full functionality.
The fish retina displays a highly conserved development and architecture. Its constant growth is mediated by retinal stem cells located in the ciliary marginal zone (CMZ).
In order to understand how retinal stem cells are established and maintained and thus how postembryonic growth and therefore scaling is mediated, I used the teleost medaka retina as a model system.

1.1 The vertebrate retina: morphogenesis and architecture

The vertebrate retina is a highly conserved organ with respect to development, cell composition and architecture [Centanin and Wittbrodt, 2014].
Eye development is initiated during gastrulation, where the eye field is specified in the anterior neuroectoderm [Chow and Lang, 2001, Sinn and Wittbrodt, 2013]. Combinatorial action of different conserved signalling pathways mediates neural induction and maintenance of neural fate [Esteve and Bovolenta, 2006, Sinn and Wittbrodt, 2013]. Suppression of Wnt-signalling [Stern, 2006] and activation of fibroblast growth factors (FGFs) [Wilson et al., 2000] prior to gastrulation promote neural induction, whereas repression of bone morphogenetic proteins (BMPs) through BMP-antagonists Follistatin, Noggin, Chordin and Cerberus is required for establishment and maintenance of

neural fate [Sinn and Wittbrodt, 2013]. A graded Wnt-activity is necessary for development of the eye anlage, telencephalon and diencephalon from the anterior neural plate [Wilson and Houart, 2004].
Subsequently, the concerted action of several homeobox-containing transcription factors is involved in early eye field specification and, as a result, allows development of the optic vesicles and establishes retinal identity. First, expression of orthodenticle homeobox 2 (Otx2) is repressed by onset of paired box 6 (Pax6) and sine oculis homeobox 3 (Six3) expression [Andreazzoli et al., 1999, Loosli et al., 1998], which in turn can be activated by Pax6 [Sinn and Wittbrodt, 2013]. Six3 acts in part by repressing Wnt, enabling optic vesicle development [Loosli et al., 1998, Loosli et al., 1999, Lagutin et al., 2003]. Secreted factors of the transforming growth factor (TGF) beta, FGF- and Sonic hedgehog (Shh)-families mediate the split of the eye field into two optic primordia [Sampath et al., 1998, Carl and Wittbrodt, 1999, Sinn and Wittbrodt, 2013], while evagination of the optic vesicles is controlled by members of the Retinal homeobox transcription factor (Rx) family [Mathers et al., 1997, Winkler et al., 2000, Loosli et al., 2001, Loosli et al., 2003, Rojas-Muñoz et al., 2005, Stigloher et al., 2006]. In medaka, *rx3* determines the migration behaviour of individual retinal progenitor cells (RPCs) to ultimately form the optic vesicle [Rembold et al., 2006]. Subsequent major morphological transformations are the basis for the development of the hemispheric bi-layered optic cup from the oval optic vesicle [Martinez-Morales and Wittbrodt, 2009, Heermann et al., 2015, Martinez-Morales et al., 2017, Sidhaye and Norden, 2017]. In zebrafish it could be shown that a gastrulation-like epithelial flow of lens-averted cells into the forming optic cup is central to this dynamic process, which is referred to as "optic flow" [Heermann et al., 2015]. The last cells flowing into the optic cup have been proposed to constitute the CMZ, making this process key for establishment of the retinal stem cell domain [Heermann et al., 2015]. Defects in this process prevent closure of the optic fissure, ultimately leading to coloboma, a major cause for blindness in humans [Onwochei et al., 2000].
Undifferentiated RPCs in the resulting pseudo-stratified epithelium are connected to both, the basal and apical laminae. Their nuclei undergo interkinetic nuclear migration, with cell divisions primarily occurring at the apical surface [Baye and Link, 2008].
Differentiation of RPCs follows a stereotypic order and is also conserved among vertebrates, with retinal ganglion cells being born first, followed by cone photoreceptors, amacrine and horizontal cells, bipolar cells and lastly, rod pho-

toreceptors and Müller glia cells [Cepko et al., 1996, Livesey and Cepko, 2001]. During neurogenesis, a wave of differentiation spreads from the centre to the periphery of the retina. In zebrafish, the optic stalk has been suggested as the source for the initiating signal for retinal differentiation [Masai et al., 2000] and FGF ligands secreted from the ventral midline, as well as Hedgehog have been shown to play a role as well [Neumann and Nuesslein-Volhard, 2000, Martinez-Morales et al., 2005, Esteve and Bovolenta, 2006].
The fully differentiated vertebrate neural retina (NR) is composed of three nuclear layers harbouring six neuronal and one glial cell type: the outer nuclear layer (ONL) is located most apically and is composed of rod and cone photoreceptor nuclei, the inner nuclear layer (INL) contains nuclei of horizontal cells, bipolar cells, Müller glia cells and amacrine cells, and the ganglion cell layer (GCL) consists of retinal ganglion cell nuclei, as well as displaced amacrine cell nuclei (Fig. 1.1). The ONL is separated from the INL by the outer plexiform layer (OPL), which contains synapses of photoreceptor cells, horizontal cells and bipolar cells. The inner plexiform layer (IPL) is located between the INL and the GCL and contains synapses of bipolar cells, amacrine cells and retinal ganglion cells. Having a structural support function, Müller glia cells span across the entire width of the retina. The NR is surrounded by the retinal pigmented epithelium (RPE), which functions in light absorption, but also in maintenance of the photoreceptor cell layer [Boulton and Dayhaw-Barker, 2001, Nasonkin et al., 2013].

1.2 The ciliary marginal zone (CMZ)

Since fish and amphibia grow life-long, neurogenesis continues postembryonically. In the retina, this is mediated by retinal stem cells (RSCs) located in the CMZ [Johns, 1977, Wetts et al., 1989, Harris and Perron, 1998, Perron and Harris, 2000, Amato et al., 2004, Fischer et al., 2013].
This circumferential structure is situated at the extreme perimeter of the retina and is composed of dormant RSCs at the outermost periphery [Tang et al., 2017], more centrally located slowly cycling RSCs and faster cycling RPCs at the border to the differentiated NR [Raymond et al., 2006, Xue and Harris, 2012, Centanin et al., 2014, Wan et al., 2016, Shi et al., 2017]. RSCs divide asymmetrically along a radial (peripheral to central) axis, giving rise to one RSC daughter cell that remains in the stem cell niche and one RPC daughter cell that is more centrally located [Centanin et al., 2014, Wan et al., 2016]. The

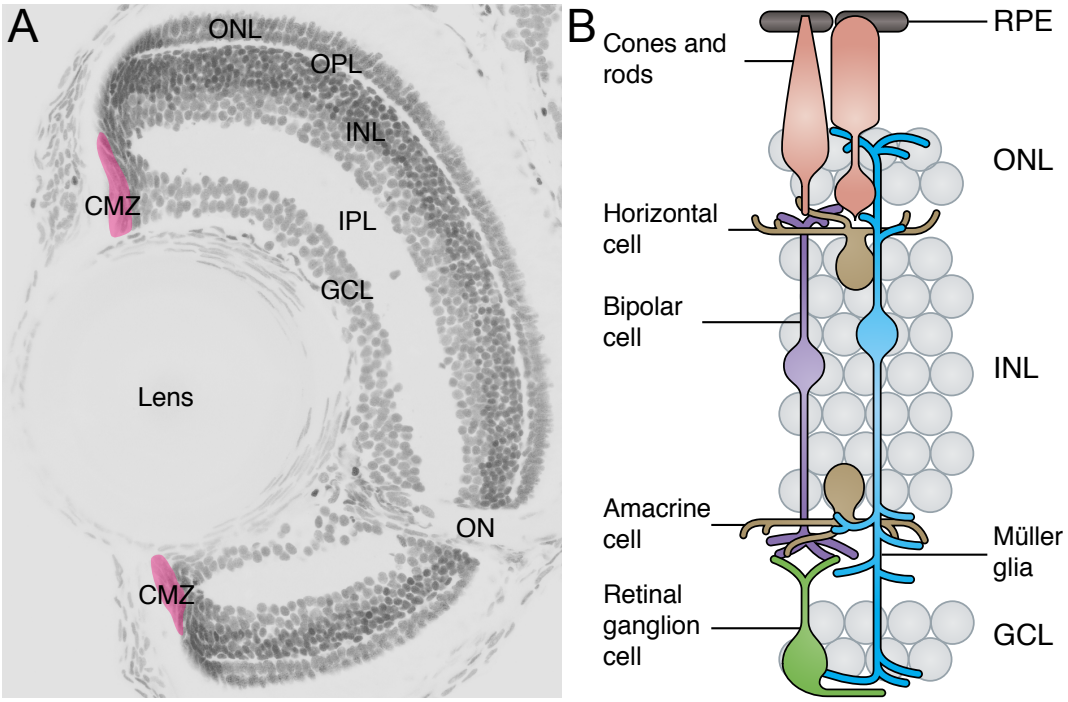

Figure 1.1: Architecture of the medaka retina. (A) DAPI staining of a central cryosection of a medaka hatchling retina. Three nuclear layers are separated by two plexiform layers. The OPL separates the ONL and the INL, the IPL separates the INL and the GCL. Axons of retinal ganglion cells located in the GCL project to the optic tectum via the ON. The CMZ, the retinal stem cell domain, is located at the periphery of the retina (marked in magenta). (B) Scheme depicting nuclear retinal layers and respective cell types. The NR is composed of the ONL, INL and GCL and is surrounded by the RPE. The ONL contains cone and rod photoreceptor nuclei, the INL contains horizontal, bipolar and amacrine cell, as well as Müller glia nuclei. The GCL contains retinal ganglion cell nuclei. Scheme adapted from [Centanin and Wittbrodt, 2014].

latter also harbours a limited proliferative potential and will finally differentiate. The resulting neuroretinal column is added at the periphery of the retina and, importantly, stays in place i.e. the organisation of the retina follows an exquisite temporal order [Straznicky and Gaze, 1971, Centanin et al., 2011]. Consequently, new concentric rings of cells are added peripherally to the growing eye, reminiscent of the growth rings of trees.

While RSCs are multipotent and continuously give rise to all seven cell types of the differentiated NR in the form of permanently growing arched continuous stripes (ArCoSs), RPCs generate short clones terminating early [Wetts et al., 1989, Harris and Perron, 1998, Centanin et al., 2011, Centanin et al., 2014]. Furthermore, it has been shown that the CMZ represents a bipartite stem cell niche, harbouring tissue-specific stem cells for the NR and the RPE [Centanin et al., 2011, Reinhardt et al., 2015, Shi et al., 2017].

There are two fundamental questions regarding the CMZ: first, how is it established and second, how is it maintained?

The CMZ has been extensively studied with regard to gene expression [Raymond et al., 2006, Parain et al., 2012], intrinsic and extrinsic cues regulating maintenance, cell cycle exit and subsequent differentiation of RPCs [Agathocleous and Harris, 2009, Cerveny et al., 2012].
In zebrafish for example, it has been suggested that differentiated neurons of the retina provide extrinsic environmental signals to restrain proliferation of RPCs emerging from the CMZ, driving them towards differentiation [Cerveny et al., 2010]. Furthermore, association with blood vessels has been shown to be required for keeping RPCs actively proliferating in the CMZ [Tang et al., 2017]. Recently identified dormant cells at the outermost tip of the CMZ have been proposed to function in maintaining active RSCs [Tang et al., 2017].
A study in Xenopus identified *hairy and enhancer of split 4 (hes4)* as a potential CMZ regulator, being expressed by the forming CMZ and later functioning in controlling cell cycle length of RSCs, thus maintaining stem cells in an undifferentiated, slowly proliferative state [El Yakoubi et al., 2012]. Interestingly, in contrast, the medaka orthologue *hairy-related 9 (her9)* is also expressed in the CMZ and has been shown to be a transcriptional modulator of stem cell features in the postembryonic retina, however repressing expression of stem cell markers and inhibiting RSC proliferation in a clonal gain-of-function scenario [Reinhardt et al., 2015].
Furthermore, opposing functions of Wnt- and Hedgehog (Hh)-signalling have been shown to regulate proliferation in the CMZ [Borday et al., 2012]. Insulin/insulin like growth factor (IGF)-signalling stimulates proliferation and neurogenesis [Fischer et al., 2002, Agathocleous and Harris, 2009], whereas glucagon-signalling inhibits proliferation in the CMZ [Fischer et al., 2008, Agathocleous and Harris, 2009].
Only recently some advances have been made regarding the establishment of the CMZ during development. *In vivo* imaging in zebrafish has been used to track back cells from the presumptive CMZ and revealed that cells making up the CMZ reach their position during the transition from the optic vesicle to the optic cup through a dynamic movement of cell-sheets, termed "optic flow" [Heermann et al., 2015]. Moreover, *in vivo* lineage analysis has identified bipotent progenitors in the zebrafish optic cup as the embryonic origin of RSCs [Tang et al., 2017].
Structures and components reminiscent of a CMZ have also been identified in higher vertebrates. In birds, a CMZ has been characterised, containing cells that are able to proliferate and differentiate under certain conditions during retinogenesis and, to a lesser degree than in fish and amphibia, also in the

adult [Fischer and Reh, 2000, Fischer et al., 2002, Moshiri et al., 2005].
Also in mammals, a CMZ has been described. Studies in mouse demonstrated the neurogenic potential of the CMZ during embryogenesis, giving rise to non-neural ciliary epithelium as well as neural retina progenies [Bélanger et al., 2017], such as retinal ganglion cells [Marcucci et al., 2016]. It is unclear however, whether and to which extent the CMZ contributes to growth of the mature mouse retina. Furthermore, proliferative cells have been identified in the ciliary body of rats [Ahmad et al., 2000] and the pars plana of mice [Kiyama et al., 2012] and have been shown to form sphere colonies *in vitro* containing multipotent retinal progenitor-like cells that can differentiate into several retinal cell types [Tropepe et al., 2000]. Moreover, a CMZ-like structure could be restored *in vivo* upon enhancement of the Shh-signalling pathway in mice [Moshiri and Reh, 2004].
Strikingly, cells expressing molecular markers of neural and retinal progenitors have been identified in the non-laminated retinal margin and ciliary body pars plana of mature primates [Fischer et al., 2001, Martínez-Navarrete et al., 2008, Bhatia et al., 2009]. Furthermore, a population of undifferentiated cells has been isolated from the human pars plicata and pars plana of the retinal ciliary margin and was shown to exhibit stem cell features both *in vitro* as well as *in vivo* after transplantation into mice and chick eyes at early developmental stages [Coles et al., 2004]. Identification of different retinal cell types at various differentiation stages by immunohistochemistry and electron microscopy provided evidence for *in vivo* neurogenesis in adult monkeys and humans [Martínez-Navarrete et al., 2008].
Additionally, when human embryonic stem cells are selectively differentiated into NR, subsequent inhibition of glycogen synthase kinase 3 (GSK3) and fibroblast growth factor receptor (FGFR) enables reversible switching to the RPE fate [Kuwahara et al., 2015]. The resulting NR-RPE boundary tissue is self-organising into a CMZ-like stem cell niche that is able to generate progenitors *de novo* [Kuwahara et al., 2015].
Altogether, the results obtained in mammals are indicative for inhibiting cues from the endogenous retinal environment, preventing establishment of a (postnatally) active CMZ *in vivo*.
The neurogenic potential of cells at the ciliary margin of mammals together with the intrinsic competence to form a CMZ suggests a progressive loss of active RSCs during vertebrate evolution [Centanin and Wittbrodt, 2014]. It further emphasises the requirement and importance of deciphering the underlying mechanisms of how the CMZ is established and maintained in lower ver-

tebrates, eventually allowing to activate these potentially dormant mammalian RSCs and thus opening up new possibilities of treating human retinopathies in the future.

1.3 *rx* genes

In order to address CMZ establishment and maintenance, I studied *retinal homeobox transcription factor* genes (*rx*) genes, which are known to be expressed in this structure.
rx genes are conserved among vertebrates and code for retina-specific proteins that belong to the family of paired-type homeodomain-containing transcription factors [Bailey et al., 2004, Orquera and de Souza, 2017]. They are among the earliest genes expressed in the presumptive eye field [Mathers et al., 1997] and play a crucial role in early eye development of several vertebrate species including medaka [Loosli et al., 2001]. While there is one *retinal and anterior neural fold homeobox (rax)* gene present in mouse, there are three copies in medaka and zebrafish (*rx1*, *rx2* and *rx3*) [Mathers et al., 1997, Chuang et al., 1999, Loosli et al., 1999, Orquera and de Souza, 2017]. In mouse, a null allele of the *rax* gene leads to an eyeless phenotype [Mathers et al., 1997], similar to *rx3*$^{-/-}$ fish, as the optic vesicles fail to evaginate due to the pivotal role of *rx* genes in eye field specification [Winkler et al., 2000, Loosli et al., 2001, Loosli et al., 2003, Kennedy et al., 2004, Rojas-Muñoz et al., 2005, Stigloher et al., 2006]. Although medaka *rx3* has been studied in great detail [Deschet et al., 1999, Winkler et al., 2000, Loosli et al., 2001] and substantial advances have been made in characterising its paralogue *rx2* [Loosli et al., 1999, Reinhardt et al., 2015], nothing is known about *rx1* expression and function.
While expression of medaka *rx3* starts already at late gastrula stages in the anterior neural plate, prior to evagination of the optic vesicles around developmental stage (st.) 16 [Deschet et al., 1999,Loosli et al., 2001], *rx1* and *rx2* are expressed from st.18 onward (*rx1*: unpublished data; *rx2*: [Loosli et al., 1999]). *rx2* is exclusively expressed in the undifferentiated retinal progenitors of the optic vesicle and, as development proceeds, becomes restricted to photoreceptors, Müller glia cells and the outer margin of the CMZ [Loosli et al., 1999, Reinhardt et al., 2015] Fig. 1.2. Furthermore, *rx2* has been identified as a molecular marker for embryonic and postembryonic multipotent RSCs in medaka [Reinhardt et al., 2015] and zebrafish [Wan et al., 2016, Tang et al., 2017], being expressed in the very periphery of the CMZ.

Moreover, Rx2 was identified as a transcriptional hub balancing stemness of NR and RPE cells in the medaka retina [Reinhardt et al., 2015].
Gain- and loss-of-function studies have been carried out in Xenopus and fish to identify the function of Rx. While overexpression or ectopic expression of Rx leads to ectopic formation of retinal tissue, partial duplication of the retina, as well as hyperproliferation and delayed neurogenesis [Mathers et al., 1997, Andreazzoli et al., 1999, Chuang and Raymond, 2001, Casarosa et al., 2003], loss-of-function results in hypoproliferation [Casarosa et al., 2003, Nelson et al., 2009], decrease in brain size and absence of eyes [Andreazzoli et al., 1999, Winkler et al., 2000, Loosli et al., 2003].
In humans, mutations in the *rax* gene have been associated with coloboma, microphthalmia (smaller eyes, either uni- or bilaterally) and anophthalmia (absence of one or both eyes) [Voronina et al., 2004, Lequeux et al., 2008, London et al., 2009, Gonzalez-Rodriguez et al., 2010, Abouzeid et al., 2012, Chassaing et al., 2014].
In this context, studying the function of *rx* genes in development may help to further understand severe (human) ocular malformations.

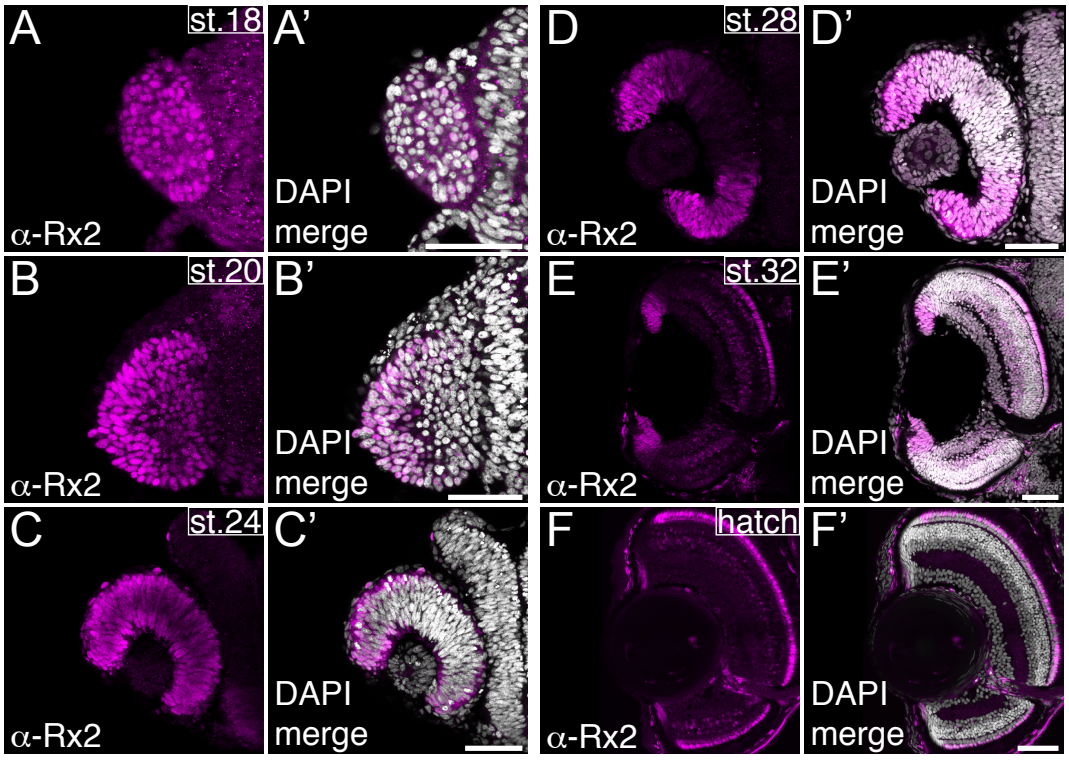

Figure 1.2: Rx2 expression at different developmental stages. Anti-Rx2 stainings at stage 18 (A, A′), 20 (B, B′), 24 (C, C′), 28 (D, D′), 32 (E, E′) and at hatching stage (F, F′). As development proceeds, Rx2 expression gets confined to the CMZ, Müller glia cells in the INL and photoreceptor cells in the ONL. Scale bars represent 50 µm.

1.3.1 Rx transcriptional network

Upstream transcriptional regulators of *rx* imply Otx2, sex determining region Y-box 2 (Sox2), Pou and Forkhead transcription factors, as well as Chordin-, Hh- and Frizzled-pathways in Xenopus [Rasmussen et al., 2001, Andreazzoli et al., 2003, Danno et al., 2008, Martinez-de Luna et al., 2010]. Furthermore, *rx* expression in the Xenopus tadpole CMZ is in part controlled by autoregulatory mechanisms [Kelly et al., 2016]. In the medaka CMZ, *rx2* expression is activated by Tailless (Tlx) and Sox2 and repressed by glioma-associated oncogene family zinc finger 3 (Gli3) and Her9 transcription factors [Reinhardt et al., 2015].

Gain- and loss-of-function studies, as well as luciferase assays have been implicated to identify downstream targets of Rx.

Interestingly, *Xenopus rx1 (Xrx1)* regulates initial Otx2 expression, which in turn regulates *Xrx1* expression, suggesting a feedback-loop [Andreazzoli et al., 1999, Terada et al., 2006, Danno et al., 2008]. Additionally, the expression of antineurogenic transcriptional repressors Hes4, Zinc finger protein of the cerebellum 2 (Zic2), and transducin like enhancer of split 2 (TLE2) preventing endomesodermal fate is activated by Xrx1 [Andreazzoli et al., 2003, Giannaccini et al., 2013]. Cell proliferation in the eye and brain has been shown to be regulated by Xrx1 via Xenopus high mobility group box 3 (Xhmgb3) [Terada et al., 2006]. In zebrafish, neurolin-like cell adhesion molecule (Nlcam) is a downstream target of Rx3, regulating cell migration during optic cup morphogenesis [Brown et al., 2010].

Furthermore, Rx is involved in photoreceptor cell maturation and survival, by regulating photoreceptor-specific genes through binding to photoreceptor conserved element 1 (PCE-1) [Kimura et al., 2000, Pan et al., 2010], as well as by activating interphotoreceptor retinoid-binding protein (IRBP) and TATA-less arrestin promoters [Kimura et al., 2000]. Moreover, Rax and Cone-rod homeobox (Crx) cooperatively transactivate *rhodopsin* and *cone opsin* promoters [Irie et al., 2015].

Importantly, all of the above mentioned genes are downstream targets of Rx3 orthologues [Orquera and de Souza, 2017].

Also recently, transcriptome data on *rx3* in zebrafish [Yin et al., 2014] and *rx1* in Xenopus have been published [Giudetti et al., 2014]. In the latter study, the transcriptome of Xenopus embryos overexpressing *rx1* was compared to embryos with an *rx1* knock-down. The stage analysed corresponds to Xenopus stage 13, when the neural plate is faintly delimited, long before

optic vesicle morphogenesis [Nieuwkoop and Faber, 1994]. Genes regulated by *Xrx1* are involved in transcriptional regulation, cell migration/adhesion and cell proliferation [Giudetti et al., 2014]. When comparing the transcriptome of *rx3*$^{-/-}$ to wild-type zebrafish embryos at 8-somite stage (13 hours post fertilisation (hpf); [Kimmel et al., 1995]), genes involved in eye development were downregulated, whereas genes involved in brain development were upregulated in the mutant [Yin et al., 2014].
Besides this, a transcriptome dataset of medaka *rx3*$^{-/-}$ embryos at different stages has been generated (Centanin, Mateo and Wittbrodt, unpublished).
In order to identify downstream targets of medaka Rx1 and Rx2, we carried out RNA sequencing (RNASeq) analysis of wild-type and *rx1*$^{-/-}$/*rx2*$^{-/-}$ double mutant optic vesicles at developmental stages 18 and 20.

1.4 Approaches for targeted gene inactivation/modification

Targeted genome editing is a powerful tool to study any gene of interest, given that its sequence is known. It enables the introduction of predetermined precise changes into the genome: genes can be deleted, either partially or entirely, modified or replaced [Wright et al., 2014].
In the past few years, enormous advances have been made in this field with the establishment of elaborate techniques such as zinc finger nucleases (ZFNs) [Kim et al., 1996b, Miller et al., 2007, Urnov et al., 2010], transcription activator-like effector nucleases (TALENs) [Joung and Sander, 2013, Sun and Zhao, 2013, Wright et al., 2014] and, most recently, clustered regularly interspaced short palindromic repeats (CRISPR)/CRISPR-associated system (Cas) [Jinek et al., 2012, Cong et al., 2013, Mali et al., 2013]. They all introduce DNA double-strand breaks (DSBs) in a sequence-specific manner, triggering endogenous DNA repair pathways, such as non-homologous end joining (NHEJ) or homology-directed repair (HDR). Sealing of the DSB by NHEJ is error-prone, being mostly accompanied by insertions and deletions, whereas HDR uses a homologous template to repair the lesion [San Filippo et al., 2008, Mladenov and Iliakis, 2011]. Thus, genes can be precisely modified by introducing a donor template containing flanking regions homologous to the target locus [Gutierrez-Triana et al., 2018].

1.4.1 transcription activator-like effector nucleases (TALENs)

The underlying principle of the TALEN technology is the fusion of a sequence-specific TALE domain to the FokI nuclease domain, which functions as a dimer and introduces the DSB. TALEs are transcriptional regulators isolated from the *Xanthomonas* plant pathogens, where they alter transcription of plant genes during pathogenesis [Kay and Bonas, 2009, Miller et al., 2011, Joung and Sander, 2013].
The TALE structure contains a DNA-binding domain, consisting of a series of amino acid tandem repeats, where each repeat is made up of 33-35 amino acids. DNA recognition specificity is mediated by highly variable amino acids at positions 12 and 13 of each repeat, the so-called repeat-variable di-residue [Boch et al., 2009, Moscou and Bogdanove, 2009, Deng et al., 2012]. Targeted genome editing using the TALEN strategy utilises a pair consisting of two TALENs, with the FokI nuclease C-terminally fused to each TALE, and can be delivered as DNA or RNA to the target cell [Miller et al., 2011, Joung and Sander, 2013, Sun and Zhao, 2013, Wright et al., 2014, Rinaldi et al., 2017].
In this thesis, I characterised medaka *rx1* and *rx2* mutants that were previously generated through the TALEN approach [Reinhardt, 2014].

1.4.2 CRISPR/Cas9

Engineering of the CRISPR/Cas system has further revolutionised targeted genome editing due to its unprecedented efficiency.
CRISPR/Cas systems have been discovered in bacteria and archea, where they act as part of the adaptive immune system, protecting against viruses and plasmids by sequence-specific targeting [Horvath and Barrangou, 2010, Bhaya et al., 2011, Terns and Terns, 2011, Jinek et al., 2012, Wiedenheft et al., 2012].
The bacterial type II CRISPR/Cas9 system of *Streptococcus pyogenes* is the most commonly engineered system used for targeted genome editing [Mali et al., 2013, Terns and Terns, 2014]. Here, a custom bipartite single guide RNA (sgRNA) provides sequence-specificity on the one hand and binding to Cas9 endonuclease on the other hand [Jinek et al., 2012, Terns and Terns, 2014]. The resulting sgRNA/Cas9 ribonucleoprotein effector complex binds the target DNA and introduces a DSB. Target sites (also called protospacers) are usually 20 nucleotides long and feature an immediately adjacent protospacer adjacent motif (PAM) (NGG in case of Cas9) [Hsu et al., 2013, Stemmer et al.,

2015]. DSBs are created 3 bp upstream of the PAM, upon which DNA repair pathways are activated to seal the cleavage site (Mali et al., 2013).
While for deletion of sequences or inactivation of genes NHEJ is sufficient, the repair and modification of genes of interest requires the precise HDR DNA repair mechanism. For instance, tagging a protein of interest with a given fluorophore requires the nucleic acid sequence of the latter to be precisely integrated without disturbing the endogenous open reading frame (ORF). Whereas NHEJ is active throughout the cell cycle, HDR is preferentially active during S/G2 phases, thus making DSB repair by HDR a rather rare event [Hustedt and Durocher, 2017,Gutierrez-Triana et al., 2018]. Furthermore, dsDNA donor sequences introduced as templates for HDR-mediated repair are likely multimerised by the highly active NHEJ mechanism, thus hindering insertions of single-copy [Gutierrez-Triana et al., 2018].
While several approaches have been undertaken to prevent NHEJ and/or favour HDR [Maruyama et al., 2015, Gutschner et al., 2016, Wang et al., 2017], these often interfere with the repair machinery on a systemic level which may introduce unwanted side-effects. We sought to focus on the dsDNA donor itself and ultimately prevent multimerisation with the notion to keep a monomeric state to favour single-copy integration.
In the framework of this thesis, I therefore developed a protocol for precise and efficient single-copy integration of modified dsDNA donors via HDR [Gutierrez-Triana et al., 2018] (in collaboration with AG, TT). This protocol was used to generate endogenously tagged medaka transgenic lines, which are characterised in this thesis.

Aims and Approaches

The aim of this study was to elucidate the role of *rx* genes in postembryonic growth, scaling and shaping of the eye, ultimately allowing to put the subfunctionalisation of *rx* genes into an evolutionary context.

I used the medaka retina and its CMZ as a model system to study the function of Rx1 and Rx2 in differentiation and proliferation of NR and RPE stem cells. As a prerequisite, it was necessary to develop tools for mosaic, systemic and conditional analyses. To this end, a CRISPR/Cas9-based approach was developed as part of this thesis, resulting in the establishment of *eGFP-FL-rx1*, *eGFP-FL-rx2* and *mCherry-FL-rx2* transgenic lines, where the respective endogenous *rx* gene is precisely tagged with a single-copy fluorophore coding sequence.

Furthermore, transplantation analyses of permanently labelled cells mutant for either *rx1* or *rx2* were carried out. Additionally, I established *rx1*$^{-/-}$/*rx2*$^{-/-}$ double mutants and analysed their phenotype at different developmental stages. In order to identify downstream targets of *rx1* and *rx2* and eventually address the transcriptional logic of lifelong proliferation and differentiation of RSCs, an RNASeq dataset of *rx1*$^{-/-}$/*rx2*$^{-/-}$ double mutant optic vesicles was generated.

Besides this, further approaches to interfere with Rx1 and Rx2 function were investigated, e.g. if targeted knock-in constructs comprising a reporter cassette and a potential transcriptional terminator could mimic a null allele situation.

In order to delineate the precise role of Rx2 in the CMZ without interfering with its function in early eye development, I characterised a conditional allele featuring a colour switch.

2

Results

2.1 Rx1 and Rx2 display different, complementary expression patterns

rx genes are among the earliest genes expressed in the presumptive eye field, with *rx3* expression starting already at late gastrula stages [Deschet et al., 1999]. *rx1* and *rx2* however, are expressed in the fully evaginated optic vesicle from stage 18/19 onward prior to the transition to the optic cup [Loosli et al., 1999, Loosli et al., 2001, Loosli et al., 2003]. So far, the expression analysis of medaka *rx1* was solely based on *in situ* hybridisation data and therefore lacked cellular resolution. *In situ* hybridisation data at early embryonic stages (*rx2*: [Reinhardt, 2014]; *rx1*: data not shown) and embryonic stage 32 were indicating spatiotemporal redundancy of *rx1* and *rx2* genes (Fig. 2.1).
Moreover, for *rx2* and *rx3*, proximal *cis*-regulatory elements have been identified [Martinez-Morales et al., 2009, Reinhardt et al., 2015], which, when controlling the expression of a fluorescent protein, indicate the respective cellular expression domain. Additionally, an anti-Rx2 antibody has been raised, revealing expression of Rx2 protein [Reinhardt et al., 2015].

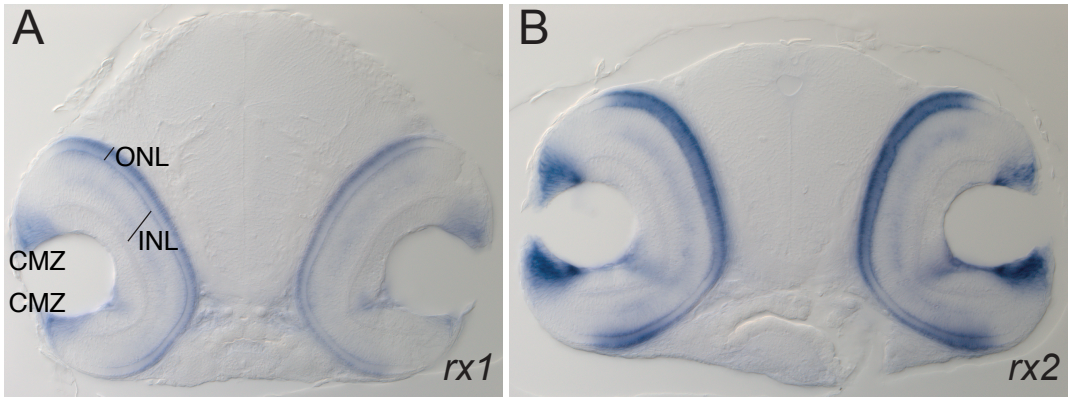

Figure 2.1: *rx1* and *rx2* expression show spatio-temporal redundancy. Vibratome sections of whole mount *in situ* hybridisation (WISH) with probes against (A) *rx1* and (B) *rx2* at embryonic stage 32 show transcripts in the CMZ, the INL and the ONL.

Nothing is known however about *rx1* expression and function in medaka.

2.1.1 Rx1 is expressed in the CMZ, in cone photoreceptor cells and in the inner nuclear layer

Using CRISPR/Cas9, I established a protocol for precise single-copy integration via HDR (in collaboration with AG, TT). Any DNA introduced into cells will concatemerise in a ligation dependent manner [Winkler et al., 1991]. To prevent this, i.e. to keep the donor DNA in a monomeric state to favour HDR-mediated integration of a single-copy, the donor was protected from multimerisation by a biotin moiety at each 5' end of the primers used for PCR amplification of the donor DNA [Gutierrez-Triana et al., 2018].
This enabled efficient endogenous tagging of *rx1* and *rx2* ORFs with a single-copy *enhanced green fluorescent protein (eGFP)* or *mCherry* coding sequence including a flexible linker (FL) as spacer [Gutierrez-Triana et al., 2018] (Fig. 2.2, Fig. 2.5). Thus, expression of medaka Rx1 was identified with cellular resolution for the first time (Fig. 2.3). Furthermore, these endogenously tagged transgenic lines allowed to compare and distinguish expression domains of *rx1* and *rx2*.

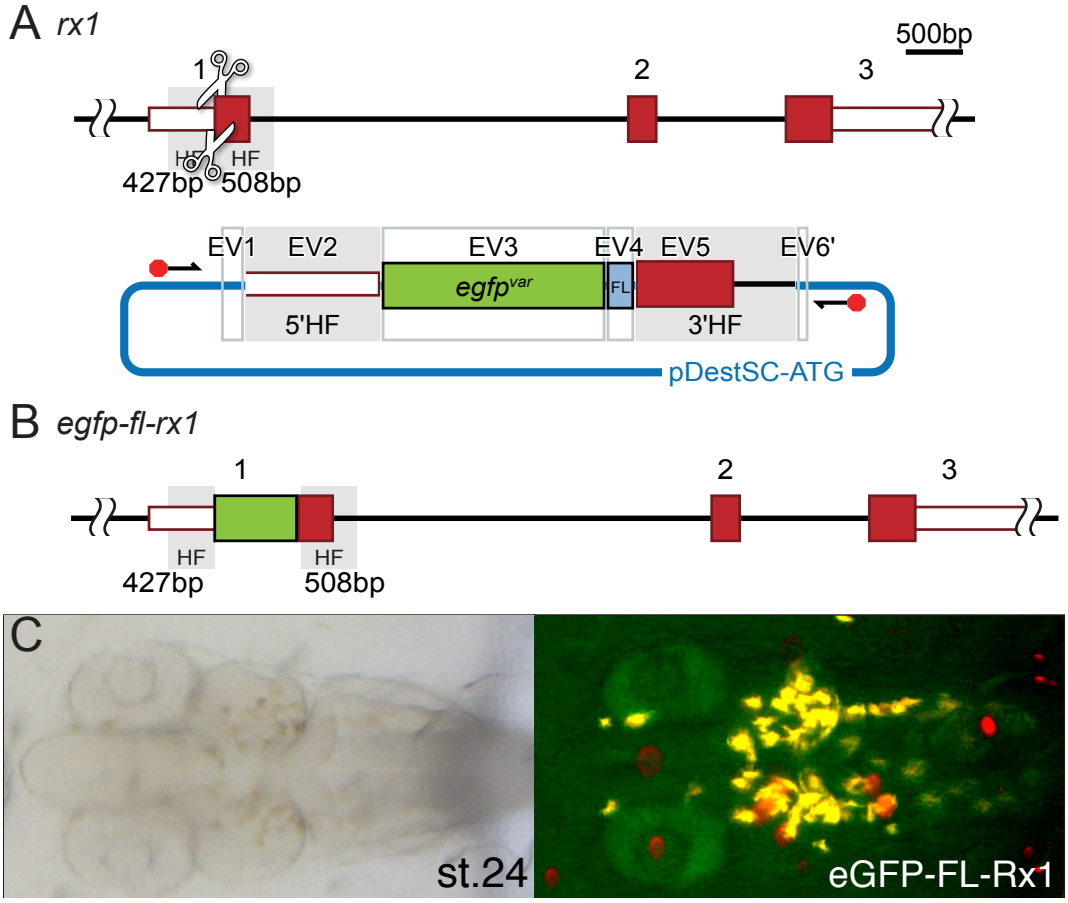

Figure 2.2: Endogenous tagging recapitulates *rx1* expression in the optic cup at embryonic stage 24. (A and B) Schematic to-scale representation of the wild-type *rx1* locus, the donor plasmid and the *rx1* locus after successful HDR-mediated integration. Golden Gate cloning [Kirchmaier et al., 2013] was used to assemble the donor plasmid, which served as a template for PCR amplification using modified (red octagon) primers flanking the donor cassette. Entry vectors (EVs) are indicated, plasmid depiction is not to scale. Untranslated region (UTR) (white boxes with red outlines), coding exons (red boxes), homology flanks (HF, grey), sgRNA target site (white scissors; located immediately after the ATG), flexible linker (FL, blue box) and eGFP (green box) are indicated. (C) *eGFP-FL-rx1* transgenic line displays eGFP expression in the *rx1* expression domain at embryonic stage 24. (Figure is adapted and modified from [Gutierrez-Triana et al., 2018], Figure 1 figure supplement 1, as well as Figure 2). Note unspecific autofluorescence of body pigmentation apparent in red and yellow.

Immunostainings for eGFP, as well as for Rx2 on homozygous hatchling retinae of the *eGFP-FL-rx1* transgenic line revealed complementary, yet not completely overlapping expression domains of Rx1 and Rx2 (Fig. 2.3). eGFP signal was mainly nuclear and could be detected in the CMZ, the INL and the ONL, partially overlapping with Rx2 signal (Fig. 2.3, filled arrowheads). Interestingly, there were also nuclei in the INL with strong eGFP signal but no or only very weak Rx2 signal (Fig. 2.3, non-filled arrowheads), suggesting a population of cells that is exclusively Rx1-positive.

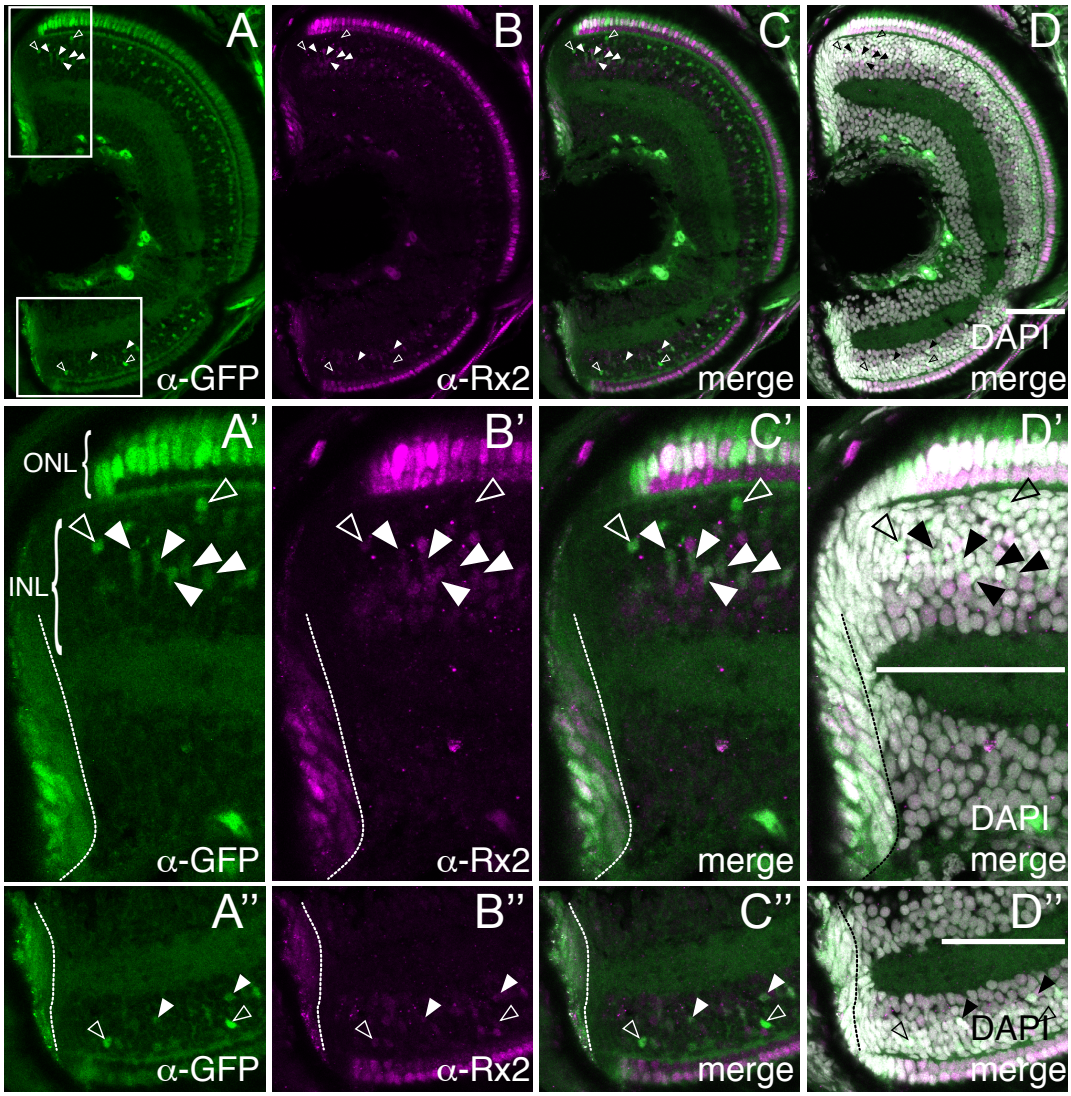

Figure 2.3: Rx1 is expressed in the CMZ, in cone photoreceptor cells and in the inner nuclear layer. (A-D) Cryosections of homozygous hatchling retinae of the *eGFP-FL-rx1* transgenic line stained for eGFP (A-A″) and Rx2 (B-B″). Overlays are shown in panels C-C″ and D-D″. Filled arrowheads point towards cells in the INL positive for both, eGFP and Rx2; non-filled arrowheads indicate cells positive for eGFP but only weakly or negative for Rx2. Regions marked with boxes in panels A-D are magnified in panels A′-D′ (dorsal) and A″-D″ (ventral). ONL, INL and CMZ (dashed line) are indicated. Upper row of nuclei in the ONL are cone photoreceptor nuclei, lower row of nuclei are rod photoreceptor nuclei. Note that eGFP signal is present in cones, but absent in rods. Scale bars represent 50 µm.

Furthermore, these nuclei were located basally to the ONL, but apically to the Müller glia cells, which were predominantly positive for both, eGFP and Rx2 (Fig. 2.3, filled arrowheads). Judged by position, these exclusively Rx1 expressing cells could either be of horizontal or bipolar cell identity. Immunostaining for the horizontal cell marker Prox1 indeed labelled a subpopulation of

Rx1 expressing cells, which however only showed weak eGFP signal (Fig. 2.4).

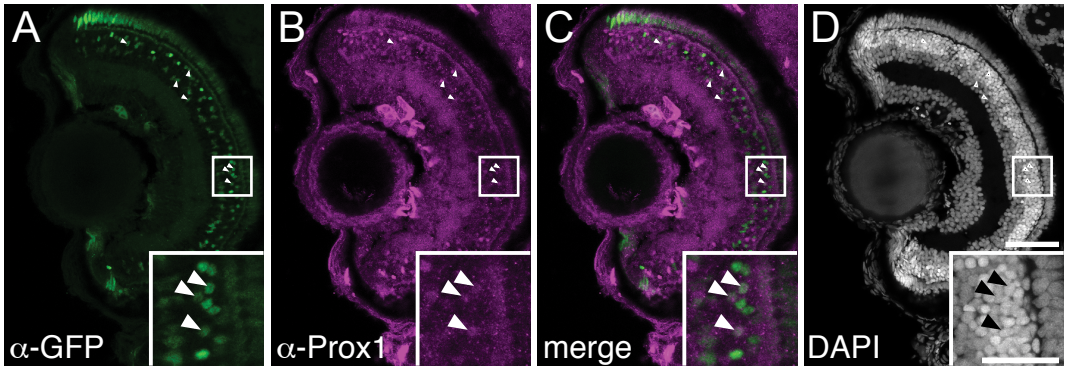

Figure 2.4: The horizontal cell marker Prox1 labels a subpopulation of (weakly) Rx1 expressing cells. Cryosections of homozygous hatchling retinae of the *eGFP-FL-rx1* transgenic line stained for eGFP (A) and Prox1 (B), which are partially overlapping in the INL (C). Note that nuclei positive for both, eGFP and Prox1 (indicated by the filled arrowheads), display only weak eGFP signal. Magnified regions of insets indicated by box in overview panels. Scale bars represent 50 µm (overview panels) or 25 µm (insets).

Also in the ONL, there was a marked difference in Rx1 expression as indicated by anti-eGFP staining and Rx2 expression as detected by the anti-Rx2 staining. While the cone photoreceptor cells were mostly positive for eGFP, rods were devoid of eGFP signal, in strong contrast to the anti-Rx2 staining which was detected in both layers, although stronger in the cones (Fig. 2.3 B-B″, Fig. 2.6). eGFP signal intensity in the cones reminded of a salt-and-pepper pattern, especially when overlaid with the anti-Rx2 staining (Fig. 2.3 C-C′). In the CMZ, nuclear eGFP signal appeared more confined than the Rx2-positive domain, indicating a (stem) cell population positive for Rx2, but negative for Rx1 (Fig. 2.3 C′).

2.1.2 Rx2 is expressed in the CMZ, in cone and rod photoreceptor cells and in Müller glia cells

A comparable analysis was carried out on homozygous hatchlings of the *eGFP-FL-rx2* transgenic line (genome targeting design see Fig. 2.5).

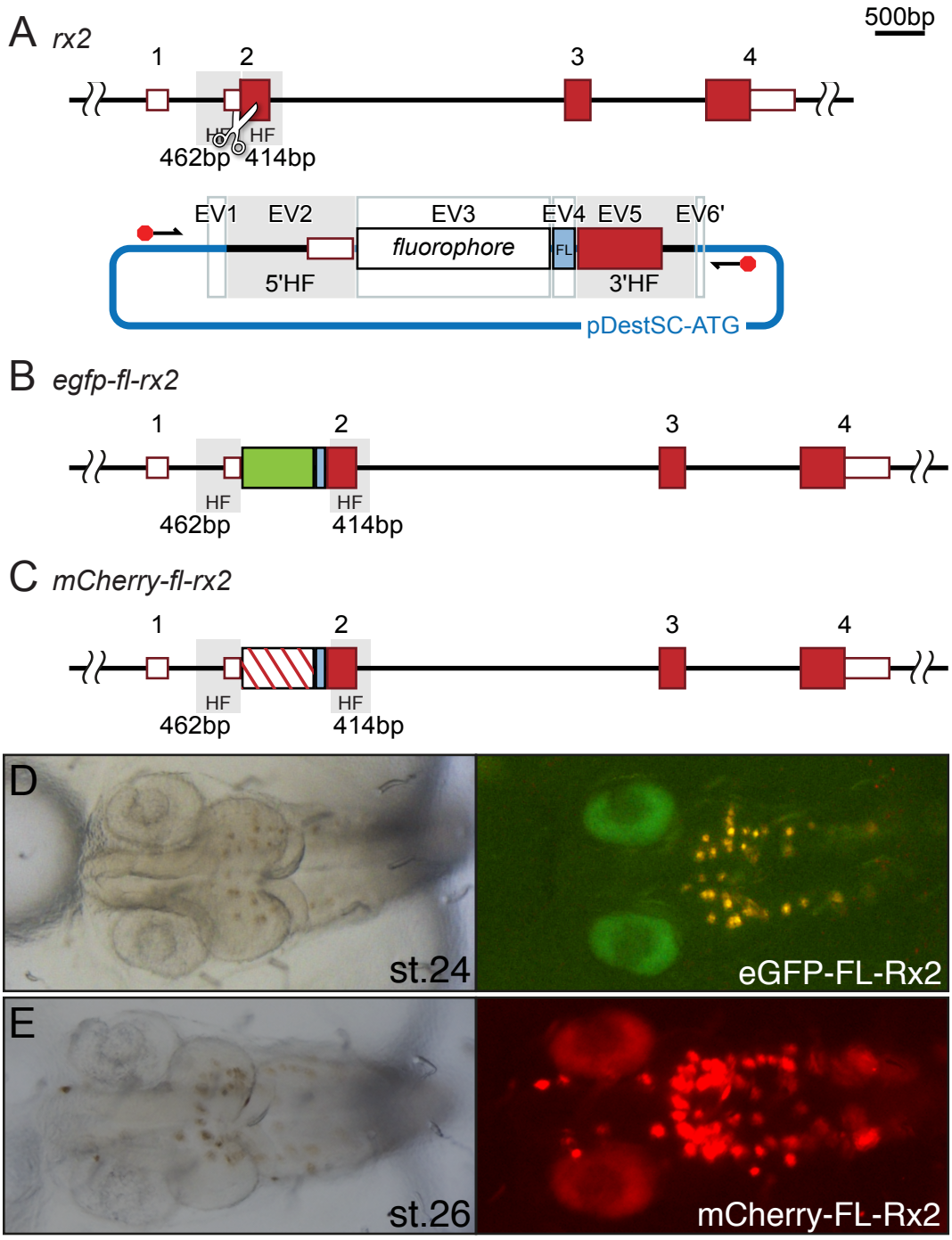

Figure 2.5: Endogenous tagging recapitulates *rx2* expression in the optic cup at embryonic stages 24 and 26. (A-C) Schematic to-scale representation of the wild-type *rx2* locus, the donor plasmid and the *rx2* locus after successful HDR-mediated integration. Golden Gate cloning [Kirchmaier et al., 2013] was used to assemble the donor plasmid, which served as template for PCR amplification using modified (red octagon) primers flanking the donor cassette. Entry vectors (EV) are indicated, plasmid depiction is not to scale. Untranslated region (UTR) (white boxes with red outlines), coding exons (red boxes), homology flanks (HF, grey), sgRNA target site (white scissors; located immediately after the ATG), flexible linker (FL, blue box), eGFP (green box) and mCherry (red-striped box) are indicated. (D) *eGFP-FL-rx2* and (E) *mCherry-FL-rx2* transgenic lines display fluorophore expression in the *rx2* expression domain at embryonic stages 24 and 26, respectively. (Panels A-C are adapted and modified from [Gutierrez-Triana et al., 2018], Figure 1 figure supplement 1, as well as Figure 2). Note unspecific autofluorescence of body pigmentation apparent in yellow (in D), as well as bright red spots on dorsal trunk (in E).

Immunostainings for eGFP, as well as for Rx2 were performed on hatchling retinae and revealed complete overlap, indicating that the tagged allele is indeed faithfully recapitulating endogenous *rx2* expression (Fig. 2.6) [Reinhardt et al., 2015]. In detail, eGFP and Rx2 signals were found in the CMZ, in Müller glia cells and in both, cone and rod photoreceptor cells, albeit appearing stronger in cone photoreceptors. Like in the case of the *eGFP-FL-rx1* transgenic line, eGFP signal was not always entirely nuclear. Especially in the CMZ, exclusive nuclear localisation of the eGFP signal was only evident in the outermost periphery (Fig. 2.6 A′, C′, A″, C″).

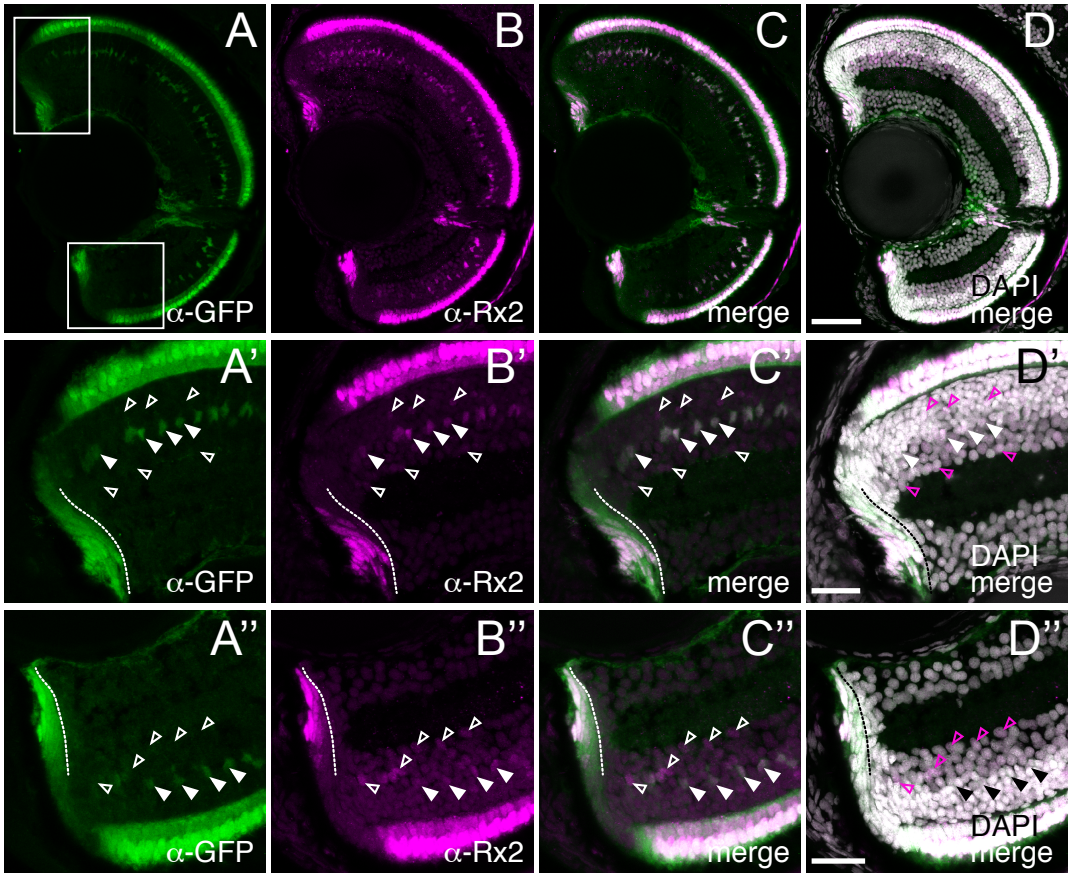

Figure 2.6: Rx2 is expressed in the CMZ, in cone and rod photoreceptor cells and in Müller glia cells. (A-D) Cryosections of homozygous hatchling retinae of the *eGFP-FL-rx2* transgenic line stained for eGFP (A-A″) and Rx2 (B-B″). Overlays are shown in panels C-C″ and D-D″. Magnifications of the dorsal (A′-D′) and the ventral retina (A″-D″) were acquired from an adjacent section of the same retina (area of magnification indicated by white boxes in A). Filled arrowheads point towards cells in the INL positive for both, eGFP and Rx2; non-filled arrowheads indicate cells weakly positive for Rx2 and negative for eGFP. CMZ (dashed line) is indicated. Scale bars represent 50 µm (D) or 20 µm (D′, D″).

2.2 Rx1 and Rx2 exhibit different, complementary functions in RSCs

In order to address the function of both, Rx1 and Rx2 in the medaka CMZ, I analysed the mutants generated through the TALEN approach by Robert Reinhardt [Reinhardt, 2014, Reinhardt et al., 2015]. Each of these mutant alleles contains a 10 bp deletion in the homeobox, leading to a frameshift and premature STOP and therefore potentially altered transcript and protein (Fig. 2.7).

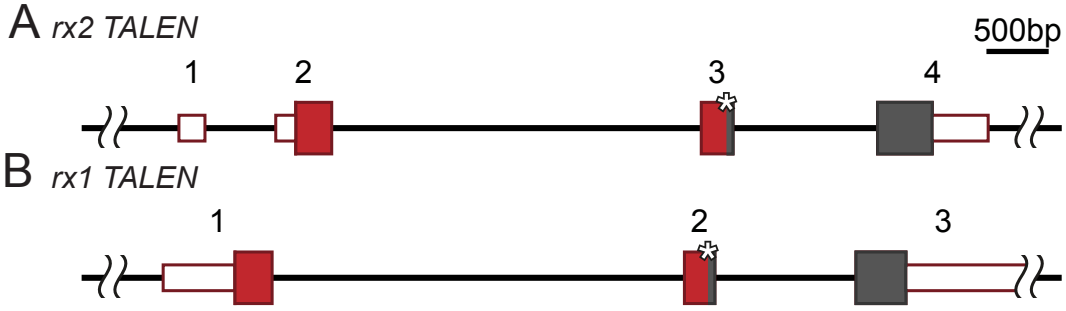

Figure 2.7: Schematic representation of the *rx1* and *rx2* loci containing the TALEN mutation. Schematic to-scale representation of *rx1* and *rx2* loci with UTR (white boxes with red outlines), coding exons (red boxes) and 10 bp deletion (TALEN mutation not to-scale; asterisk, potential frameshift in grey) in the homeobox.

Homozygous *rx1*$^{-/-}$ or *rx2*$^{-/-}$ mutant fish do not display any apparent (macroscopic) phenotype, potentially due to partial functional redundancy of the *rx* paralogues [Reinhardt et al., 2015]. Therefore, I carried out cell transplantions at blastula stage (developmental stage 10-11) to analyse the capacity of *rx1* and *rx2* mutant cells to contribute to growth of the retina. Permanently labelled wild-type cells were transplanted into a homozygous mutant background (*rx2*$^{-/-}$: [Reinhardt et al., 2015]), and homozygous mutant cells were challenged by a wild-type environment. In all cases retinal cells were tested for their ability to generate ArCoSs, as a readout for contribution to retinal growth [Centanin et al., 2011].

When wild-type blastula cells are transplanted into a wild-type blastula host, they contribute to both, NR and RPE stem cell populations, as indicated by their capacity to form ArCoSs in both retinal layers [Reinhardt et al., 2015]. Here, the number of RPE ArCoSs is equal (Fig. 2.8 A, A′, D) or slightly reduced (Fig. 2.9 A, A′, D) compared to the number of NR ArCoSs.

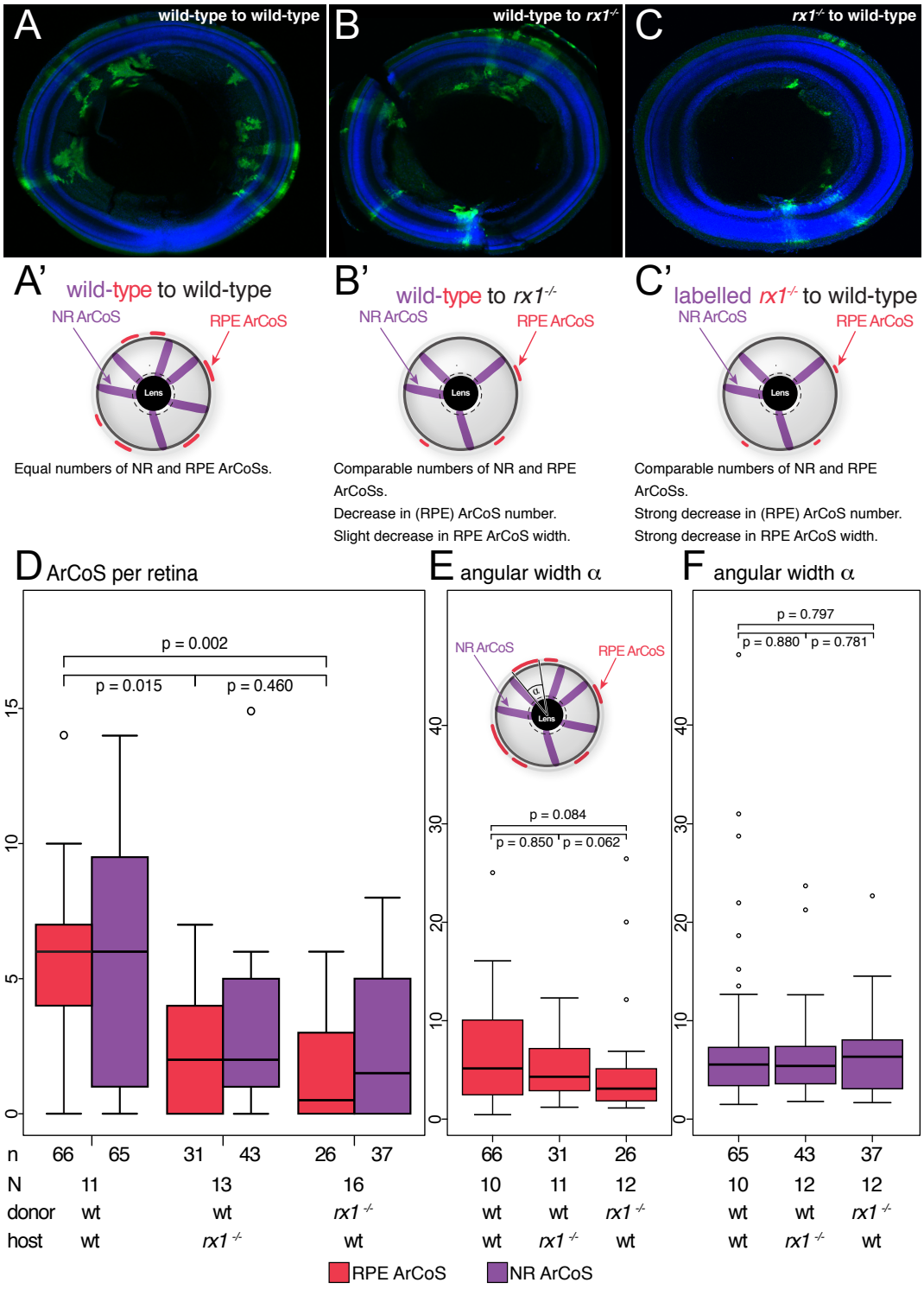

Figure 2.8: Loss of *rx1* cell-autonomously impacts on RPE clone expansion. Transplantation of permanently labelled donor blastula cells into a host blastula results in formation of both, NR and RPE ArCoSs. Transplantation of (A) labelled wild-type donor cells into a wild-type blastula host, (B) labelled wild-type donor cells into a *rx1*$^{-/-}$ blastula host, (C) labelled *rx1*$^{-/-}$ cells into a wild-type blastula host. (A′-C′) Schematic representations of the respective transplantation outcomes. Boxplots showing numbers of ArCoS per retina (D), as well as angular width α of RPE (E) and NR ArCoSs (F) as a proxy for ArCoS width for each transplantation. The scheme in (E) shows how angular width α was determined. P-values were calculated using the Wilcoxon Sign Test, since data were not normally distributed, as tested with the Shapiro-Wilk test. n represents the number of ArCoSs, N the number of retinae analysed; wt (wild-type).

2.2.1 Loss of *rx1* impacts on expansion of RPE clones in a cell-autonomous manner

However, when analysing wild-type blastula cells transplanted into a *rx1*$^{-/-}$ background, the overall number of ArCoSs decreased with a trend towards narrower RPE ArCoSs (Fig. 2.8 B, B′, D, E).
This tendency is even more pronounced when *rx1*$^{-/-}$ cells are challenged in a wild-type environment, with a fraction of *rx1*$^{-/-}$ cells giving rise to RPE ArCoSs taking up only 0.3 % of the retinal perimeter (Fig. 2.8 C, C′, D, E). Also, the overall number of ArCoSs further decreased, accounting for a 60 % decrease in the number of RPE ArCoSs compared to the wild-type situation. The width of NR ArCoSs remained unaffected (Fig. 2.8 F).

2.2.2 Loss of *rx2* favours the formation of RPE in a non-autonomous manner

Parts of the transplantation data regarding *rx2*$^{-/-}$ mutant cells have already been published [Reinhardt et al., 2015] (Fig. 2.9 A, B). When transplanted to a *rx2*$^{-/-}$ environment, wild-type cells preferentially gave rise to NR ArCoSs (Fig. 2.9 B, B′, D). This data indicated that Rx2 activity is required for balancing of cell fates and numbers between NR and RPE stem cells [Reinhardt et al., 2015].
Consistent with this, transplantation of *rx2*$^{-/-}$ cells into a wild-type background led to formation of more and wider RPE ArCoSs, with a fraction of *rx2*$^{-/-}$ cells giving rise to RPE ArCoSs taking up to 20 % of the retinal perimeter (Fig. 2.9 C, C′, D, E). In comparison, wild-type RPE ArCoSs usually take up 1-6 % of the retinal perimeter. The increase in RPE ArCoS number accounted for 60 % compared to the wild-type situation. Furthermore, when re-analysing the already published dataset, I could show that wild-type cells in a *rx2*$^{-/-}$ environment not only preferentially give rise to NR ArCoSs, but that these are also wider compared to the wild-type situation (Fig. 2.9 B, B′, F).

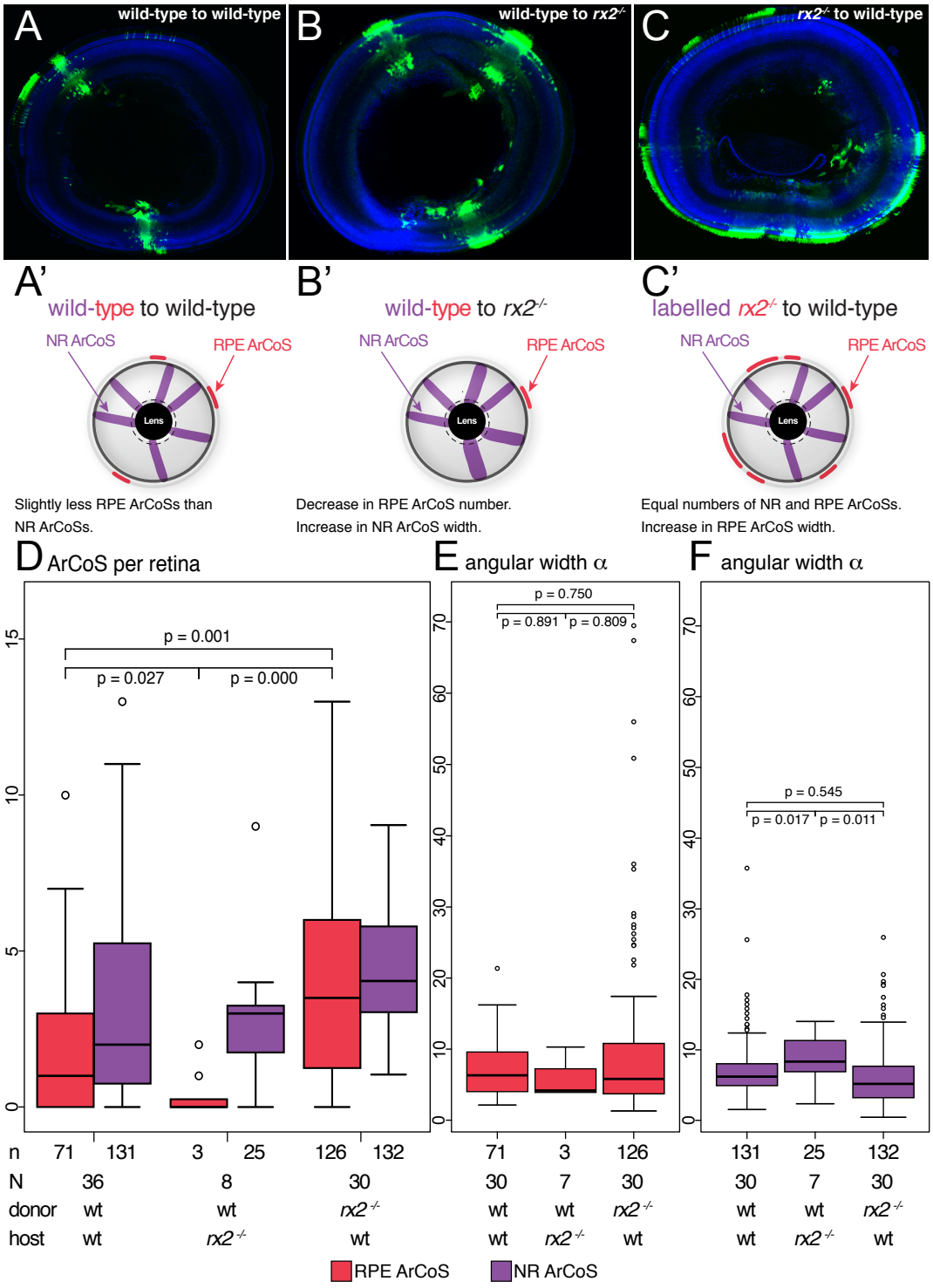

Figure 2.9: Loss of *rx2* favours the formation of RPE in a non-autonomous manner. Transplantation of permanently labelled donor blastula cells into a host blastula results in formation of both, NR and RPE ArCoSs. Transplantation of (A) labelled wild-type donor cells into a wild-type blastula host, (B) labelled wild-type donor cells into a *rx2*$^{-/-}$ blastula host, (C) labelled *rx2*$^{-/-}$ cells into a wild-type blastula host. (A′-C′) Schematic representations of the respective transplantation outcomes. Boxplots showing numbers of ArCoS per retina (D), as well as angular width α of RPE (E) and NR ArCoSs (F) as a proxy for ArCoS width for each transplantation. P-values were calculated using the Wilcoxon Sign Test, since data were not normally distributed, as tested with the Shapiro-Wilk test. n represents the number of ArCoSs, N the number of retinae analysed; wt (wild-type). Panels A and B are adapted and modified from [Reinhardt et al., 2015], Figure 8 C and D.

Taken together, the transplantation experiments indicate different, complementary functions for Rx1 and Rx2 in RSCs. While the loss of Rx1 function impacts on the width of RPE clones in a cell-autonomous manner, the loss of Rx2 function favours the formation of RPE in a non-autonomous manner.

2.3 *rx1*$^{-/-}$/*rx2*$^{-/-}$ double mutants exhibit microphthalmia

Since fish homozygous for the respective single *rx1* or *rx2* TALEN mutation did not show an apparent (macroscopic) phenotype, I generated homozygous double mutants (*rx1*$^{-/-}$/*rx2*$^{-/-}$ double mutant) by subsequent crossings. These double mutants exhibited severe microphthalmia phenotypes macroscopically detectable from developmental stage 24 onwards (Fig. 2.10 - Fig. 2.16).

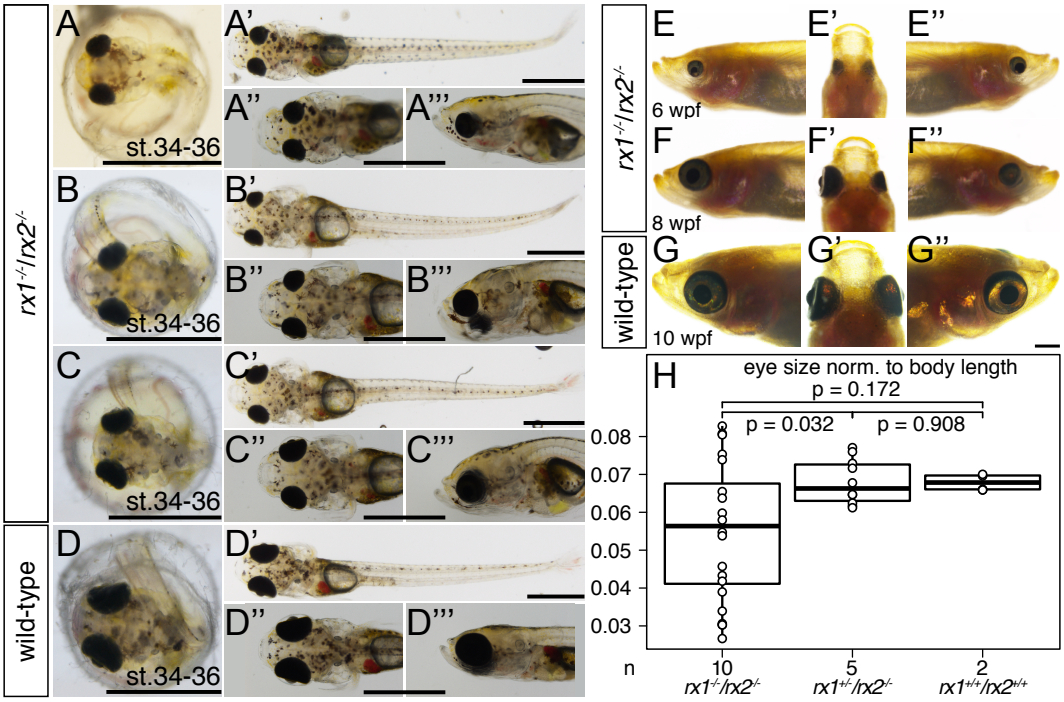

Figure 2.10: *rx1*$^{-/-}$/*rx2*$^{-/-}$ double mutant fish show microphthalmia phenotypes from embryonic stages onwards. *rx1*$^{-/-}$/*rx2*$^{-/-}$ double mutant (A-A‴, B-B‴, C-C‴) stage 34-36 embryos and hatchlings show micropthalmia phenotypes, which are still evident in adult stages (E-E″, F-F″). Wild-type stages for reference (D-D‴, G-G″). (H) Boxplot shows eye size normalised to body length of adult fish of different genotypes: *rx1*$^{-/-}$/*rx2*$^{-/-}$ double mutant, *rx1*$^{+/-}$/*rx2*$^{-/-}$ and *rx1*$^{+/+}$/*rx2*$^{+/+}$ (wild-type). Eyes of *rx1*$^{-/-}$/*rx2*$^{-/-}$ double mutant fish are in general smaller than wild-type eyes, whereas eyes of *rx1*$^{+/-}$/*rx2*$^{-/-}$ heterozygotes are not significantly different from wild-type size. P-values were calculated using two-sample t-test, since data were normally distributed, as tested with the Shapiro-Wilk test. n indicates number of fish analysed; wpf = weeks post fertilisation. Scale bars represent 1 mm.

Notably, *rx1*$^{-/-}$/*rx2*$^{-/-}$ double mutant fish showed high phenotypic variability (Fig. 2.10 E-G″), including cases where both eyes were affected equally and others where one eye seemed to be affected to a larger extent compared to the second eye (Fig. 2.10, Fig. 2.14). Interestingly, the variability of phenotypes observed by immunostaining correlated with the macroscopic variability of the *rx1*$^{-/-}$/*rx2*$^{-/-}$ double mutant eye phenotypes (Fig. 2.14).

2.3.1 *rx1*$^{-/-}$/*rx2*$^{-/-}$ double mutant embryos exhibit morphogenetic defects reminiscent of an optic flow and show reduced retinal proliferation

In order to address the early consequences of *rx1* and *rx2* loss-of-function, I carried out bromodeoxyuridine (BrdU) pulse-chase experiments of *rx1*$^{-/-}$/*rx2*$^{-/-}$ double mutants and wild-type embryos at stage 28 and 32-34 (Fig. 2.11 A, H, Fig. 2.12 A, H).
Embryos were dechorionated with hatching enzyme, incubated in 2.5 mM BrdU solution for 1 hour, cryosectioned and analysed by immunohistochemistry. Antibodies against BrdU and Islet-1 (Isl-1) were used to visualise the proportion of actively proliferating and differentiating retinal cells, respectively (Fig. 2.11) [Bejarano-Escobar et al., 2015, Martín-Partido and Francisco-Morcillo, 2015]. In addition, a phosphorylated histone H3 (PH3) antibody was used to identify mitotic cells. Immunostainings at stage 28 revealed a morphogenetic phenotype, suggesting the presence of a hitherto not described optic flow in wild-type medaka (Fig. 2.11, compare panel E to L) [Heermann et al., 2015]. Furthermore, development of the ventral retina of *rx1*$^{-/-}$/*rx2*$^{-/-}$ double mutants seemed to be delayed compared to wild-type. Moreover, patterning defects as well as reduced proliferation as indicated by overall reduced numbers of PH3-positive cells compared to wild-type were observed (Fig. 2.11, compare panels C, E, F to J, L, M). Anti-Isl-1 staining revealed a neuronal differentiation delay compared to wild-type retinae (Fig. 2.11, compare panel B to I). Staining for S-phase marker BrdU seemed unaffected in *rx1*$^{-/-}$/*rx2*$^{-/-}$ double mutant retinae (Fig. 2.11, compare panels D, E, F to K, L, M). Furthermore, the coherence of cryosections was severely reduced when compared to wild-type sections processed in parallel, suggesting reduced tissue integrity of *rx1*$^{-/-}$/*rx2*$^{-/-}$ double mutant retinae.

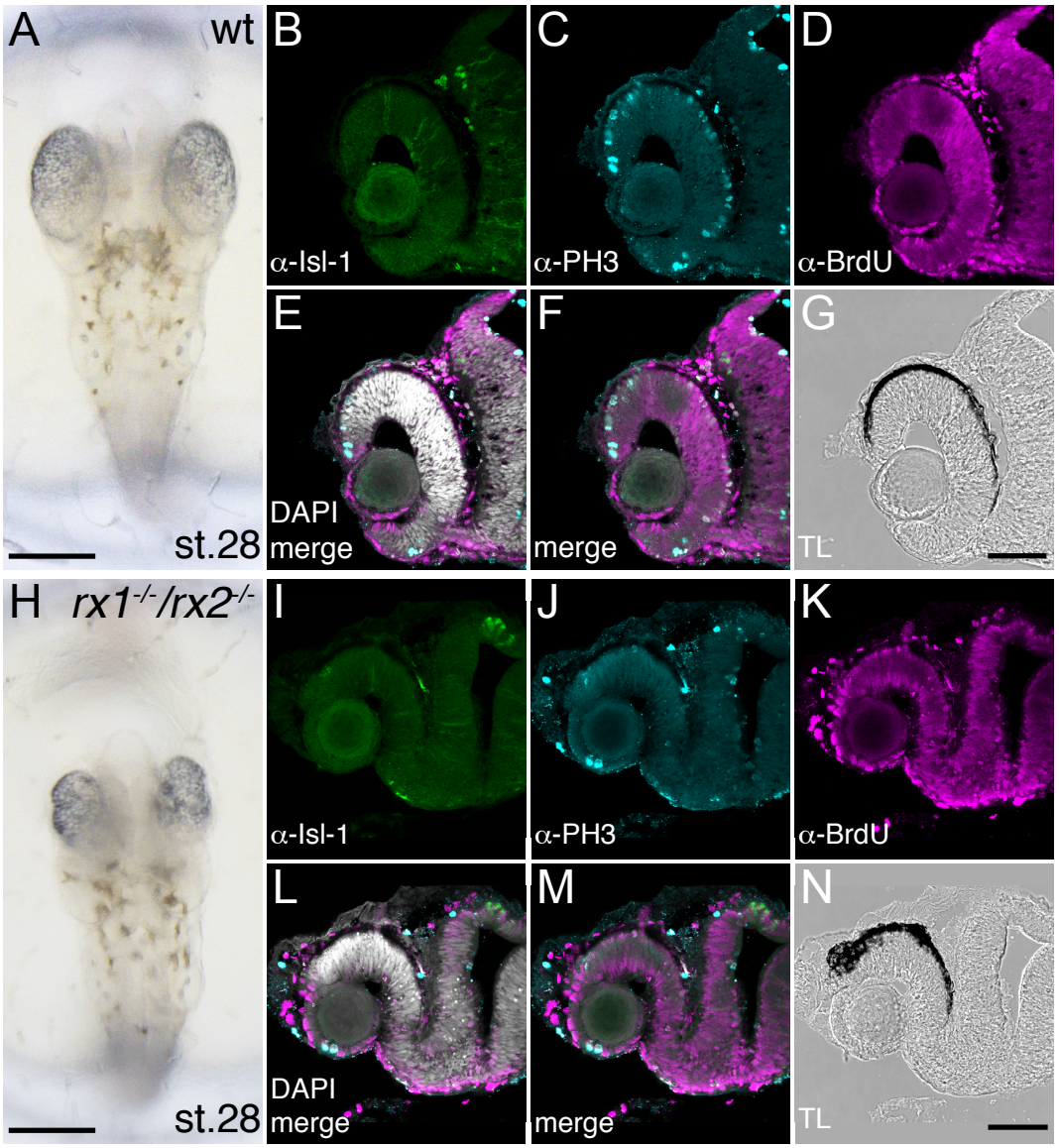

Figure 2.11: *rx1*$^{-/-}$*/rx2*$^{-/-}$ double mutant retinae display defects reminiscent of optic flow aberrations and reduced proliferation. Wild-type (A) and *rx1*$^{-/-}$*/rx2*$^{-/-}$ double mutant (H) stage 28 embryos were incubated in 2.5 mM BrdU solution for 1 hour, subjected to cryosectioning and analysed by immunohistochemistry. DAPI staining revealed a morphogenetic phenotype in *rx1*$^{-/-}$*/rx2*$^{-/-}$ double mutant retinae reminiscent of an optic flow (E, L). Reduced anti-Isl-1 staining (B, E, F, I, L, M) indicated a neuronal differentiation delay and reduced anti-PH3 staining (C, E, F, J, L, M) revealed reduced proliferation in *rx1*$^{-/-}$*/rx2*$^{-/-}$ double mutant retinae. Staining for S-phase marker BrdU (D-F, K-M) seemed unaffected in *rx1*$^{-/-}$*/rx2*$^{-/-}$ double mutant retinae. Sections are shown in transmission light in panels G and N. Scale bars represent 200 µm (A, H) or 50 µm (G, N).

2.3.2 *rx1*$^{-/-}$*/rx2*$^{-/-}$ double mutants show misfating of neurons and retinal lamination defects

Corresponding analyses of *rx1*$^{-/-}$*/rx2*$^{-/-}$ double mutants and wild-type embryos at stage 32-34 revealed misfating of neurons and severe retinal lamination de-

fects (Fig. 2.12).

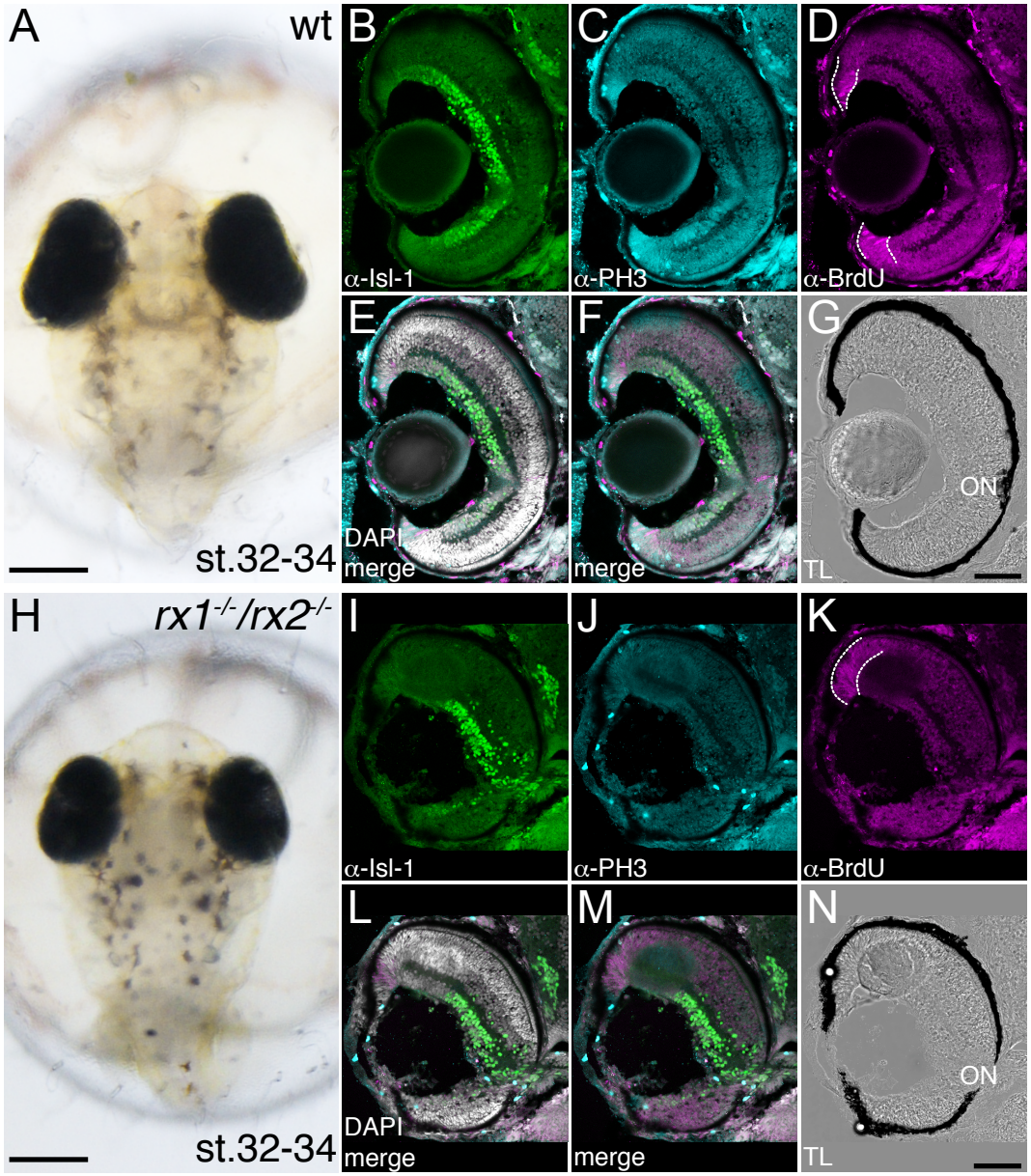

Figure 2.12: *rx1*$^{-/-}$*/rx2*$^{-/-}$ double mutant retinae exhibit misfating of neurons and retinal lamination defects. Wild-type (A) and *rx1*$^{-/-}$*/rx2*$^{-/-}$ double mutant (H) stage 32-34 embryos were incubated in 2.5 mM BrdU solution for 1 hour, subjected to cryosectioning and analysed by immunohistochemistry. DAPI staining revealed lamination defects more pronounced in the ventral retina of *rx1*$^{-/-}$*/rx2*$^{-/-}$ double mutants (E, L). Misfating of neurons in *rx1*$^{-/-}$*/rx2*$^{-/-}$ double mutant retinae is evident by mislocated anti-Isl-1 staining in the optic nerve (ON) (B, E, F, I, L, M), reduced proliferation is indicated by reduced anti-PH3 staining (C, E, F, J, L, M). Only cells in the dorsal CMZ show (weak) anti-BrdU staining in *rx1*$^{-/-}$*/rx2*$^{-/-}$ double mutant retinae (D-F, K-M; indicated by dashed lines in D and K). Sections are shown in transmission light in panels G and N, position of the optic nerve (ON) is indicated. Scale bars represent 200 µm (A, H) or 50 µm (G, N).

While reduced anti-PH3 staining at stage 28 suggested either a lack or a delay of the initial, massive proliferation phase in *rx1*$^{-/-}$*/rx2*$^{-/-}$ double mutant

retinae, analysis at stage 32-34 confirmed that it is rather absent (Fig. 2.12, compare panels C, E, F to J, L, M). Compared to wild-type, only the dorsal retina of *rx1*$^{-/-}$/*rx2*$^{-/-}$ double mutants showed (weak) anti-BrdU staining in the CMZ (Fig. 2.12, compare panels D and K). The neuronal differentiation delay observed in stage 28 resulted in misfating of cells in stage 32-34, with many Isl-1-positive cells located at the optic nerve, which was never seen as extensively in wild-type controls (Fig. 2.12, compare panel B to I). Although delayed at stage 28, the ventral retina is eventually formed in *rx1*$^{-/-}$/*rx2*$^{-/-}$ double mutants. However, lamination as well as differentiation seemed to be overall more affected in the ventral part than in the dorsal part of the retina, as indicated by both, DAPI- and anti-Isl-1 staining (Fig. 2.12, compare panels B and E to I and L).

Similar results were obtained when analysing hatchlings subjected to a 21-hour BrdU pulse followed by an immediate chase. Cryosections were analysed by immunohistochemistry using anti-BrdU to identify cells in S-phase, and anti-Parvalbumin (Pvalb) to identify amacrine cells, which are amongst the first retinal neurons to differentiate [Centanin and Wittbrodt, 2014] (Fig. 2.13). DAPI staining revealed strong retinal lamination defects, again to a greater extent in the ventral retina (Fig. 2.13, compare panel D to I). In general, the retinae of *rx1*$^{-/-}$/*rx2*$^{-/-}$ double mutant hatchlings showed less anti-Pvalb staining compared to wild-type, but in addition Pvalb-positive cells were found more frequently at the optic nerve region (Fig. 2.13, compare panels B, D, E to G, I, J). Furthermore, BrdU-positive cells were not only found in the dorsal CMZ, but also in the optic nerve region, which was never observed to the same extent in wild-type controls (Fig. 2.13, compare panels C-E to H-J). In conclusion, the ventral CMZ seemed to be absent in *rx1*$^{-/-}$/*rx2*$^{-/-}$ double mutants (Fig. 2.13 H-J).

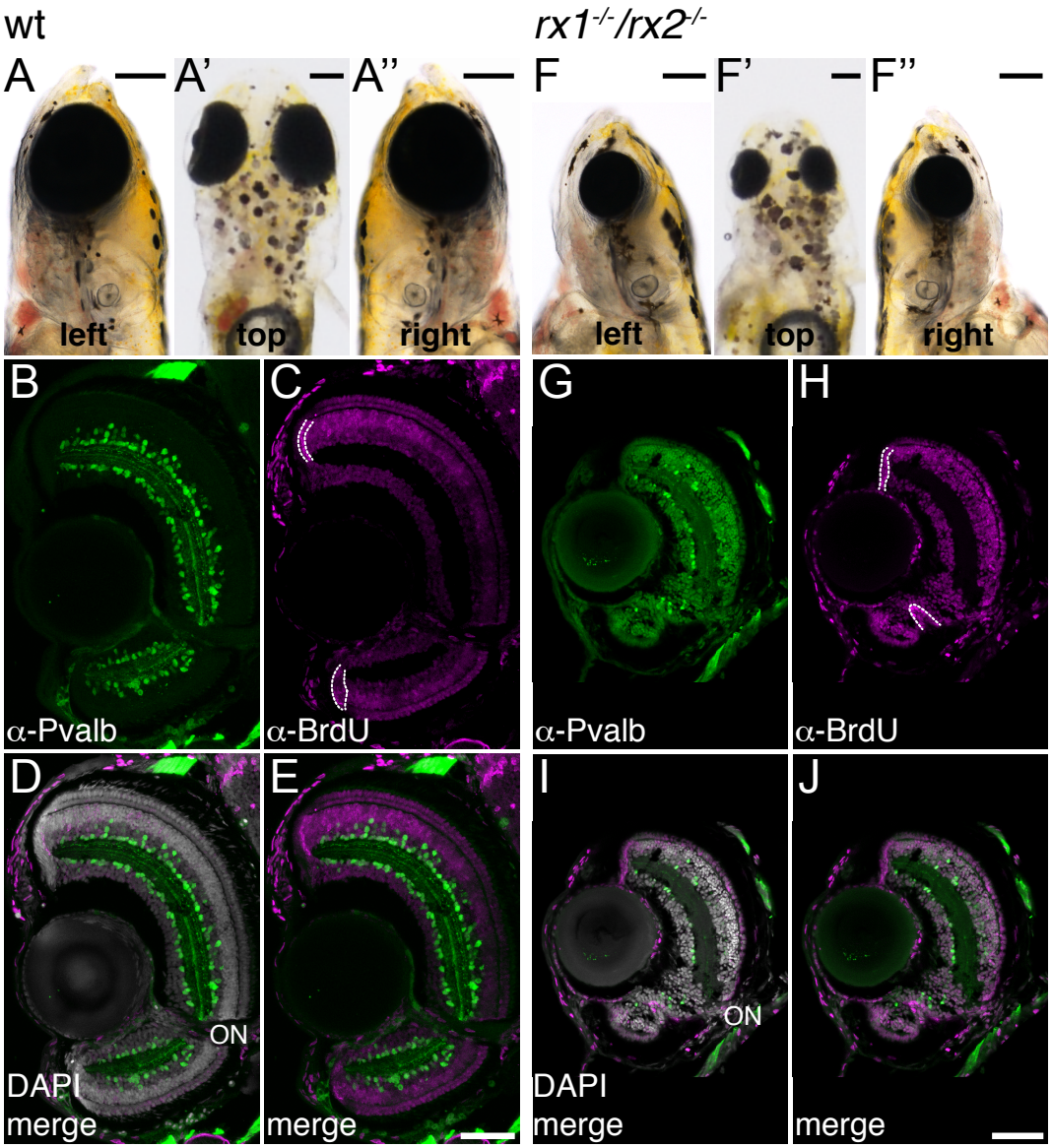

Figure 2.13: Misfating of neurons and retinal lamination defects of *rx1*$^{-/-}$/*rx2*$^{-/-}$ double mutant fish persist to hatching stage. Wild-type (A) and *rx1*$^{-/-}$/*rx2*$^{-/-}$ double mutant (F) hatchlings (left side, top, right side views) were incubated in 2.5 mM BrdU solution for 21 hours, subjected to cryosectioning and analysed by immunohistochemistry. Strong lamination defects in *rx1*$^{-/-}$/*rx2*$^{-/-}$ double mutant retinae most pronounced in the ventral retina are evident by DAPI staining (D, I). Anti-Pvalb staining is weaker and mislocates to the optic nerve (ON) region in *rx1*$^{-/-}$/*rx2*$^{-/-}$ double mutant retinae (B, D, E, G, I, J). Cells in the dorsal CMZ and in the optic nerve (ON) region of *rx1*$^{-/-}$/*rx2*$^{-/-}$ double mutant retinae show anti-BrdU staining (C-E, H-J; indicated by dashed lines in C and H), whereas the ventral CMZ seems to be absent. Position of the optic nerve (ON) is indicated. Scale bars represent 200 µm (A-A″, F-F″) or 50 µm (E, J).

When analysing adult stages it became clear that even eyes which macroscopically appeared to be wild-type sized and shaped, exhibited lamination defects as well, although not as pronounced as eyes with severe microphthalmia (Fig. 2.14). Coinciding with the previous analyses, the ventral retina was more affected than the dorsal retina.

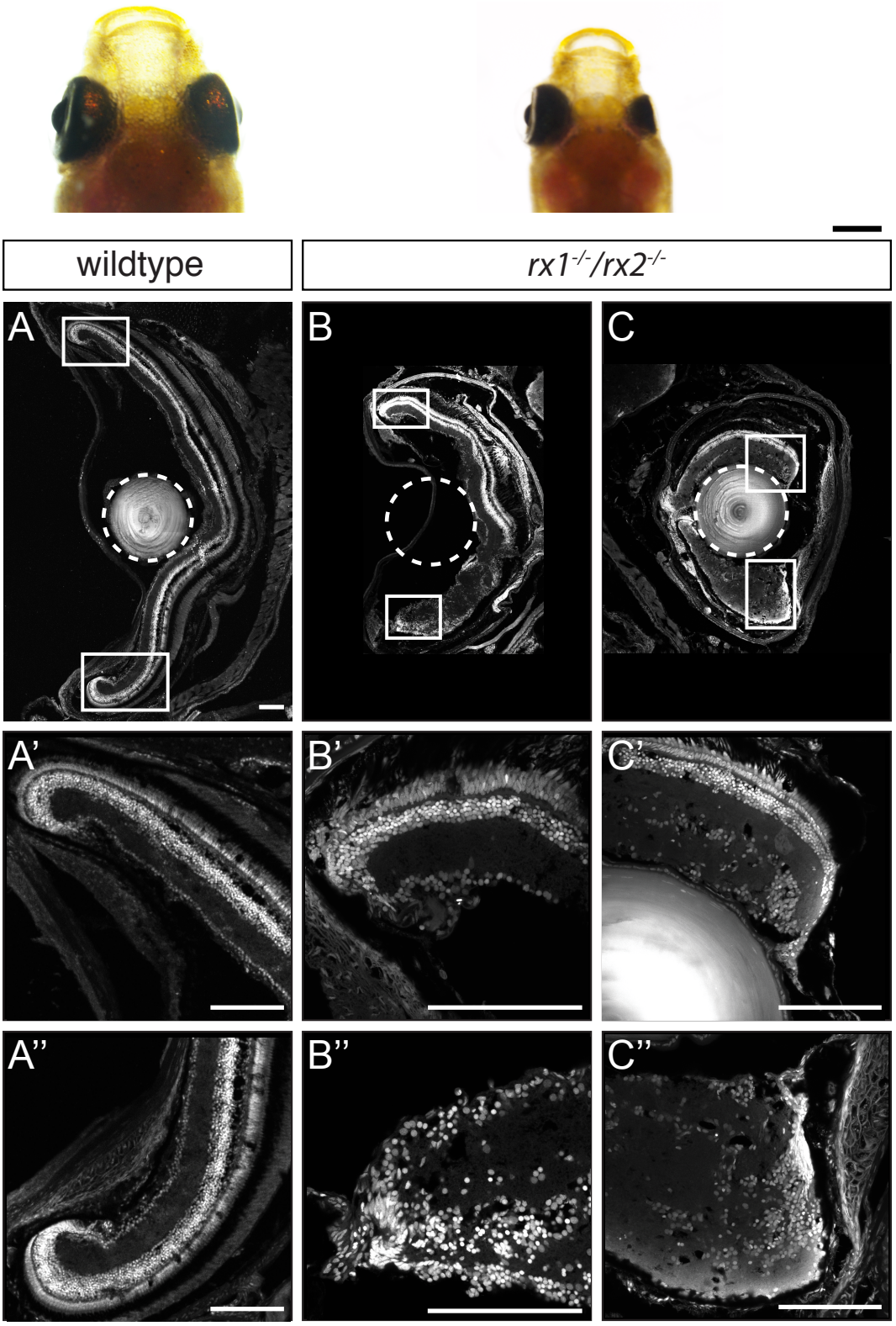

Figure 2.14: *rx1*$^{-/-}$/*rx2*$^{-/-}$ double mutant adult retinae exhibit extensive retinal lamination defects, irrespective of their size. DAPI stainings of wild-type (A-A″) and *rx1*$^{-/-}$/*rx2*$^{-/-}$ double mutant (B-B″, C-C″) adult retinae reveal massive lamination defects. While the retina shown in B-B″ macroscopically appears wild-type sized and shaped, retinal lamination is affected to a higher extent on the ventral compared to the dorsal side. This phenotype is even more pronounced in smaller eyes (C-C″). Note: retinae in B and C from same fish. Magnified regions indicated by boxes in panels A-C, respectively. Wild-type fish was 10 wpf, *rx1*$^{-/-}$/*rx2*$^{-/-}$ double mutant fish was 8 wpf. Dashed circle indicates position of the lens. Scale bars represent 1 mm (adult heads) or 100 µm (A-C″).

Anti-HuC/D staining revealed that the majority of the optic cup is filled with unordered neuronal cells (Fig. 2.15 E′, E″, F′, F″) [Kim et al., 1996a, Akamatsu et al., 2005]. Furthermore, staining for the cone photoreceptor cell marker Zinc finger protein 1 (Zpr-1) at adult stages showed that the small retina in *rx1*$^{-/-}$/*rx2*$^{-/-}$ double mutant fish is only patterned dorsally in a narrow stripe (Fig. 2.15 G′, G″).

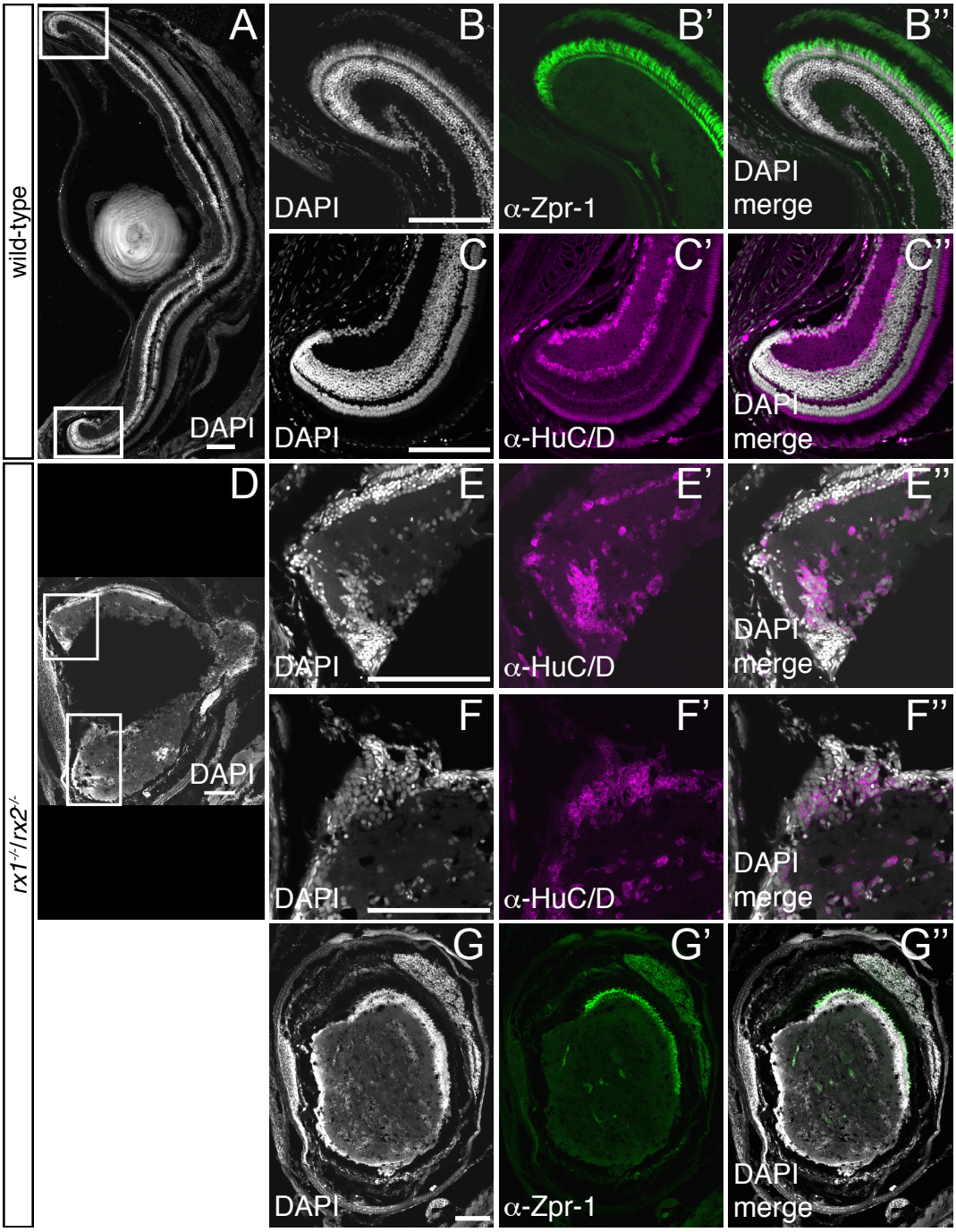

Figure 2.15: *rx1*$^{-/-}$*/rx2*$^{-/-}$ double mutant adult retinae are only patterned dorsally. Overview DAPI stainings of a wild-type (A) and a *rx1*$^{-/-}$*/rx2*$^{-/-}$ double mutant retina (D, G-G″). White boxes indicate magnified regions shown in panels B-B″, C-C″ and E-E″, F-F″, respectively. Retinal lamination defects are visible by DAPI staining (A, B, C, D, E, F, G). Cells of *rx1*$^{-/-}$*/rx2*$^{-/-}$ double mutant small retinae express the neuronal marker HuC/D (E′, E″, F′, F″; wild-type control in panels C′, C″). The cone photoreceptor marker Zpr-1 is expressed only in the dorsal retina of *rx1*$^{-/-}$*/rx2*$^{-/-}$ double mutant fish (G′, G″; wild-type control in panels B′, B″). Scale bars represent 100 µm.

2.3.3 *rx1*$^{-/-}$/*rx2*$^{-/-}$ double mutant retinal lamination defects are variable across the nasal/temporal axis

Notably, the retinal lamination defects observed in *rx1*$^{-/-}$/*rx2*$^{-/-}$ double mutant fish not only varied with respect to the dorso-ventral axis but also appeared in different phenotypic manifestations across the nasal-temporal axis, being more pronounced nasally and most pronounced in central, ventral position (Fig. 2.16).

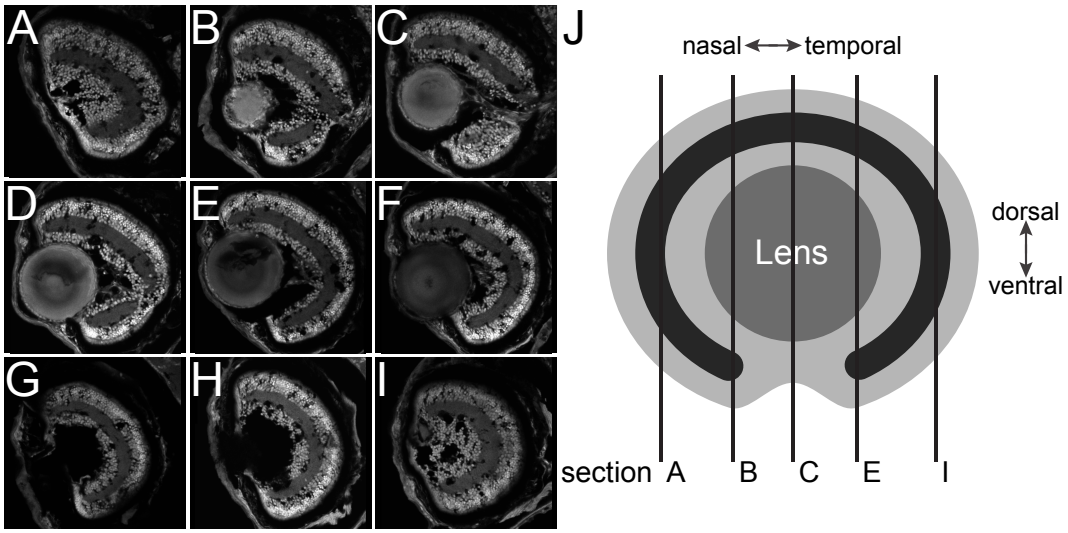

Figure 2.16: *rx1*$^{-/-}$/*rx2*$^{-/-}$ double mutant retinae exhibit variable phenotypic manifestations on the nasal-temporal and dorso-ventral axis. DAPI stainings of consecutive sections (nasal to temporal; A - I) of a *rx1*$^{-/-}$/*rx2*$^{-/-}$ double mutant hatchling retina. Schematic representation of retina (lateral view) with position of sections indicated (J). Note: Phenotype is most pronounced in central, ventral sections.

Taken together, analysis of *rx1*$^{-/-}$/*rx2*$^{-/-}$ double mutant retinae at different stages revealed a non-exclusive stem cell phenotype, representing the accumulated consequences of an early and late loss-of-function.

Phenotypes at embryonic stages prior to establishment of the CMZ (Fig. 2.11) indicate an early function of *rx* genes in retinal development, whereas phenotypes at hatching (Fig. 2.13) and adult stages (Fig. 2.14, Fig. 2.15) point towards a function in retinal stem cell maintenance.

2.4 RNASeq analysis of *rx1*$^{-/-}$/*rx2*$^{-/-}$ double mutant optic vesicles to identify differentially expressed genes

Based on the results from phenotypic analyses in embryos, hatchlings and adult fish, I hypothesise that *rx1* and *rx2* genes confer retinal (stem) cell identity early on in eye development and, as also indicated by the transplantation experiments, later on function in maintaining this identity. Additionally, the clonal analyses showed that *rx1* and *rx2* genes function in specification of NR and RPE stem cells from a pool of retinal stem cells. Following up on these results and to get mechanistic insight into this mode of action, single optic vesicles of wild-type and *rx1*$^{-/-}$/*rx2*$^{-/-}$ double mutant embryos were dissected just after their formation at stage 18 and stage 20 and right optic vesicles were subjected to whole transcriptome sequencing (RNA sequencing, RNASeq) (in collaboration with NS, DI, JM). Importantly, the chosen stages are prior to the onset of the macroscopically distinguishable phenotype but correspond to the onset of *rx1* and *rx2* expression (*rx2*: [Reinhardt, 2014]; *rx1*: data unpublished).

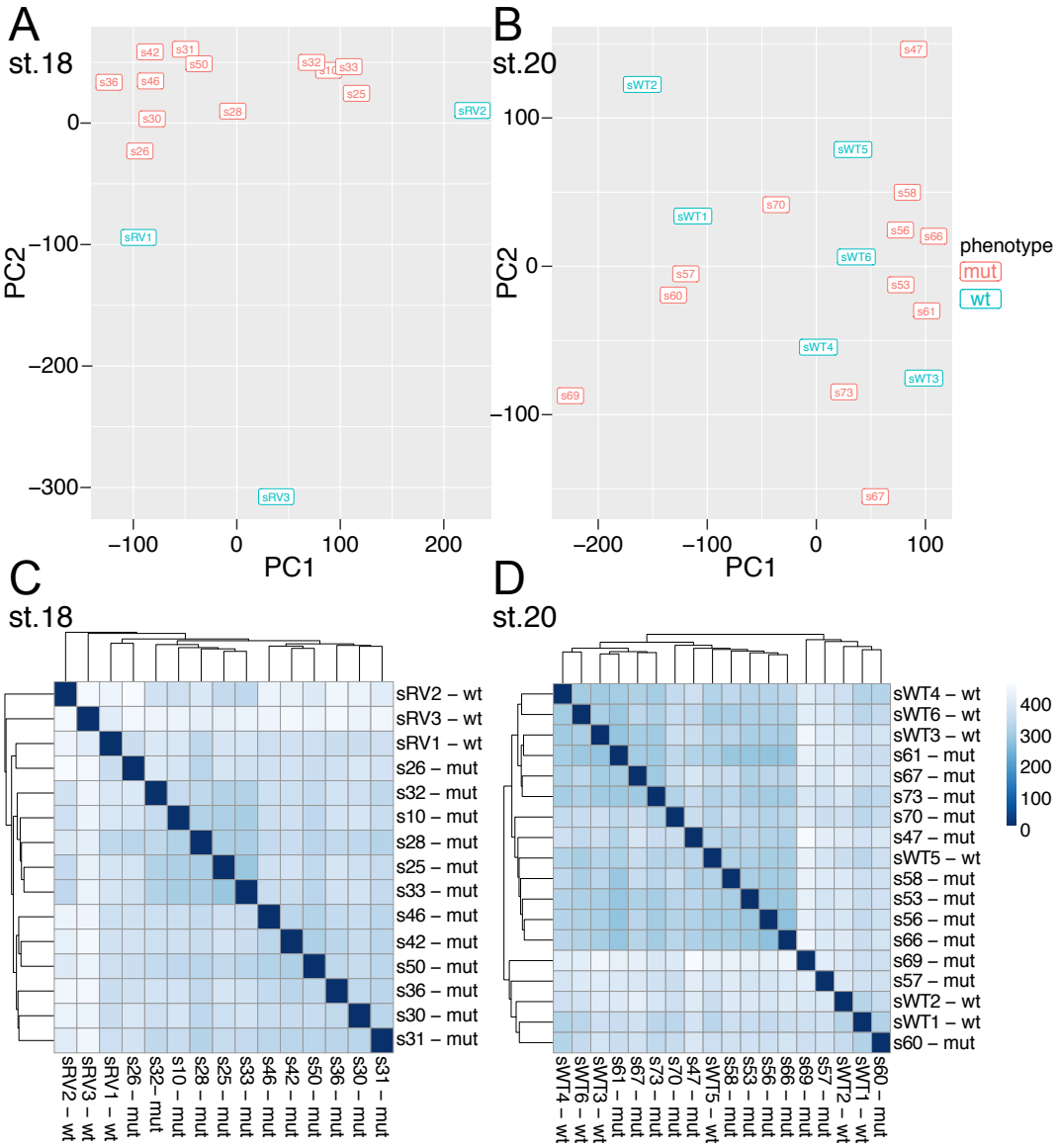

Figure 2.17: RNASeq dataset plots. Principal component analysis (PCA) of RNASeq datasets obtained from single optic vesicles of stage 18 (A) and 20 (B) embryos from wild-type (turquoise) and *rx1*$^{-/-}$/*rx2*$^{-/-}$ double mutant samples (red). Heatmaps of RNASeq datasets obtained from stage 18 (C) and 20 (D). Both plots show a good separation between wild-type and mutant samples for stage 18, but not stage 20, potentially due to more indirect effects of the mutation at stage 18. wt (wild-type); mut (mutant).

Preliminary analysis of the data indicated a good separation between wild-type and mutant samples for stage 18, but not stage 20, potentially due to more direct effects of the mutation at stage 18 (Fig. 2.17).

Furthermore, a high variability between mutant samples was detected (Fig. 2.17). The analysis of the datasets is still ongoing with the aim to find differentially expressed genes compared to respective wild-type stages ultimately revealing the consequences of *rx1* and *rx2* loss-of-function in retinal progenitor cells on the transcriptome level.

2.5 Establishing a labelled potential null allele of *rx1* and *rx2* using a fluorescent reporter featuring the ocean pout transcriptional terminator (OPT) cassette

In order to investigate further possibilities for generating null alleles other than relying on out-of-frame indel mutations, potentially still leading to hypomorphic versions of genes of interest, I investigated if a potential transcriptional terminator cassette could be used for targeted inhibition of gene expression (in collaboration with TT). In addition, this cassette featured a fluorescent protein (FP) sequence to facilitate screening for respective founders. The ocean pout transcriptional terminator (OPT) is a regulatory element consisting of a strong polyadenylation signal, transcriptional terminator and putative border element [Sivasubbu et al., 2006, Clark et al., 2011]. It was isolated from the arctic ocean pout fish, where it regulates the expression of an anti-freeze gene, ensuring survival in subzero environments. Taking advantage of its capacity to efficiently stop transcription (with $> 97\%$ knock-down as described in [Clark et al., 2011]), we designed knock-in cassettes for both, *rx1* and *rx2*, containing a nuclear-localised fluorophore fused to the OPT to be inserted immediately after the respective ATG (Fig. 2.18 A, A′, B, B′). Embryos injected at one-cell stage with both, the *h2b-egfp-opt-rx1* and the *h2b-rfp-opt-rx2* cassettes showed fluorophore expression exclusively in the *rx1* and *rx2* expression domains (Fig. 2.18 C-E). Once founders are identified, expression analysis will be performed on homozygous OPT individuals, investigating the amount of (residual) expression from the respective locus. Ideally, labelled *rx1* and *rx2* RNA null mutants will be obtained. The generation of double-fluorescent *rx1 OPT*, *rx2 OPT* transgenic lines and potentially resulting (enhanced) microphthalmia phenotypes will give further insight into *rx1* and *rx2* loss-of-function with cellular resolution.

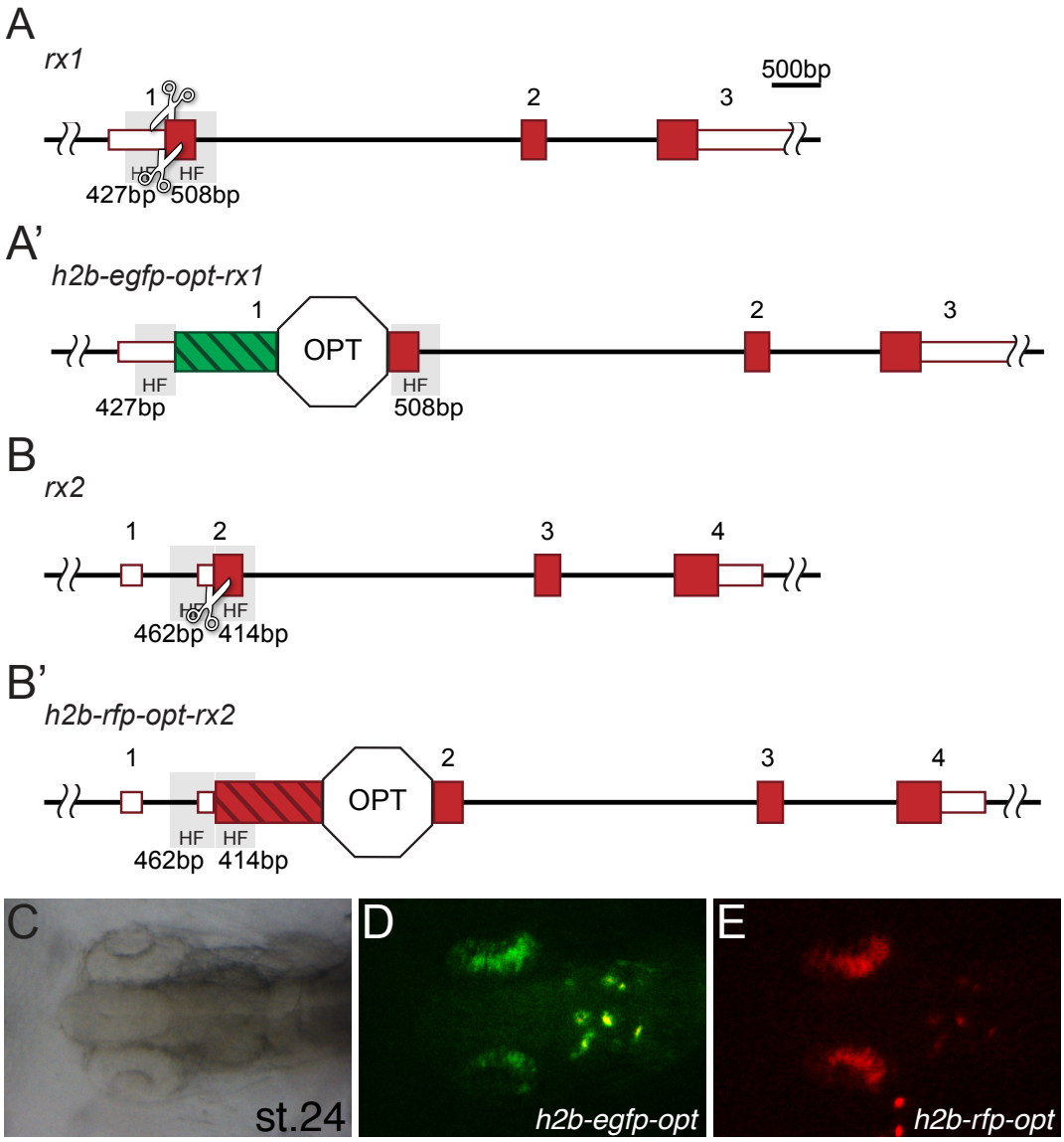

Figure 2.18: Design of the *rx opt* alleles. Schematic to-scale representation of the wild-type *rx1* (A) and *rx2* loci (B). *rx1* and *rx2* loci after successful HDR-mediated integration of the OPT N-terminally fused to a nuclear-localised fluorophore (H2B-eGFP in case of *rx1*; H2B-RFP in case of *rx2*) are shown in A′ and B′. Untranslated region (UTR) (white boxes with red outlines), coding exons (red boxes), homology flanks (HF, grey), sgRNA target site (white scissors; located immediately after the respective ATG), H2B-eGFP (green striped box), OPT (octagon) and H2B-RFP (red striped box) are indicated. Embryo injected with (D) *h2b-egfp-opt-rx1* and (E) *h2b-rfp-opt-rx2* constructs displays mosaic fluorophore expression in the *rx1* and *rx2* expression domains at embryonic stage 24 (contrast increased). Note unspecific autofluorescence of body pigmentation apparent in yellow (in D), as well as bright red spots on dorsal trunk (in E).

2.6 Establishing a conditional allele to address the late function of *rx2*

Since the phenotype observed in the *rx1*$^{-/-}$/*rx2*$^{-/-}$ double mutants represents the accumulated consequences of *rx1* and *rx2* loss-of-function early in retinal development, as well as in RSCs, a conditional allele was established for *rx2* [Stemmer, 2015] to be able to differentiate between its early and late function. Specifically, this allele was generated using HDR and the CRISPR/Cas9 system. The utilised donor plasmid features the complete *rx2* locus fused at the N-terminus via a flexible linker to *egfp* and flanked by LoxP sites followed by an out-of-frame *h2b-rfp* cassette to label the loss of *rx2* function upon recombination via Cre-recombinase (Fig. 2.19 A, B). I confirmed the nature and functionality of the generated allele on the level of the genome, both by PCR and Southern Blot analysis (Fig. 2.19 C, D), transcript (Fig. 2.19 E) and protein (Western Blot data not shown) and could show that it is a single-copy integration replacing the wild-type *rx2* locus.

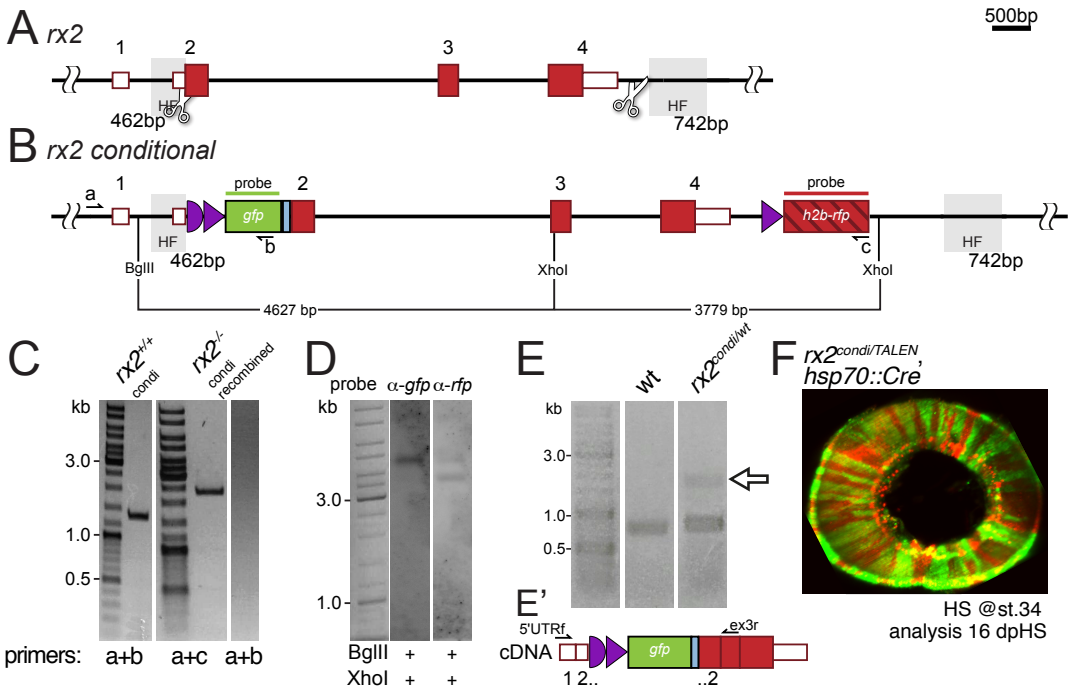

Figure 2.19: Design and characterisation of the *rx2 conditional* allele. Schematic to-scale representation of the wild-type *rx2* locus (A) and the *rx2 conditional* locus (B). The entire *rx2* gene is replaced by a floxable version, where the *rx2* gene is fused to an *egfp* via a flexible linker. The entire sequence is flanked by LoxP sites. The *rfp* cassette functions as a loss-of-function reporter, getting under the control of the *rx2* promoter after recombination [Stemmer, 2015]. LoxP (purple triangle) and FRT (purple semicircle) sites are not to scale. Untranslated region (UTR) (white boxes with red outlines), coding exons (red boxes), homology flanks (HF, grey), sgRNA target site (white scissors), flexible linker (FL, blue box), primer binding sites used for PCR genotyping (a, b, c), probe binding sites as well as restriction sites used for Southern Blot analysis are indicated. (C) Individual embryo PCR genotyping shows bands indicative for the homozygous *rx2 conditional* allele before (*rx2*$^{+/+}$ *conditional (condi)*; 1337 bp) and after recombination (*rx2*$^{-/-}$ *condi recombined*; 2345 bp). (D) Southern Blot analysis of pools of embryos reveals a single band for a digestion scheme cutting outside the 5' donor cassette and in exon 3/after the 3'UTR indicating precise single-copy donor integration. Blot was hybridised first to a anti-*gfp* probe, signal was detected and blot was stripped and re-probed using a anti-*rfp* probe. (E) RT-PCR analysis on mRNA isolated from a pool of heterozygous stage 34 embryos indicates the transcription of a *egfp-rx2* fusion mRNA (arrow; schematic representation in E′) in comparison to the shorter wild-type *rx2* mRNA. (F) The *rx2 conditional* allele can be recombined *in vivo*. Embryos were injected at one-cell stage with *hsp70::Cre* plasmid, heatshocked (HS) at stage 34 and fixed 16 days post heatshock (dpHS). Anti-eGFP staining reveals non-recombined cells expressing the default *rx2 conditional* allele and anti-RFP staining reveals the knock-out reporter after successful recombination.

Furthermore, I could show that this single-copy conditional allele codes for a functional Rx2 tagged with eGFP that is lost and switched to nuclear red (H2B-RFP) in the presence of Cre-recombinase (Fig. 2.19 F, in collaboration with MS). Moreover, the conditional loss-of-function allele shows severe microphthalmia phenotypes in an *rx1*$^{-/-}$ background, comparable to the *rx1*$^{-/-}$/*rx2*$^{-/-}$ double mutants (Fig. 2.20).

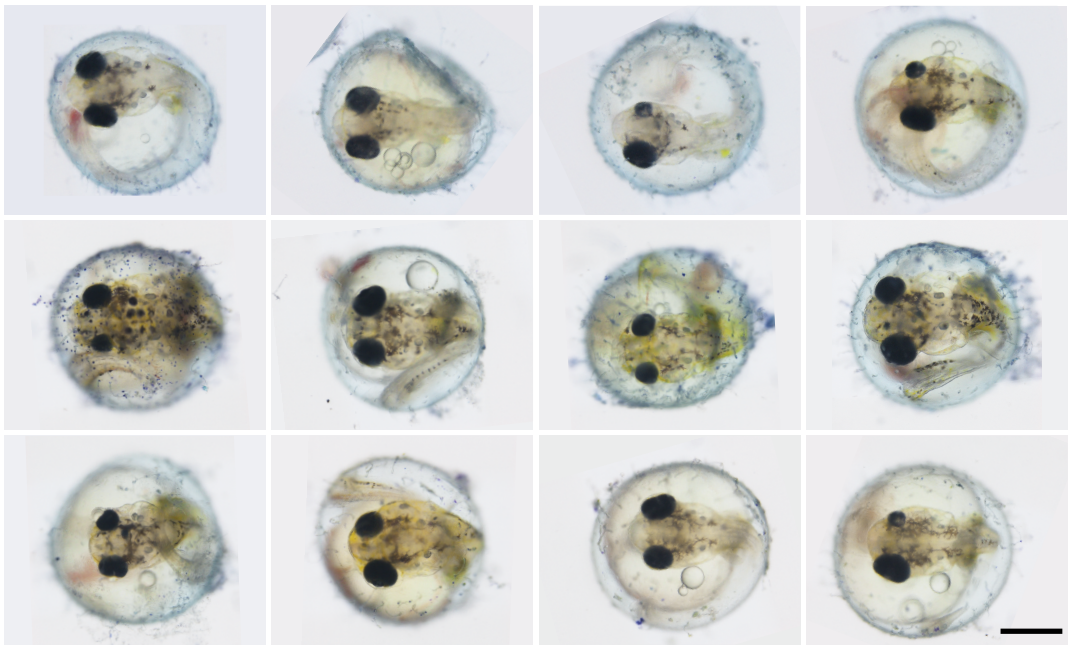

Figure 2.20: The *rx2* conditional loss-of-function allele shows severe microphthalmia phenotypes in an *rx1*$^{-/-}$ background. Embryos homozygous for the conditional loss-of-function allele (*rx2*$^{-/-}$ *condi recombined*) in an *rx1*$^{-/-}$ background were assessed for phenotypes at developmental stage 32-34. Phenotypes are comparable to those of the *rx1*$^{-/-}$/*rx2*$^{-/-}$ double mutants, however embryos tend to appear more affected. Scale bar represents 500 µm.

3
Discussion

In this thesis I identified functional aspects of medaka *rx1* and *rx2*, two genes coding for retina-specific homeobox-containing transcription factors. I carried out cellular expression analysis, clonal single mutant and systemic double mutant analyses, and established genetic tools for future detailed analysis of early and late conditional function of *rx* genes.
Based on the transplantation data, Rx1 and Rx2 function in the specification of NR and RPE stem cells from a pool of retinal stem cells.
Furthermore, the phenotypic analysis of the microphthalmic *rx1*$^{-/-}$/*rx2*$^{-/-}$ double mutants at different developmental stages point towards a function of *rx1* and *rx2* during the specification of RSCs from a pool of neural stem cells. The early morphogenetic defect in retinogenesis coincides with reduced retinal proliferation and is followed by misfating of neurons and retinal lamination defects, ultimately resulting in retinal growth defects. Mechanistic insight into these processes will be achieved by analysis of the RNASeq dataset generated in the course of this thesis from optic vesicles of developmental stages 18 and 20, which correlate to the onset of *rx1* and *rx2* expression.
Moreover, the *rx2 conditional* allele characterised here will allow to differentiate between early and late function of *rx2*.

3.1 Rx1 and Rx2 exhibit different, complementary expression patterns and functions

First I identified the complementary yet different expression patterns of *rx1* and *rx2* by endogenous precise tagging with a single-copy fluorophore (Fig. 2.2, Fig. 2.3, Fig. 2.5 Fig. 2.6). While Rx1 is expressed in cone but not rod photoreceptor cells, Rx2 is expressed in both of these cell types, albeit stronger in cones. Interestingly, in the zebrafish ONL, *rx1* and *rx2* are expressed exclu-

sively in cones, but not in rods [Chuang et al., 1999].
Both proteins are expressed in Müller glia cells, Rx1 however, is also expressed in a second cell population in the INL, as reported by strong eGFP signal. This cell population could indeed reflect two different cell types, i.e. horizontal cells (due to partially overlapping anti-Prox1 staining, Fig. 2.4) or bipolar cells (due to localisation). Furthermore, simultaneous staining for Rx2 using an anti-Rx2 antibody revealed that strong eGFP-positive cells are either Rx2-negative or weakly stained for Rx2, indicating a cell population expressing Rx1 but not Rx2. Both genes are expressed in the CMZ, (nuclear) eGFP signal in the *eGFP-FL-rx1* transgenic line however seemed to be more confined compared to both the *eGFP-FL-rx2* transgenic line and to the anti-Rx2 staining, indicating a cell population within the RSC domain that is positive for Rx2, but negative for Rx1.
Moreover, expression in the CMZ suggests that Rx1 could function as an RSC marker. Future lineage tracing approaches utilising Cre recombinase expressed in the *rx1* expression domain will decipher whether Rx1-positive cells in the CMZ are *bona fide* stem cells.
Furthermore, in both transgenic lines, the eGFP signal appeared not always entirely nuclear, specifically in the CMZ the eGFP signal seemed to fade out in a gradient from the periphery towards the centre of the retina. This could potentially reflect posttranslational cleavage of the eGFP and the attached Rx protein. Both fusions have been shown to be precise on the genomic as well as on the transcriptomic level and furthermore in the homozygous case the fusion transcript is the only existing transcript transcribed from the respective locus [Gutierrez-Triana et al., 2018]. On the protein-level, however, it is conceivable that a fraction of fusion proteins is cleaved posttranslationally. Western Blot analysis will be carried out in the future to address this point.
Moreover, analysis of the *eGFP-FL-rx1*, *mCherry-FL-rx2* double transgenic line will reveal the complementary yet different expression pattern of these two paralogous genes in greater detail. Especially *in vivo* imaging will be of major importance to identify *rx1* and *rx2* expression dynamics to see whether there are cells which turn on expression of one paralogue after just having turned off expression of the other. Regarding the CMZ, this would point towards a delicate balance and interplay of these two transcription factors ensuring proper cell fate of retinal stem cells. Strikingly, when qualitatively comparing expression levels of both eGFP-fusion lines, eGFP expression coming from the *eGFP-FL-rx2* line always appeared considerably stronger, in living embryos as well as on cryosections after staining for eGFP. This suggests that endogenous

expression levels of *rx2* are higher than those of *rx1*, a scenario that could be addressed using qPCR analysis. However, an elegant genetic approach will be constituted by analysis of the tagged allele in a background mutant for the other paralogue, as for instance *eGFP-FL-rx1*$^{+/+}$ in the *rx2*$^{-/-}$ TALEN background. Thus, compensatory effects will be revealed, provided respective changes in *egfp* expression levels and potentially also domains are detectable.
Second, mosaic clonal analyses at blastula stage indicated complementary yet different functional aspects of medaka *rx1* and *rx2*, reminiscent of what was shown for zebrafish *rx1* and *rx2*, whose functions also overlap only partially [Nelson et al., 2009]. However, the precise functions of *rx1* and *rx2* themselves in medaka and zebrafish may indeed differ.
While the loss of *rx2* favoured the formation of RPE in a non-autonomous manner, the loss of *rx1* impacted on expansion of RPE in a cell-autonomous manner. When *rx2*$^{-/-}$ cells were transplanted into a wild-type environment, they preferentially give rise to more and wider RPE ArCoSs and consequently prevent wild-type cells from contributing to RPE in the reciprocal experiment. In contrast, when *rx1*$^{-/-}$ cells were transplanted into a wild-type environment, they formed less and narrower RPE ArCoSs compared to the wild-type control, suggesting a reduced proliferation rate, as well as a lower frequency of symmetric cell division.
These results point towards a function for both, Rx1 and Rx2, in balancing cell fates and numbers between NR and RPE stem cells. Potentially this is further regulated by different expression levels of the two paralogues as already indicated by the expression analysis (Fig. 2.3, Fig. 2.6).

3.2 Simultaneous loss of *rx1* and *rx2* function leads to defects in retinal morphogenesis and architecture

The lack of a macroscopic phenotype in the homozygous single mutants suggests a potential functional redundancy of *rx1* and *rx2*. Only when both, *rx1* and *rx2* function was homozygously lost (*rx1*$^{-/-}$, *rx2*$^{-/-}$ double mutant), a phenotype was detectable. *rx1*$^{-/-}$/*rx2*$^{-/-}$ double mutant fish exhibited severe microphthalmia phenotypes with extensive retinal lamination defects, most prominent in central, ventral position of the retina.

The CMZ has been subdivided according to gene expression [Harris and Perron, 1998, Raymond et al., 2006]. The spatial order of gene expression within the CMZ from peripheral to central reflects the temporal sequence of retinogenesis, as genes expressed in the periphery of the CMZ are expressed early on during retinogenesis [Perron et al., 1998, Harris and Perron, 1998, Ohnuma et al., 2002, Wan et al., 2016]. Furthermore, *rx* genes have been implicated in proliferation and retinal specification [Mathers et al., 1997, Harris and Perron, 1998, Andreazzoli et al., 1999, Chuang and Raymond, 2001, Andreazzoli et al., 2003, Casarosa et al., 2003, Nelson et al., 2009]. Consistent with this, the loss of *rx1* and *rx2*, two genes expressed at the very periphery of the CMZ, also had severe effects early on in retinogenesis.

Analyses of *rx1*$^{-/-}$, *rx2*$^{-/-}$ double mutant embryonic stages prior to formation of the CMZ revealed morphogenetic defects, indicating the presence of an optic flow in medaka, similar to what has been described for zebrafish [Heermann et al., 2015]. Here, formation of the optic fissure by epithelial flow in the ventral optic cup is key for development of the ventral NR. Consistent with this, analyses of *rx1*$^{-/-}$, *rx2*$^{-/-}$ double mutants at later embryonic stages, as well as at hatching and adult stages revealed extensive differentiation and lamination defects in the ventral NR. Furthermore, also the observed optic nerve defects are most likely resulting from reduced tissue flow during optic cup morphogenesis leading to a defective optic stalk [Eckert et al., 2017]. Also the phenotypic variability in the *rx1*$^{-/-}$/*rx2*$^{-/-}$ double mutant retinae across the dorso-ventral and nasal-temporal axes with the most affected part being the central, ventral position, can be explained by the nature of the optic flow, being strongest at exactly this position [Heermann et al., 2015].

DAPI stainings reveal the whole history of a retina, since cells in the medaka retina maintain their relative position while the retina grows [Centanin et al., 2011]. Thus, analyses of adult *rx1*$^{-/-}$, *rx2*$^{-/-}$ double mutant retinae led to the conclusion that not only early retinal progenitors are affected by the simultaneous loss of both *rx* paralogues, but that also maintenance of post-embryonic retinal growth mediated by the CMZ is affected. Furthermore, the ventral CMZ seemed to be absent in *rx1*$^{-/-}$, *rx2*$^{-/-}$ double mutant retinae. This is in line with studies suggesting that RSCs originate from optic flow [El Yakoubi et al., 2012, Heermann et al., 2015], a process where *rx2*-expressing retinal progenitor cells are involved in zebrafish [Heermann et al., 2015, Eckert et al., 2017].

Moreover, microphthalmia or anophthalmia phenotypes due to mutations in *rx* genes have been described for Xenopus [Fish et al., 2014], fish [Winkler et al.,

2000,Loosli et al., 2003,Kennedy et al., 2004,Nelson et al., 2009], mice [Mathers et al., 1997,Tucker et al., 2001,Voronina et al., 2005,Muranishi et al., 2011,Muranishi et al., 2012,Rodgers, 2017]and humans [Voronina et al., 2004,Lequeux et al., 2008,London et al., 2009,Gonzalez-Rodriguez et al., 2010,Abouzeid et al., 2012,Chassaing et al., 2014]. Strikingly, *rx1* and *rx2* expression is downregulated upon loss of *rx3* in zebrafish [Loosli et al., 2003].

In an embryonic conditional *rax* mouse mutant, retinal progenitors are depleted as indicated by decreased BrdU and proliferating cell nuclear antigen (PCNA)-labelling [Rodgers, 2017]. Also in the *rx1*$^{-/-}$, *rx2*$^{-/-}$ double mutants the BrdU-positive domain in the dorsal CMZ appeared to be smaller, whereas the ventral CMZ was absent.

Future detailed analyses of the *rx1*$^{-/-}$, *rx2*$^{-/-}$ double mutants will reveal whether and which differentiated cell types are missing, especially in the ventral retina, like in the conditional *rax* mouse, where late-born retinal cell types are absent in affected regions of the postnatal retina [Rodgers, 2017]. Initial results in adult *rx1*$^{-/-}$, *rx2*$^{-/-}$ double mutants showed absence of cone photoreceptors in the ventral retina, consistent with the proposed role for Rx in photoreceptor cell maturation and survival in zebrafish [Nelson et al., 2008, Nelson et al., 2009], Xenopus [Pan et al., 2006, Wu et al., 2009, Pan et al., 2010] and mouse [Muranishi et al., 2011, Irie et al., 2015, Rodgers, 2017].

Intriguingly in Xenopus, *rax*-deficient tissue normally fated to become retina forms tissue with diencephalic and telencephalic character [Fish et al., 2014]. Accordingly, overexpression of *rx1* and *rx2* in zebrafish leads to ectopic retinal tissue formation in areas normally fated to become forebrain [Chuang and Raymond, 2001].

These transformations of cell fate mediated by *rx* indicate that it prevents brain fate and are in agreement with the hypothesis based on the results of this thesis that medaka *rx1* and *rx2* confer retinal identity early on. Future analysis of *rx1*$^{-/-}$/*rx2*$^{-/-}$ double mutants will reveal whether the unordered, HuC/D-positive neuronal cells [Kim et al., 1996a, Akamatsu et al., 2005] in the ventral retina are brain neurons lacking retinal specification or whether these are indeed retinal ganglion cells [Inoue and Wittbrodt, 2011]. Furthermore, morphometric analysis by X-ray computed tomography [Weinhardt et al., 2018] will identify potential morphological brain defects, which have been described for *rax* loss-of-function in mouse [Mathers et al., 1997].

The fact that the penetrance and variability of the phenotype in *rx1*$^{-/-}$/*rx2*$^{-/-}$ double mutants is quite high also suggests that *rx1* and *rx2* can not only complement each other but that their function is highly balanced by a mechanism

yet to be uncovered. One such mechanism has been identified in the cavefish *Astyanax mexicanus*, where eye size variation is phenotypically masked by Hsp90 [Rohner et al., 2013].
Rescue experiments using mRNA of single *rx* paralogues as well as combinatorial injections will further address subfunctionalisation and compensation aspects. It is conceivable that the phenotype is either completely rescued, or only partially, for instance eye size may be rescued, whereas the retinal lamination defect may persist or vice versa.
Taken together, the phenotypic analysis of the *rx1*$^{-/-}$/*rx2*$^{-/-}$ double mutants at different developmental stages indicates a function of *rx1* and *rx2* in specification of retinal fate.

3.3 RNASeq analysis of *rx1*$^{-/-}$/*rx2*$^{-/-}$ double mutant optic vesicles will help to decipher *rx* downstream transcriptional logic

In order to reveal the transcriptional logic downstream of *rx1* and *rx2* and to get mechanistic insight into their function in stem cell specification, RNASeq analysis of wild-type and *rx1*$^{-/-}$/*rx2*$^{-/-}$ double mutant optic vesicles at stages 18 and 20 was carried out. These stages are prior to the macroscopically visible phenotype and correspond to the onset of *rx1* (unpublished data) and *rx2* [Reinhardt, 2014] expression. First analyses indicated a high variability at both developmental stages, which could be due to the high developmental speed, resulting in slight temporal differences corresponding to "early" and "late" stage 18 and 20. Furthermore, the high variability between mutant samples could point towards a mechanism involving *rx1* and *rx2* that is highly buffered in the wild-type, and disturbed to different amounts in the double mutant. If true, this would be reflected in the obtained data, meaning that for validation, not only the top 10 transcripts differentially expressed in wild-type and mutant optic vesicles should be considered, but also transcripts that are highly variable within the mutant samples. Candidates will be validated and analysed by whole mount *in situ* hybridisation at different stages, including those where retinal, neuroretinal and RPE identity is specified. Stages after the formation of the CMZ will be included to address the later function of *rx* genes with respect to their contribution in stem cell proliferation and specification. This approach will also allow to differentiate between genes downstream

of Rx that are continuously expressed versus those that are expressed only at later stages in the CMZ. Ultimately, the most promising and interesting candidates (based on expression and proposed function) will be analysed via CRISPR/Cas9-mediated targeted inactivation. Gross morphological analysis of the retinal phenotype will indicate a potential function for the candidates in retinal differentiation and growth.

Furthermore, the RNASeq dataset will be compared to the DNA adenine methyltransferase identification (DamID) dataset, which contains potential direct targets of Rx2 [Gutierrez-Triana et al., 2016]. Based on both, the potential morphogenetic flow defect observed in *rx1*$^{-/-}$*/rx2*$^{-/-}$ double mutants and the role for BMP that has been described in this process in zebrafish [Heermann et al., 2015, Knickmeyer et al., 2018], the DamID dataset has been analysed and contains indeed some BMP-pathway related candidates. Specifically, BMP has been implicated in inhibition of optic flow in zebrafish. When BMP activity is artificially increased, optic flow ceases [Heermann et al., 2015, Knickmeyer et al., 2018]. Therefore it has been proposed that repression of BMP signaling is crucial for this movement of cells during optic cup formation. In medaka, this repression could potentially be mediated by *rx1* and/or *rx2*, either directly or indirectly by e.g. activating BMP antagonists like Noggin [Smith and Harland, 1992, Zimmerman et al., 1996], Chordin [Sasai et al., 1995], Follistatin [Fukui et al., 1993, Iemura et al., 1998], Cerberus [Piccolo et al., 1999], Gremlin [Hsu et al., 1998], or Bambi [Onichtchouk et al., 1999]. Consequently, loss of *rx* would lead to elevated BMP-signalling. If the hypothesis is true, that *rx* genes activate expression of BMP antagonists, I would expect to find these downregulated in the RNASeq dataset. Moreover, it is known from the literature, that during eye development, neural fate is established and maintained by repression of BMPs [Sinn and Wittbrodt, 2013] and BMP4 has been shown to inhibit neural fate in Xenopus [Wilson and Hemmati-Brivanlou, 1995]. Even though *rx1*$^{-/-}$*/rx2*$^{-/-}$ double mutant retinae still express neural markers like HuC/D, they lack proper lamination, suggesting the lack of proper neuroretinal specification signals [Amini et al., 2018]. Conceivably, a transient inhibition of the potentially elevated BMP-signalling could partially rescue the *rx1*$^{-/-}$*/rx2*$^{-/-}$ double mutant phenotype.

The candidates obtained from the RNASeq of *rx1*$^{-/-}$*/rx2*$^{-/-}$ double mutant optic vesicles will also be compared to published transcriptome datasets from Xenopus and zebrafish [Giudetti et al., 2014, Yin et al., 2014]. Importantly, it has to be considered that these published datasets are all based on Rx3 orthologues [Orquera and de Souza, 2017]. Therefore it is likely that the targets will

not match completely.
Moreover, in the studies mentioned above, whole embryos were subjected to transcriptomic analysis. In this thesis in contrast, single optic vesicles of *rx1*$^{-/-}$/*rx2*$^{-/-}$ double mutant and wild-type embryos were dissected, thus allowing to detect also minor changes with respect to gene expression.
Future analysis of the combined RNASeq and DamID datasets will reveal the mode of action of *rx* genes regulating the hypothetical optic flow, as well as stem cell specification of neural towards retinal stem cells, but also of retinal stem cells towards NR and RPE stem cells.

3.4 The *rx2 conditional* allele will be instrumental to differentiate between early and late function of *rx2*

Since the phenotypes observed in the *rx1*$^{-/-}$/*rx2*$^{-/-}$ double mutants represented the accumulated consequences of early and late loss-of-function, I further characterised a *rx2 conditional* allele established by Manuel Stemmer [Stemmer, 2015]. This transgenic line will allow to differentiate between early and late functions of Rx2. Cells expressing wild-type, functional *rx2* are labelled with eGFP, while cells lacking *rx2* function express a nuclear red fluorophore (H2B-RFP) after Cre-mediated recombination. Importantly, the dual colour switch makes this conditional allele rather distinct from the published mouse *rax conditional* alleles and will for instance allow (long term) *in vivo* tracking and investigating the proper integrity of individual stem cells with induced loss of *rx2* versus their neighbouring wild-type cells that serve as internal control [Voronina et al., 2005, Muranishi et al., 2011, Muranishi et al., 2012, Rodgers, 2017]. The *rx2 conditional* allele will be used in combination with different Cre-driver lines expressed in different domains of the CMZ to study the late function of *rx2* in RSCs. Importantly it should be noted here that in this case the readout will be restricted to cells usually expressing *rx2*: RSCs, Müller glia cells and photoreceptor cells. Transplantation experiments analogous to what has been performed in case of the *rx2* TALEN mutants will help to further characterise this allele. Cells homozygous for the recombined *rx2* allele are expected to phenocopy *rx2*$^{-/-}$ TALEN cells, whereas cells homozygous for the wild-type tagged *rx2* allele should represent wild-type cells. Of course it is conceivable that cells homozygous for the recombined *rx2 conditional* allele show an even stronger

phenotype than *rx2*$^{-/-}$ TALEN cells, as the latter are still expressing an altered *rx2* transcript.

Furthermore, this conditional allele will be an instrumental tool to address whether stem cell fate decisions in the RSC domain are dynamic or rather deterministic. A set of experiments combining transplantation and recombination will allow to analyse whether the CMZ reacts to changes in *rx2* levels e.g. by sorting stem cells and positioning them accordingly in the niche (Fig. 3.1). In detail, cells homozygous for the wild-type, tagged conditional *rx2* allele, as well as expressing a source of Cre (e.g. *hsp70::Cre*) will be transplanted at blastula stage to an albino blastula host. This transplantation should result in a comparable outcome as the wild-type to wild-type transplantations carried out in this work. 15 days post fertilisation (dpf), a heat shock will lead to recombination and therefore loss of *rx2*, indicated by a colour switch from green to nuclear red. This time span allows the RSCs to contribute to retinal growth and form (pre-)ArCoSs. In case the RSC domain is dynamic, there should be a fraction of green NR ArCoSs switching to red RPE ArCoSs. This fate-switch from NR to RPE in the CMZ would implicate Rx2 in balancing fate decisions of retinal stem cells not only early on in retinal development [Reinhardt et al., 2015], but also late in the already established RSC domain.

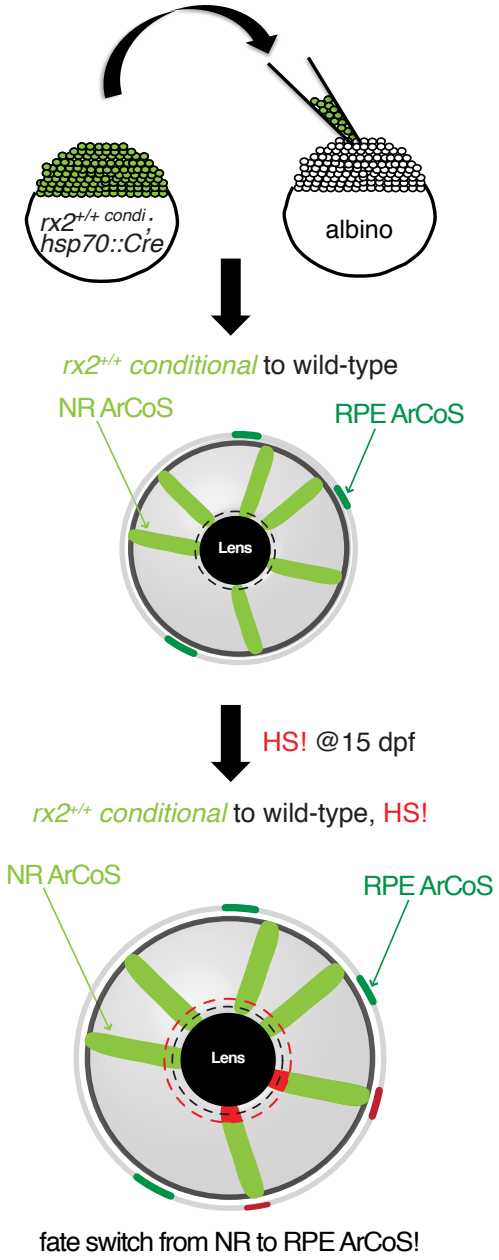

Figure 3.1: Experimental design for studying retinal stem cell niche dynamics using the *rx2 conditional* allele. Cells homozygous for the wild-type, tagged conditional *rx2* allele, as well as expressing a source of Cre (e.g. *hsp70::Cre*) will be transplanted at blastula stage to an albino blastula host. RSCs will contribute to retinal growth and form (pre-)ArCoSs. At 15 dpf, recombination induced by heat shock will lead to loss of *rx2*, indicated by a colour switch from green to nuclear red. In case the RSC domain is dynamic, a fraction of green NR ArCoSs are hypothesised to switch to red RPE ArCoSs.

3.5 Alternative approaches for genetic interference

In the framework of this thesis, I established a CRISPR/Cas9-based protocol for precise single-copy insertions via HDR (in collaboration with AG, TT). *rx1* and *rx2* served as test cases, eventually leading to the establishment of two precisely endogenously tagged transgenic lines. Besides identification of cellular expression of genes of interest, the simplicity and reproducibility of our method will be of relevance for other applications requiring precise insertion/replacement of DNA elements. One such application is the inducible acute knock-down of fluorophore-labelled proteins via degradation technologies targeting GFP, which absolutely requires a precise, seamless single-copy fusion of the fluorophore sequence to the ORF of the gene of interest.
Studying protein function, deGradFP [Caussinus et al., 2012] and degradation of GFP by auxin-dependent nanobodies [Daniel et al., 2018] constitute excellent alternatives to the elaborate generation of conditional alleles, which require laborious cloning strategies. Furthermore, proper analyses of conditional alleles require a loss-of-function genetic background (mutated/silenced second allele), whereas conveniently, for degradation of GFP-tagged proteins, homozygous tagged alleles are sufficient. Further advantages of acute protein knock-down include reversibility and temporal control of the approach [Daniel et al., 2018]. Importantly, proper protein functionality of the GFP-tagged protein of interest has to be ensured.
Besides this, interference on the transcript level may be possible by insertion of transcriptional terminator cassettes into genes of interest, like e.g. the ocean pout terminator cassette described in this thesis. Moreover, the resulting loss of transcript will be visualised by the fluorophore preceding the terminator cassette on the construct. This opens up the exciting possibility to generate fluorescently labelled null alleles of the targeted gene.
In this thesis, I provided the basis to further conditionally interfere with Rx1 and Rx2 function on the genome- and protein-level, as well as systemically on the transcriptional level.

3.6 An evolutionary perspective

It is well conceivable that multiple copies of *rax* correlate with subfunctionalisation of this gene. While *rax* in mouse is expressed early on in eye development and acts in eye field specification [Furukawa et al., 1997, Mathers et al., 1997], this role is taken over by *rx3* in fish. *rx1* and *rx2* however, are expressed later on in specific cell types of the retina, while *rx3* expression is eventually restricted to the INL and the hypothalamus [Deschet et al., 1999, Loosli et al., 2001]. *rax* expression is maintained throughout retinogenesis and eventually is restricted to the brain and the outer and inner nuclear layer of the retina [Mathers et al., 1997]. Strikingly, *rax* is also expressed in the ciliary body of adult mice, the tissue which contains mammalian retinal progenitor-like cells which are proliferatively active and neurogenic in culture [Amato et al., 2004, Tropepe et al., 2000, Kiyama et al., 2012]. Therefore, the combined expression patterns of *rx* in species with multiple copies reflects the *rax* expression pattern. It is tempting to speculate that the subfunctionalisation of *rx* genes correlates with the presence of an active CMZ, placing *rx* as a central player in evolution of the CMZ. In other words, subfunctionalisation of *rx* genes enabled an evolutionary strategy of postembryonic growth in the retina, like in fish and amphibia. On the contrary, in species with only one *rx* gene, postembryonic growth of the retina is absent, like in mammals.

However, only recently, phylogenetic as well as genomic analyses distinguished two groups of vertebrate Rax proteins, the Rax1 and the Rax2 subgroups [Orquera and de Souza, 2017]. *rax-like* genes, such as the human *QRX* gene have been associated with the *rax2* subgroup, along with medaka and zebrafish *rx1* and *rx2*. Interestingly, *QRX* is expressed in the outer and inner nuclear layer, like fish *rx1* and *rx2* [Wang et al., 2004]. Still, rodents and lagomorphs possess only one *rax* gene and thus, it has been proposed that originally, there were two *rax* genes in mammals, but *rax2* was secondarily lost in a common ancestor of rodents and lagomorphs [Orquera and de Souza, 2017].

Among all vertebrates analysed, more than two *rax* genes have been only identified in *Xenopus laevis* and in teleost fish. While in *Xenopus leavis* the two closely related paralogues *rx1a* and *rx2a* belong to the *rax1* subgroup and *rxl* belongs to the *rax2* subgroup, *rx3* of teleosts belongs to the *rax1* subgroup and *rx1* and *rx2* to the *rax2* subgroup [Orquera and de Souza, 2017]. It has been suggested that the three *rx* genes in teleosts originated in the whole-genome duplication at the base of the teleost radiation, subsequently resulting in the

loss of one *rx3* paralogue and retaining of *rx1* and *rx2* [Furutani-Seiki and Wittbrodt, 2004, Orquera and de Souza, 2017].
Rax proteins typically contain three conserved protein motifs: an N-terminal octapeptidemotif, a central homeodomain region that binds to DNA and a C-terminal OAR domain [Orquera and de Souza, 2017]. Interestingly, all Rax2 proteins of tetrapods are shorter and lack the octapeptide motif.
Speculating even further, it is conceivable that a regulatory element, potentially interacting with Rx and preventing differentiation of retinal progenitors, is present in anamniotes but absent in mammals.
Furthermore, on an evolutionary note, according to the concept of the "nocturnal bottleneck" of mammalian evolution, the early placental mammals were active at night to avoid their enemies the dinosaurs, which were the dominant taxon at the time [Walls, 1942, Gerkema et al., 2013]. The evolution of mammalian activity patterns, aspects of vision such as eye shape and orbit have already been associated with the "nocturnal bottleneck" concept [Heesy and Hall, 2010, Hall et al., 2012, Gerkema et al., 2013].
In view of this, lifelong growth of the retina may be a feature that was lost during the early nocturnal evolution of mammals, when big eyes were essential for survival already at the time of birth.

4
Conclusions

The results of this thesis suggest a role for the two paralogous genes *rx1* and *rx2* in both, establishment and maintenance of the medaka CMZ and therefore in postembryonic growth, scaling and shaping of the retina.
During retinogenesis, *rx1* and *rx2* are necessary for the morphogenetic processes leading to optic cup and eventually also to CMZ formation. Simultaneous loss of *rx1* and *rx2* results in a phenotype reminiscent of optic flow, as a consequence of which the ventral CMZ is not established.
Based on the results presented in this thesis, I hypothesise an early role for *rx1* and *rx2* in specifying retinal identity of neural stem cells during retinogenesis. Later on, they control the bifunctionality of the CMZ by specifying stem cells for the NR and RPE, respectively. Furthermore, they have a function in proliferation and cell fate specification and thus proper lamination of the retina.
Only recently NR stem cells of the medaka CMZ have been shown based on a computational agent based model to actively control postembryonic growth of the retina [Tsingos et al., 2018]. Based on the results of this thesis, this is most likely regulated by *rx* genes.

5

Materials & Methods

5.1 Materials

5.1.1 Transgenic fish lines

Medaka stocks and transgenic lines used in this thesis are summarised in Table 5.1.

Table 5.1: Medaka stocks and transgenic lines used in this work. "Source" indicates whether the transgenic fish line was generated during the course of this work.

Medaka fish line used	Internal stock number	Source
wild-type Cab F61-F68	5266, 5692, 6097, 6480, 6857, 7239, 7524, 7796	lab stock
rx1 TALEN mutant	6486, 6772, 6922	lab stock
rx2 TALEN mutant	5781, 5869, 6114, 6326, 6856	lab stock
wimbledon	5713, 6249, 6352	lab stock
rx1$^{-/-}$/*rx2*$^{-/-}$ double mutant	6423, 6431, 6682, 7181, 7182, 7422, 7423, 7438, 7461, 7497, 7820, 7864	this work
eGFP-FL-rx2	7280, 7428, 7583, 7755, 8083	this work, Gutierrez-Triana et al., 2018
eGFP-FL-rx1	7513, 7650, 7767, 8032	this work, Gutierrez-Triana et al., 2018
mCherry-FL-rx2	8066, 8220	this work
H2B-mRFP-OPT-rx2	7717	this work
H2B-EGFPwCR13-OPT-rx1	7718	this work

Medaka fish line used	Internal stock number	Source
rx2 conditional	6443, 6562, 6588, 6619, 6635, 6663, 6732, 6733, 6749, 6751, 6752, 6773, 6796, 6797, 6821, 6822, 6846, 6956, 7012, 7013, 7022, 7087, 7088, 7089, 7509, 7510, 7679, 7689, 7742, 7836, 8079, 8087, 8101, 8102, 8116, 8170, 8174, 8240, 8276, 8277	lab stock

All transgenic fish lines were generated by injection into one-cell stage medaka embryos.
rx1 and *rx2* TALEN mutant lines were generated by Robert Reinhardt [Reinhardt, 2014].
All other transgenic fish lines were generated using the CRISPR/Cas9 system. Specifically, the transgenic lines carrying the ocean pout terminator cassette, as well as the *rx2 conditional* cassette [Stemmer, 2015] were generated via the *in vivo* linearisation approach described by [Stemmer et al., 2015]. The tagged lines were generated using the modified PCR-product based approach described by [Gutierrez-Triana et al., 2018].

5.1.2 Plasmids

Plasmids used to generate new transgenic fish lines are listed in Table 5.2.
The ocean pout terminator (OPT) sequence was subcloned from pDB770 (GBT-RP2), which was a gift from Darius Balciunas (Temple University, Philadelphia, USA) [Clark et al., 2011].

Table 5.2: Plasmids used to generate transgenic fish lines in this work. "Number" indicates internal lab plasmid stock number, "Source" indicates whether the plasmid was generated during the course of this work.

Number	Alias	Source
3922	eGFP-FL-rx2	lab stock/ Manuel Stemmer
4367	*rx2* conditional	lab stock/ Manuel Stemmer
4974	eGFP-FL-rx1	this work

Number	Alias	Source
5152	mCherry-FL-rx2	this work
5166	H2B-EGFPwCR13-OPT-rx1	this work
M820	H2B-mRFP-OPT-rx2	lab stock/ Thomas Thumberger

Plasmids used to generate *in situ* probes are listed in Table 5.3.

Table 5.3: Plasmids used to generate *in situ* probes in this work. "Number" indicates internal lab plasmid stock number, "Source" indicates whether the plasmid was generated during the course of this work.

Number	Probe against	Source
467	*rx2*	lab stock
1080	*rx1*	lab stock

5.1.3 sgRNAs

sgRNAs used to generate new transgenic fish lines are listed in Table 5.4.

Table 5.4: sgRNAs used to generate new transgenic fish lines in this work. "Number" indicates internal lab sgRNA number, corresponding lab plasmid stock numbers of constructs used with the respective sgRNA are listed in column "Donor".

Number	Target	Target sequence	Donor
13	target site for *in vivo* linearisation	GGCGAGGGCGATGCCACCTA[CGG]	#4367, #5166, M#820
40	first coding exon of *rx2*	GCATTTGTCAATGGATACCC[TGG]	#3922, #4367, #5152, M#820
108	3' UTR of *rx2*	AAGTATATCTCTAAATTGCA[GGG]	#4367
214	first coding exon of *rx1*	AAATGCATGAGAGCGTCT[GGG]	#4974
215	first coding exon of *rx1*	CTCTCATGCATTTATCAC[TGG]	#4974, #5166

5.1.4 Primers

Oligonucleotides used in this work are listed in Table 5.5. All oligonucleotides named with "JW..." were ordered from Eurofins Genomics. Oligonucleotides with a 5' modification and oligo-$dT_{30}VN$ were ordered from Sigma-Aldrich, IS-PCR oligos were ordered from Biomers and Template Switching Oligos (TSOs) were ordered from Exiqon. For further information on the latter three, refer to [Picelli et al., 2014].

Table 5.5: Oligonucleotides used in this work. "Name" indicates internal lab primer name.

Name	Alias	Sequence 5'-3'
JW0942	*rx2* TALEN genotyping fwd	AACAGTGAGTAGCGGGTCGT
JW0943	*rx2* TALEN genotyping rev	TCTGAGGGATGGAATTCTGG
JW1381	*rx1* 3' UTR rev	CAAGCAGGATTCATTTGATGT
JW1408	GFP rev	AAACGCTCGACCAGGATGGGCA
JW1458	GFP probe Southern Blot fwd	GTGAGCAAGGGCGAGGAGCT
JW1550	*rx1* TALEN genotyping fwd	TCTCGTCCTCCAAACAGACA
JW1549	*rx1* TALEN genotyping rev	ATTCGTCCGTGTGGACCTGT
JW1745	GFP probe Southern Blot rev	TTACTTGTACAGCTCGTCCATG
JW1955	pGGDest fwd	ATTACCGCCTTTGAGTGAGC
JW2051	*rx2* tagging genotyping fwd	TGCATGTTCTGGTTGCAACG
JW2052	*rx2* tagging genotyping rev	AGGGACCATACCTGACCCTC
JW2175	*rx1* tagging genotyping fwd	CTTTGCTGTTTTGAGAATTGCACC
JW2176	*rx1* tagging genotyping rev	GAGACCGAACGATGACAATAACAC
JW2428	*rx2* exon 3 rev	GGTACGGTTTCTTCTGTGCTTTTT
JW2891	RFP rev	AGCTTCAGCCTCATCTTGATCTCG
JW3550	*rx2* exon 3 fwd	GCTGACGGCTCTCCTAAGTC
JW3553	*rx2* exon 4 rev	GAGCTCATGAACCCCGGAAT
JW3566	RFP rev and RFP probe Southern Blot rev	GCCGGTACCTTAGGCGCCGG TGGAGTGGCGGCC
JW3840	RFP probe Southern Blot fwd	TAATACGACTCACTATAGGGAGAGC CACCATGGCCTCCTCCGAG

Name	Alias	Sequence 5'-3'
JW3863	*rx2* conditional genotyping fwd	TAGGTTAGCAATGGCCTCCCTCTG
JW4124	*rx2* conditional genotyping rev	GAATGATGCTGTGAGCTGTC
JW4342	*rx2* exon 3 rev	CGGCTGTAGACGTCTGGATA
JW4826	*rx2* exon 2 fwd	TAGGATGGTGGACGATAGCGGACA
JW5590	*rx1* exon 1 rev	CTGCTCTTTGGGGCCCCG
JW5601	*rx1* 5' UTR fwd	TCCAGCTGGACTGCTAGTTT
JW5581	pGGDest fwd	GACAGGTATCCGGTAAGCGG
JW6021	rx1 full fwd	GCTCTAGATCCAGCTGGACTGCTA GTTTC
JW6022	rx1 full rev	TCATTACATGGGTTGCCATGTTTTG TC
JW6026	rx1 Q5 mut fwd	CCGGGAGGAGCTGGCCATGAAG
JW6027	rx1 Q5 mut rev	CTGGATAGTGGGACTTCTCGAAGG CG
JW6028	rx2 Q5 mut fwd	GGAGGAACTGGCAACGAAGGTCA ACCTG
JW6029	rx2 Q5 mut rev	CGTCTGGATAGTGGGACTTCTC GAAGG
JW6689	mCherry fwd	GCCGGTCTCAACCTCTGGATCCA TGGTGAGCAAGGGCGAGGA
JW6690	mCherry rev	GCCGGTCTCATAGTGGTACCCTT GTACAGCTCGTCCATGC
JW6718	*rx2* 3' UTR rev	GCGACAGCTATTCCACATAAAAAC
JW8002	OPT fwd	GTACAGCTACCAGAGAAGCTTGA
JW8003	OPT rev	GGTTTTGACATGTTCAGTTAACGG
pCS2 f mod	modified primer fwd	5'moiety-C*C*A*T*T*CAGGCTGCGCAACTG
pCS2 r mod	modified primer rev	5'moiety-C*A*C*A*C*AGGAAACAGCTATGAC
oligos for RNA Sequencing		
	ISPCR oligo	AAGCAGTGGTATCAACGCAGAGT

Name	Alias	Sequence 5'-3'
	Template Switching Oligos (TSO)	AAGCAGTGGTATCAACGCAGAGT ACATrGrG+G
	oligo-dT_{30}VN (100 µM)	AAGCAGTGGTATCAACGCAGAGT ACT30VN

5.1.5 Chemicals and Reagents

Chemicals and reagents used in this work are listed in Table 5.6.

Table 5.6: Chemicals and Reagents used in this work.

Chemical/Reagent	Company
2-mercaptoethanol	Roth
4',6-Diamidino-2-Phenyindole, Dilactate (DAPI)	Sigma-Aldrich
Acetone	Sigma-Aldrich
Acrylamide, 30 % (29:1)	Bio-Rad
Agar	Roth
Agarose	Sigma-Aldrich
Agarose low melting	Roth
Ampicillin	Roth
APS (ammonium persulfate)	Roth
ATP (100 mM)	Thermo Fisher Scientific
Bacto-Trypton	Gibco
BCIP (5-bromo-4-chloro-3-indolyl phosphate)	Roche
Betaine	Sigma-Aldrich
Blocking reagent	Roche
Borax anhydrous	Fluka
Bovine Serum Albumin (BSA)	Sigma-Aldrich
BrdU (5-Bromo-2-deoxyuridine)	Sigma-Aldrich
Bromphenol Blue	Sigma-Aldrich
Calcium chloride ($CaCl_2$)	AppliChem
Calcium chloride dihydrate ($CaCl_2 \cdot 2\,H_2O$)	AppliChem

Chemical/Reagent	**Company**
CDP-Star®	Roche
Chloroform	Sigma-Aldrich
DigUTP (100 mM)	Roche
Dimethyl sulfoxide (DMSO)	Roth
Disodium hydrogen phosphate (Na_2HPO_4)	Sigma-Aldrich
Disodium hydrogen phosphate dihydrate ($Na_2HPO_4 \cdot 2\,H_2O$)	Sigma-Aldrich
dNTPs (10 mM)	Sigma-Aldrich
DTT (dithiothreitol) (100 mM)	Thermo Fisher Scientific
Ethanol 70 % (denatured)	Roth
Ethanol 96 % (denatured)	Roth
Ethanol 99 %	Sigma-Aldrich
Ethidium bromide (EtBr)	Sigma-Aldrich
Ethylenediamine tetraacetic acid (EDTA)	AppliChem
Ficoll Type 400	Amersham Biosciences
Formamide	Sigma-Aldrich
Glacial acetic acid	Merck
Glycerol	Merck
Glycine	Sigma-Aldrich
H_2O, 0.1 µm sterile filtered	Sigma-Aldrich
Heparin	Gibco
HEPES (4-(2-hydroxyethyl)-1-piperazineethanesulfonic acid)	Roth
Hydrochloric acid (HCl)	Merck
Hydrogen peroxide (H_2O_2)	Sigma-Aldrich
Isopropanol (C_3H_7OH)	Sigma-Aldrich
Kanamycin	Roth
Magnesium chloride ($MgCl_2$)	AppliChem
Magnesium sulfate heptahydrate ($MgSO_4 \cdot 7\,H_2O$)	AppliChem
Maleic acid 99 %	Roth
Methanol (MeOH)	Roth
Methylene blue trihydrate	Sigma-Aldrich
Milk Powder	Roth

Chemical/Reagent	Company
Nail polish	essence
NBT (4-nitro blue tetrazolium chloride)	Roche
Normal Goat Serum (NGS)	Gibco
Orange G	Sigma-Aldrich
Paraformaldehyde (PFA)	Sigma-Aldrich
Penicillin-Streptomycin (Pen/Strep)	Sigma-Aldrich
Phenol-Chloroform-Isoamylalcohol (25:24:1) pH 8 (PCI)	Roth
Phosphoric acid (H_3PO_4)	Grüssing
Ponceau S solution 0.2 % in 3 % TCA	Serva
Potassium acetate (CH_3CO_2K)	AppliChem
Potassium chloride (KCl)	AppliChem
Potassium dihydrogen phosphate (KH_2PO_4)	Merck
Potassium hydrogen phosphate (K_2HPO_4)	Merck
Potassium hydroxide (KOH)	Merck
Proteinase K	Roche
rNTPs (ATP, CTP, GTP, UTP, 100 mM each)	Roche
Sheep Serum	Sigma-Aldrich
Sodium chloride (NaCl)	Sigma-Aldrich
Sodium dodecyl sulfate (SDS)	Roth
Sodium hydrogen carbonate ($NaHCO_3$)	Merck
Sodium hydroxide (NaOH)	AppliChem
Sodium tetraborate ($Na_2B_4O_7$)	Sigma-Aldrich
Sucrose	Sigma-Aldrich
Tamoxifen	Sigma-Aldrich
TEMED (tetramethylethylenediamine)	Roth
Tricaine ($C_9H_{11}NO_2 \cdot CH_4SO_3$)	Sigma-Aldrich
Tris base	Roth
Tri-sodium citrate dihydrate ($C_6H_5Na_3O_7 \cdot 2\,H_2O$)	Sigma-Aldrich
Triton X-100	Sigma-Aldrich
TRIzol	Life Technologies
Tryptone bacterial	Roth

Chemical/Reagent	Company
Tween20	Sigma-Aldrich
X-Gal (5-bromo-4-chloro-3-indolyl-$beta$-D-galactopyranoside)	Thermo Fisher Scientific
Xylene Cyanol FF	Serva
Yeast extract	Roth

5.1.6 Molecular materials

Molecular materials used in this work are listed in Table 5.7.

Table 5.7: Molecular materials used in this work.

Material	Company
Agencourt Ampure XP beads	Beckman Coulter
Anti-Digoxigenin-AP Fab fragments	Roche
cOmplete™, Mini, EDTA-free Protease Inhibitor Cocktail	Roche
DNA Loading Dye	homemade
GeneRuler DNA Ladder Mix	Thermo Fisher Scientific
MachT1 cells	Thermo Scientific
PageRuler Prestained Protein Ladder	Thermo Fisher Scientific, 26616
RiboLock RNase Inhibitor	Thermo Fisher Scientific
Recombinant RNase Inhibitor	Clontech
RNA from torula yeast Type VI	Sigma-Aldrich
RNA Loading Dye 2x Rapid	Thermo Fisher Scientific

5.1.7 Enzymes

Enzymes used in this work are listed in Table 5.8.

Table 5.8: Enzymes used in this work.

Enzyme	Company
AccI	NEB
BsaI-HF	NEB
BsrGI-HF	NEB
CutSmart Buffer	NEB
DpnI	NEB
Eco31I FD	Thermo Fisher Scientific
Hatching enzyme	homemade
KAPA HiFi HotStart ReadyMix	KAPA Biosystems
Klenow enzyme	Roche
Phosphatase, alkaline	Roche
Proteinase K (10 mg/ml)	Thermo Fisher Scientific
Proteinase K powder; stock solution 20 mg/ml	Roche
Q5 High-Fidelity DNA Polymerase and 5x Q5 Reaction Buffer	NEB
Restriction enzymes and buffers	Thermo Fisher Scientific/NEB
RNase A, DNase- and protease-free (10 mg/ml)	Thermo Fisher Scientific
T4 DNA Ligase (5 U/µl) and 10x T4 DNA Ligase Buffer	Thermo Fisher Scientific
T4 DNA Ligase (30 U/µl) and 10x T4 DNA Ligase Buffer	Thermo Fisher Scientific
T4 Polynucleotide Kinase (T4 PNK)	Thermo Fisher Scientific
Taq Polymerase EP0621 (5 U/µl) and 10x Taq Buffer	Thermo Fisher Scientific
Turbo DNase (2 U/µl)	Thermo Fisher Scientific

5.1.8 Kits

Kits used in this work are listed in Table 5.9.

Table 5.9: Kits used in this work.

Kit	Company
Agilent DNA 1000 Kit	Agilent Technologies
Agilent high-sensitivity DNA Kit	Agilent Technologies
innuPREP DOUBLEpure Kit	Analytik Jena
mMESSAGE mMACHINE™ Sp6 Transcription Kit	Thermo Fisher Scientific
mMESSAGE mMACHINE™ T3 Transcription Kit	Thermo Fisher Scientific
mMESSAGE mMACHINE™ T7 Transcription Kit	Thermo Fisher Scientific
Nextera XT DNA sample preparation kit, 96 samples	Illumina
PCR DIG Probe Synthesis Kit	Roche
Plasmid Midi Kit	Qiagen
QIAprep® Spin Miniprep Kit	Qiagen
QIAquick® Gel Extraction Kit	Qiagen
QIAquick® Nucleotide Removal Kit	Qiagen
Qubit dsDNA High-Sensitivity Kit	Thermo Fisher Scientific
RevertAid First Strand cDNA Synthesis Kit	Thermo Fisher Scientific
RNeasy Mini Kit	Qiagen
SuperSignal West Femto Trial Kit	Thermo Fisher Scientific
TNT® Quick Coupled Transcription/Translation System (SP6 promoter)	Promega
TruSeq Dual-Index Sequencing Primer Kit	Illumina

5.1.9 Antibodies

Primary antibodies used in this work are listed in Table 5.10.

Table 5.10: Primary antibodies used in this work. Working concentration is given in column "concentration".

Primary antibody	Species	Concentration	Company
anti-BrdU	rat	1:100	AbD Serotec, BU1/75
anti-EGFP	chicken	1:500	Life Technologies, A10262
anti-GFP	rabbit	1:250, 1:500	Invitrogen, A11122

Primary antibody	Species	Concentration	Company
anti-HuC/D	mouse	1:50	Thermo Fisher Scientific, A-21271
anti-Islet-1	mouse	1:100	DSHB, 39.4d5-c
anti-Parvalbumin	mouse	1:200	Millipore, MAB1572
anti-PCNA	mouse	1:100	Millipore, CBL407
anti-pH3 (Ser10)	rabbit	1:250	Millipore, 06-570
anti-PKCα	rabbit	1:100	Santa Cruz, sc-208
anti-Prox1	rabbit	1:100	Millipore, AB5475
anti-Rx2	rabbit	1:250	homemade (Reinhardt et al., 2015)
anti-Zpr-1	mouse	1:100	ZIRC, 021009 CM + Na Azide

Secondary antibodies used in this work are listed in Table 5.11.

Table 5.11: Secondary antibodies used in this work. Working concentration is given in column "concentration".

Secondary antibody	Species	Concentration	Company
anti-chicken DyLight488	donkey	1:250 (whole mount staining) - 1:500 (sections)	Jackson, 703-485-155
anti-mouse 488	goat	1:500	Life Technologies, A-11029
anti-mouse Alexa546	goat	1:500	Life Technologies, A-11030
anti-mouse 647	donkey	1:500	Jackson, 715-605-151
anti-rabbit Alexa488	goat	1:500	Life Technologies, A-11034
anti-rabbit DyLight549	goat	1:500	Jackson, 112-505-144
anti-rabbit Alexa647	goat	1:500	Life Technologies, A-21245
anti-rabbit HRP	goat	1:10000 (Western Blot)	Agrisera, AS09602
anti-rat Alexa647	donkey	1:500	Jackson 712-605-157

5.1.10 Consumables

Consumables used in this work are listed in Table 5.6.

Table 5.12: Consumables used in this work.

Consumable	Company
Blades to cut from agarose gels	Roth
Cell saver tips 200 µl, 1000 µl	Biozym
Cell strainer	Greiner
Cover slips	Roth
Cryosection Superfrost Plus slides	Thermo Fisher Scientific
D1000 ScreenTape	Agilent Technologies
Filter paper	Whatman
Filter tips 10 µl, 20 µl, 200 µl, 1.25 ml	Starlab
Filter Tips TipOne® RPT (sterile), 10 µl, 20 µl, 200 µl	Starlab
Folded filters	Sartorius
Glass beads	Roth
Glass dishes for microscopy	MatTek
Glass petri dishes STERIPLAN® 4 cm, 9 cm	Roth
Glass vials for hatching enzyme treatment	Roth
Hybond-N^+ membrane	Amersham
Injection moulds	homemade
Injection needles GC100F-10	Harvard Apparatus
Latex gloves	Semperguard
Microloader tips for microinjection	Eppendorf
Microloader tips for Western Blot	VWR
Micro pestles 0.5/1.5 ml	Laborversand Hartenstein
Micro pestles 1.5/2.0 ml	Eppendorf
Microscopy slides	Roth
Microtome blades C35	Feather
Molding cups	Polysciences
Needles BD Microlance, 0.3 mm x 13 mm	BD

Consumable	Company
Nitrile gloves	Starlab
Parafilm® M	Bemis
PCR stripes	Sarstedt
PCR tubes	Kisker
PCR tubes, thin-walled, 0.2 ml	Eppendorf
Petri dishes 3.5 cm, 6 cm, 9 cm	Sarstedt
Phase Lock Gel tubes 1.5 ml, 2 ml	Eppendorf
Pipette tips	Steinbrenner
Plastic pipettes 2 ml, 5 ml, 10 ml, 25 ml	Sarstedt
PVDF membrane	Bio-Rad
Reaction tubes 1.5 ml, 2 ml	Sarstedt
Safe-Lock reaction tubes 1.5 ml, 2 ml	Eppendorf
Sandpaper 1000 grit	Bauhaus
Superglue	Uhu
Syringe	BD
Syringe filters 0.22 µm, 0.44 µm	Millipore
Syringe filter 0.2 µm	Whatman
Tissue Freezing Medium	Jung, Leica Microsystems
Transplantation moulds	homemade
Transplantation needles GC100-10	Harvard Apparatus
Tubes 15 ml, 50 ml	Sarstedt
Well plates, 6-well, 12-well, 24-well, 96-well	Roth, Corning
Whatman® Paper	Whatman®

5.1.11 Equipment

Equipment used in this work is listed in Table 5.13.

Table 5.13: Equipment used in this work.

Equipment	Company
Bacterial Shaker INNOVA 44	New Brunswick

Equipment	Company
Bioanalyzer 2100	Agilent Technologies
Blot Documentation System	Intas
Camera Nikon DS-Ri1	Nikon
Centrifuge 5417C	Eppendorf
Centrifuge 5430 R	Eppendorf
Centrifuge 5810 R	Eppendorf
Cold light source for stereomicroscope KL 1500 LCD	Schott
Cryostat CM 3050S	Leica
DeNovix DS-11 spectrophotometer	DeNovix
Electrophoresis chambers and combs for agarose gels	homemade and Peqlab
FemtoJet express and Microinjector 5242	Eppendorf
Fish incubators	Heraeus instruments and RuMed
Forceps 5, 55 Inox stainless steel	Dumont
Forceps 110 mm, straight	NeoLab
Freezer -20 °C	Liebherr
Freezer -80 °C	Thermo Fisher Scientific
Fridge 4 °C	Liebherr
Hybridisation oven Hybaid Micro-4	MWG Biotech
Incubator 32 °C, 37 °C, 60 °C	BINDER
InjectMan NI2	Eppendorf
Leica SP8	Leica
Leica SPE	Leica
Microwave	Sharp
Milli-Q water filtration station	Millipore Corporation
Mini-centrifuge	Sarstedt
Mortar and Pestle	Roth
MS1Minishaker	IKA
Multitemp II Thermostatic circulator 2219	LKB Bromma
Needle puller P-30	Sutter Instrument Co USA
Needle puller P-97	Sutter Instrument Co USA

Equipment	Company
NextSeq 500 system	Illumina
Nikon SMZ18 stereomicroscope	Nikon
Olympus SZX7	Olympus
PCR C100 Touch™ Thermal Cycler	Bio-Rad
pH-Meter	Sartorius
PipetMan	Gilson
Pipettes 2 µl, 10 µl, 20 µl, 200 µl, 1 ml	Gilson
Power supply Power-PAC Basic	Bio-Rad
Rotating Arm	homemade
Scale	Sartorius
SDS-PAGE gel chamber and combs	Bio-Rad
Semi-Dry-Blot-System for Western Blot	Bio-Rad
Shaker CAT S 20	NeoLab
Shaker DRS-12	NeoLab
Shaker GFL 3005	HILAB
Staining container for immunohistochemistry on cryosections	homemade
Stereomicroscope Zeiss Stemi 2000	Zeiss
Stratalinker™ UV Crosslinker	Stratagene
TapeStation 4200	Agilent Technologies
Thermocycler	Bio-Rad
Thermomixer Compact	Eppendorf
ThermoMixer® F1.5	Eppendorf
UV-Gel Documentation System	Intas
UV table	Vilber Lourmat
Vibratome Leica VT 1000S	Leica
Vortex	Scientific Industries
Water bath	GFL
Zeiss Axio Imager M1	Zeiss

5.1.12 Solutions for fish husbandry

Solutions for fish husbandry used in this work are listed in Table 5.14.

Table 5.14: Solutions for fish husbandry.

Solution	Ingredients	Final concentration
10x ERM (Embryo Rearing Medium)	NaCl	17 mM
	KCl	0.4 mM
	$CaCl_2 \cdot 2\,H_2O$	0.27 mM
	$MgSO_4 \cdot 7\,H_2O$	0.66 mM
	HEPES pH 7.3	17 mM
	pH 7.1	
10x Medaka Hatch Medium	NaCl	17 mM
	KCl	0.4 mM
	$CaCl_2 \cdot 2\,H_2O$	0.27 mM
	$MgSO_4 \cdot 7\,H_2O$	0.66 mM
	HEPES pH 7.3	17 mM
	Methylene blue trihydrate	0.0001 %
	pH 7.1	
20xTricaine	$C_9H_{11}NO_2 \cdot CH_4SO_3$	4 g/l
	$Na_2HPO_4 \cdot {}_2H_2O$	10 g/l
	pH 7-7.5 (adjust with 1 N HCl)	
Fixation of fish		
32 % PFA stock solution	paraformaldehyde	500 g
	Millipore H_2O	ad 1562 ml
store at 4℃		
16 % PFA stock solution	32 % PFA stock solution	200 ml
	Millipore H_2O	ad 360 ml
	dissolve at 60℃ while stirring	
	adjust to pH 7 with 1 M NaOH	
	Millipore H_2O	ad 400 ml

Solution	Ingredients	Final concentration
store at 4℃		

5.1.13 Solutions for bacterial work

Solutions for bacterial work are listed in Table 5.15.

Table 5.15: Solutions for bacterial work.

Solution	Ingredients	Final concentration
LB-Bacterial Plates	Bacto-Tryptone	10 g/l
	Yeast extract	5 g/l
	NaCl	10 g/l
	Agar	18 g/l
LB-Medium	Bacto-Tryptone	10 g/l
	Yeast Extract	5 g/l
	NaCl	5 g/l
TB-medium	Bacto-Tryptone	12 g/l
	Yeast extract	24 g/l
	Glycerol	0.4 %
	KH_2PO_4	2.13 g/l
	K_2HPO_4	12.54 g/l

5.1.14 Antibiotics

Antibiotics used in this work are listed in Table 5.16.

Table 5.16: Antibiotics used in this work.

Antibiotic	Stock concentration	Working concentration
bacterial work		
Ampicillin	100 mg/ml	100 µg/ml

Antibiotic	Stock concentration	Working concentration
Kanamycin	50 mg/ml	50 µg/ml
fish work		
Penicillin Streptomycin	10000 U/ml Pen	50 U/ml Pen in 1x ERM
	10 mg/ml Strep	0.05 mg/ml Strep in 1x ERM

5.1.15 Solutions for DNA and RNA work

Solutions for DNA and RNA work used in this work are listed in Table 5.17.

Table 5.17: Solutions for DNA and RNA work.

Solution	Ingredients	Composition
6x DNA loading dye	Ficoll	15 %
	Xylene cyanol	0.05 %
	Bromphenol Blue	0.05 %
	Orange G	0.2 %
	Ponceau S	0.2 %
10x DNA orange loading dye	sucrose	20 g in 40 ml Millipore H_2O
	Orange G	100 mg
	Millipore H_2O	ad 50 ml
EtBr Bath	EtBr (10 mg/ml)	0.02 %
	1x TAE	
Fin-Clip buffer	Tris-HCl pH 8.5	100 mM
	EDTA pH 8	10 mM
	NaCl	200 mM
	SDS	2 %
Fin-Clip buffer/Proteinase K mix	Proteinase K (20 mg/ml)	1:20 in Fin-Clip buffer
Oligo Annealing Buffer	Tris pH 7.5-8	10 mM
	NaCl	30 mM

Solution	Ingredients	Composition
P1 buffer	Tris-HCl pH 8	50 mM
(resuspension buffer)	EDTA	10 mM
	RNase A	100 µg/ml
sterile filtered and stored at 4℃		
P2 buffer (lysis buffer)	NaOH	8 g/l
	SDS	1 %
sterile filtered and stored at RT		
P3 buffer	Potassium acetate (CH_3CO_2K)	294.45 g/l
(neutralisation buffer)	96 % Glacial acetic acid	22.08 %
adjust to pH 5.5 with Glacial acetic acid		
2x RNA loading dye	Bromphenol blue	0.25 %
	Xylene cyanol	0.25 %
	SDS	0.025 %
	EDTA pH 8	5 mM
	Formamide	95 %
TEN-9 buffer	Tris-HCl pH 8.5	100 mM
	EDTA	10 mM
	NaCl	200 mM
	SDS	1 %
50xTris-Acetate-EDTA	Tris base	2 M
Buffer (TAE)	Glacial acetic acid	1 M
	EDTA pH 8	500 mM
	pH 8.5	

5.1.16 Solutions for Southern Blot analysis

Solutions for Southern Blot analysis are listed in Table 5.18.

Table 5.18: Solutions for Southern Blot analysis.

Solution	Ingredients	Composition
10x Blocking Reagent	Blocking Reagent	10 %
	10x DIG1	1x DIG1
Church hybridisation buffer	1 M NaPi	50 ml
	20 % SDS	35 ml
	0.5 M EDTA pH 8	200 µl
	Millipore H_2O	ad 100 ml
Church washing buffer	1 M NaPi	40 ml
	20 % SDS	50 ml
	Millipore H_2O	ad 1 l
Denaturation solution	NaOH	0.5 N
	NaCl	1.5 M
Depurination solution	HCl	0.25 M
10x DIG1	Maleic acid	1 M
	NaCl	1.5 M
adjust to pH 7.5 with NaOH pellets		
1x DIG1	10x DIG1	1x DIG1
1x DIG1 + 0.3 % Tween20		
1x DIG2	Blocking Reagent	1 %
	1x DIG1	
1x DIG3	Tris pH 9.5	0.1 M
	NaCl	0.1 M
1x DIG3 + CDP Star (6 µl/ml)		
1 M NaPi	Na_2HPO_4	0.5 M
adjust to pH 7.2 with H_3PO_4 acid		
50 mM NaPi	1 M NaPi	
Neutralisation buffer	Tris	0.5 M

Solution	Ingredients	Composition
	NaCl	1.5 M
adjust to pH 7.2-7.4 with 32 % HCl (approx. 50 ml for 1 l buffer)		
20xSSC (saline sodium citrate buffer)	NaCl	175.3 g
	sodium citrate ($Na_3C_6H_5O_7$)	88.22 g
	Millipore H_2O	ad 1 l
adjust to pH 7 with HCl		
10xSSC	20x SSC	

5.1.17 Solutions for Western Blot analysis

Solutions for Western Blot analysis are listed in Table 5.19.

Table 5.19: Solutions for Western Blot analysis.

Solution	Ingredients	Composition
20 % APS	APS Powder	
Store at 4 ℃ in the dark.		
3 % Blocking Solution for antibody	Skim Milk Powder	1.5 g
	TBS-T	
4 % Blocking Solution	Skim Milk Powder	2 g
	TBS-T	
1x Blotting Buffer	Methanol	20 %
	SDS	0.0375 %
Store at 4 ℃ in case of wet blot.		
10x Blotting Buffer	Tris	480 mM
	Glycine	390 mM
2.5x Laemmli Sample Buffer	SDS	5 %
	Glycerol	25 %
	Tris-HCl pH 6.8	0.1575 M

Solution	Ingredients	Composition
	Bromphenol Blue	0.05 %
freshly add 2-mercaptoethanol	2.5x Laemmli Sample Buffer	
	12.5 % 2-mercaptoethanol	
RIPA Buffer	Tris-HCl pH 8	50 mM
	NaCl	150 mM
	EDTA	5 mM
	$MgCl_2$	15 mM
	Triton X-100	1 %
Freshly add 1 tablet cOmplete™, Mini, EDTA-free Protease Inhibitor Cocktail (Roche) to 10 ml of RIPA Buffer.		
This mix can be stored at -20 °C.		
10x SDS Running Buffer	Tris	2.25 M
	Glycine	1.92 M
	SDS	ad 1 %
4x Separation Buffer	Tris	1.5 M
	SDS	0.4 %
adjust pH to 8.8 by carefully titrating HCl (1 N or 2 N); store at 4 °C		
4x Stack Buffer	Tris	0.5 M
	SDS	0.4 %
adjust pH to 6.8 by carefully titrating HCl (1 N or 2 N); store at 4 °C		
TBS-T Buffer	Tris-HCl pH 7.5	10 mM
	Tween20	0.05 %
	NaCl	154 mM

5.1.18 Solutions for immunohistochemistry

Solutions used for immunohistochemistry in this work are listed in Table 5.20.

Table 5.20: Solutions for immunohistochemistry.

Solution	Ingredients	Composition
Bleaching solution	30 % H_2O_2	100 ml
	10 % KOH	50 ml
	1xPTW	ad 1 l
Borax PTW	saturated Borax solution	4 ml
	1x PTW	6 ml
2 mg/ml DAPI - stock solution	DAPI	10 mg
	DMSO	ad 5 ml
HCl nuclear denaturation solution	2 N HCl	42.5 ml
	10x PBS	5 ml
	10 % Triton X-100	0.5 ml
10x Phosphate-buffered saline	NaCl	70.1 g
(PBS)	Na_2HPO_4	49.8 g
	KH_2PO_4	3.4 g
	de-ionised H_2O	ad 1 l
adjust to pH 7.3 and autoclave		
2xPhosphate-buffered saline	10x PBS pH 7.3	200 ml
with Tween (2x PTW)	20 % Tween20	5 ml
	Millipore H_2O	ad 1 l
sterile filtered		
1xPhosphate-buffered saline	10x PBS pH 7.3	100 ml
with Tween (PTW)	20 % Tween20	5 ml
	Millipore H_2O	ad 1 l
sterile filtered		
Saturated Borax solution	Sodium tetraborate ($Na_2B_4O_7$)	6 g
	Millipore H_2O	ad 100 ml
crystallisation indicates that the solution is saturated		
30 % sucrose	Sucrose	15 g

Solution	Ingredients	Composition
	1x PTW	ad 50 ml
stored at 4 ℃		
Whole mount antibody blocking solution	Sheep serum	400 µl
	100 mg/ml BSA-solution (sterile filtrate)	100 µl
	DMSO	100 µl
	1x PTW	ad 10 ml

5.1.19 Solutions for *in situ* hybridisation

Solutions for *in situ* hybridisation are listed in Table 5.21.

Table 5.21: Solutions for *in situ* hybridisation.

Solution	Ingredients	Final concentration
20x SSC (saline sodium citrate buffer)	NaCl	3 M
	tri-sodium citrate dihydrate ($C_6H_5Na_3O_7 \cdot 2\,H_2O$)	300 mM
adjust to pH 7 with 1 N HCl		
autoclave		
4x SSCT	20x SSC	4x
	20 % Tween20	0.1 %
2x SSCT	20x SSC	2x
	Tween20	0.1 %
0.2x SSCT	20x SSC	0.2x
	Tween20	0.1 %
10 % Blocking Reagent	2x Maleate buffer pH 7.5	
Blocking Buffer	2x Maleate buffer	1x
	10 % Blocking Reagent	2 %

Solution	Ingredients	Final concentration
	Tween20	0.1 %
Hybridisation Mix (Hyb-Mix)	Formamide	50 %
	20x SSC	5x
	Heparin	150 µg/ml
	Ribonucleic acid from torula yeast Type VI	5 mg/ml
	Tween20	0.1 %
2x Maleate Buffer	Maleic acid	200 mM
	NaCl	300 mM
	Tween20	0.1 %
adjust pH to 7.5 with 10 N NaOH		
Pre-staining buffer	Tris-HCl, pH 7.5	100 mM
	NaCl	100 mM
	Tween20	0.1 %
Staining buffer	Tris-HCl, pH 9.5	100 mM
	NaCl	100 mM
	$MgCl_2$	50 mM
	Tween20	0.1 %

5.2 Methods

5.2.1 Fish maintenance

All fish are maintained in closed stocks at Heidelberg University. Medaka (*Oryzias latipes*) husbandry (permit number 35–9185.64/BH Wittbrodt) and experiments (permit number 35-9185.81/G-145/15 Wittbrodt) were performed according to local animal welfare standards (Tierschutzgesetz §11, Abs. 1, Nr. 1) and in accordance with European Union animal welfare guidelines [Bert et al., 2016]. The fish facility is under the supervision of the local representative of the animal welfare agency. Medaka was raised and maintained as described

previously [Köster et al., 1997].

5.2.2 Microinjection into fertilised Medaka eggs

Embryos were injected at one-cell stage according to [Stemmer et al., 2015]. The following concentrations were used: Cas9 mRNA 150 ng/µl, sgRNAs between 15 and 30 ng/µl, plasmid donors 10 ng/µl. All components were diluted in nuclease-free H_2O (Sigma-Aldrich).
The tagged lines were generated using the modified PCR-product based approach described by [Gutierrez-Triana et al., 2018].
The evening before injection male fish were separated from the females. The next day the fish were put back together for mating. While fish were left mating for 15-25 min, the injection plate was prepared by pouring 1.5 % agarose dissolved in H_2O into a 9 cm Petri dish. A plastic mould was put into the agarose to create the grooves for positioning the embryos for injection. After solidifying, the mould was removed and the agarose covered with ice-cold 1x ERM. Fertilised eggs were then collected, separated by using two tweezers and sorted into the grooves of the injection plate. Injection needles were pulled with the needle puller P-30 fromSutter Instrument Co USA prior to injection. The capillaries were filled with 2-3 µl injection mix (previously prepared and kept on ice) and the needle was opened by gently touching the chorion. A pressure injector with a holding pressure of 80-100 hPa (=P3) and an injection pressure of 450-850 hPa (=P2) depending on the needle was used. The needle was inserted through the chorion into the cytoplasm of one-cell stage embryos and a small amount (1/10th of the visually estimated cell volume) was injected. After injection, the embryos were raised in 1x ERM at either 28°C, 26°C or 18°C to the appropriate stage for further analysis.

5.2.3 Transplantation at blastula stage

Embryos were collected in 1x ERM and kept in the 28°C incubator for approximately 3 hours. In order to perforate the chorion, the embryos were rolled on sandpaper (1000 grit) until the hairs on the chorion were not visible anymore. The embryos were transferred to glass vials, the medium was removed completely, the embryos were covered with hatching enzyme and incubated at 28°C until the chorion was detached (this took approximately 1 h 20 min). The hatching process was monitored by regular assessment under the stereomicroscope. From this step onwards, it is essential that the embryos do not

get into contact with air. Once few embryos hatched, the hatching solution was diluted by careful addition of 1x ERM and 3 further washes with 1x ERM. The embryos were carefully transferred to a glass Petri dish filled with 1x ERM supplemented with Pen/Strep (1 ml Pen/Strep in 200 ml 1x ERM).
Transplantation plates were prepared by pouring 1.5 % agarose dissolved in H_2O into a 9 cm Petri dish. A transplantation mould was put into the agarose to create the slots for positioning the blastula-staged embryos for transplantation. After solidifying, the mould was removed and the agarose covered with 1x ERM/Pen/Strep.
For the actual transplantation, blastula stage embryos (stage 10-11, [Iwamatsu, 2004]) were transferred into the slots of the transplantation plate using a pipette with a cell saver tip, always surrounded by medium, not coming into contact with air. The donor and host blastulae were positioned in a way that allows distinguishing them.
Transplantation needles were pulled with the needle puller P-97 from Sutter Instrument Co USA using the following settings: heat 505; pull 25; vel 250; time 10. The needle tip was cut off using a razor blade to create an opening that fits the cells. After calibration of the transplantation needle, it was filled with 1x ERM/Pen/Strep. Blastomeres were aspirated from the central-most and superficial-most region (future eye field) of a donor embryo and transferred to the same position in the corresponding host embryos. For standard transplantations, where no donor-genotyping was necessary, each donor was used to transplant 10-25 cells into 3-5 hosts each.
When donors needed to be genotyped, each donor was used to transplant cells into up to 3 hosts. Donors were then transferred into individual PCR tubes filled with 25 µl Fin-Clip buffer/Proteinase K mix (1 ml Fin-Clip buffer + 50 µl Proteinase K) and incubated at 60°C for 3 hours in the PCR cycler before continuing with the genotyping protocol.
After transplantation, the embryos were kept in a fresh glass Petri dish filled with 1x ERM/Pen/Strep at 28°C. The medium was carefully exchanged every day until the embryos started swimming. Two to three days after the transplantation, embryos were selected for GFP-positive cells in the retina. Positively screened embryos were raised under standard conditions.

5.2.4 BrdU incorporation

BrdU solution was prepared in 1x ERM in a Falcon tube wrapped in aluminium foil. In order to properly dissolve, the solution was shaken at 37°C for approximately 30 min .
For BrdU incorporation at hatching stage, fish were incubated in 2.5 mM BrdU solution at 28°C for respective amounts of time. Afterwards, fish were euthanised with 20x tricaine, heads were cut off using a scalpel and immediately fixed individually in 4 % PFA/2x PTW. Individual tails were transferred into 25 µl Fin-Clip buffer/Proteinase K mix and incubated at 60°C overnight for genotyping.
For BrdU incorporation at embryonic stages, dechorionated embryos were incubated in 2.5 mM BrdU solution at 28°C for respective amounts of time. Afterwards, heads were cut off using tweezers and immediately fixed individually in 4 % PFA/2x PTW. Individual tails were transferred into 25 µl Fin-Clip buffer/Proteinase K mix and incubated at 60°C overnight for genotyping.

5.2.5 Fish fixation

After the fish were euthanised with 20x tricaine, they were fixed with 4 % paraformaldehyde (PFA). For this, fish were briefly washed with 1x PTW and then incubated in 4 % PFA/2x PTW at 4°C overnight for hatchlings or up to 2 days for 2 weeks old or older fish. Afterwards, the fish were washed 5x for 10 min with 1x PTW prior to preparation for cryosectioning, whole mount immunohistochemistry or *in situ* hybridisation. In case of long-term storage, the fish were dehydrated with consecutive dilutions (25 %, 50 %, 75 % and 100 %) of either ethanol or methanol in 1x PTW for 5 min each on a horizontal shaker and kept in 100 % ethanol or methanol at -20°C.

5.2.6 Genotyping of blastulae

After transplantation into up to 3 hosts, donor blastulae were transferred into individual PCR tubes filled with 25 µl Fin-Clip buffer/Proteinase K mix (1 ml Fin-Clip buffer + 50 µl Proteinase K) using a 200 µl cell saver tip and incubated at 60°C for 3 hours in the PCR cycler. The solution was then briefly centrifuged and transferred from the PCR tube to an 1.5 ml Eppendorf tube. 50 µl H_2O were added to the sample, mixed by pipetting up and down and incubated at 95°C for 15 min to inactivate the Proteinase K. The sample was then centrifuged at full speed for 1 min and the supernatant containing the

genomic DNA was transferred to a fresh Eppendorf tube. The genomic DNA can be directly used for PCR genotyping (max. 5 µl in a 50 µl reaction volume) or stored at 4°C for later analysis.

5.2.7 Genotyping of embryos

Embryos were collected in a 1.5 ml Eppendorf tube. The medium was removed completely, 20-30 µl Fin-Clip buffer/Proteinase K mix were added for single embryos, 30-50 µl for pools of embryos, and embryos were ground using micro pestles (0.5/1.5 ml; one pestle per tube). The sample was briefly centrifuged and then incubated at 60°C overnight. The solution was then briefly centrifuged, two volumes of H_2O were added and mixed by pipetting up and down, followed by an incubation step at 95°C for 15 min to inactivate the Proteinase K. The sample was then centrifuged at full speed for 1 min and the supernatant containing the genomic DNA was transferred to a fresh Eppendorf tube. The genomic DNA can be directly used for PCR genotyping (max. 5 µl in a 50 µl reaction volume) or stored at 4°C for later analysis.

5.2.8 Genotyping of hatchlings

After the fish were euthanised with 20x tricaine, the body was cut off with a scalpel and transferred to a 1.5 ml Eppendorf tube. The medium was removed completely, 25 µl Fin-Clip buffer/Proteinase K mix were added and the sample was incubated at 60°C overnight. The solution was then briefly centrifuged, two volumes of H_2O were added and mixed by pipetting up and down, followed by an incubation step at 95°C for 15 min to inactivate the Proteinase K. The sample was then centrifuged at full speed for 1 min and the supernatant containing the genomic DNA was transferred to a fresh Eppendorf tube. The genomic DNA can be directly used for PCR genotyping (max. 5 µl in a 50 µl reaction volume) or stored at 4°C for later analysis.

5.2.9 Genotyping of adult fish

Fish were sedated using 1x tricaine. A piece of the tail fin was cut off with a scalpel and collected in a 1.5 ml Eppendorf tube. 50-100 µl (depending on the size of the fin) Fin-Clip buffer/Proteinase K mix were added and the sample was incubated at 60°C overnight. The solution was then briefly centrifuged, two volumes of H_2O were added and mixed by pipetting up and down, followed by an incubation step at 95°C for 15 min to inactivate the Proteinase K.

The sample was then centrifuged at full speed for 1 min and the supernatant containing the genomic DNA was transferred to a fresh Eppendorf tube. The genomic DNA can be directly used for PCR genotyping (max. 5 µl in a 50 µl reaction volume) or stored at 4°C for later analysis.

5.2.10 Probe synthesis for *in situ* hybridisation

Qiagen Plasmid Midi prep template plasmids (#467 for *rx2*, #1080 for *rx1*) were linearised with SmaI (*rx2*) or HindIII (*rx1*) and purified using the innuPREP DOUBLEpure kit (Analytik Jena). rNTP mix (15.4 mM each of ATP, CTP and GTP; 10 mM UTP) was prepared according to Table 5.22.

Table 5.22: rNTP mix for probe synthesis for *in situ* hybridisation.

Component	volume per reaction
100 mM ATP	46.2 µl
100 mM CTP	46.2 µl
100 mM GTP	46.2 µl
100 mM UTP	30 µl
Millipore H_2O	ad 300 µl

Transcription reactions were set up as described in Table 5.23.

Table 5.23: Probe synthesis for *in situ* hybridisation.

Component	volume per reaction
linearised template	3 µg
100 mM DTT	2 µl
rNTP mix	1.3 µl
10 mM DigUTP	0.7 µl
RiboLock	0.5 µl
10x Transcription buffer	2 µl
T7 RNA polymerase	2 µl
H_2O	ad 20 µl

The mix was incubated for 2 h at 37°C. After that, 1 µl Turbo DNase was added and the mix was incubated at 37°C for 15 min. The RNA was purified with the Qiagen RNeasy Mini Kit and eluted twice with 25 µl H_2O. For analysis, a 2 µl aliquot was mixed with 5 µl 2x RNA loading dye and 1 µl H_2O, incubated for 10 min at 80°C and run on a 1% TAE agarose gel. The remaining transcription product was mixed with 150 µl hybridisation mix, mixed by finger tipping and stored at -20°C.

5.2.11 Whole mount *in situ* hybridisation

Whole mount *in situ* hybridisation (WISH) was performed on Heino medaka. The incubation steps were done at room temperature in tubes on a rotator (so that the tubes rotated sideways and not over head) if not stated otherwise. The steps at 65°C were done in a water bath without rotation. The fixed and dechorionated st.32 embryos were rehydrated in successive steps of 75 %, 50 % and 25 % methanol in 1x PTW for 5 min each. Next they were washed 2x for 5 min each in 1x PTW. Then they were permeabilised by incubating with 10 µg/ml Proteinase K in 1x PTW (stock: 20 mg/ml) for 1 h 10 min without rotation. The Proteinase K was then inactivated by rinsing 2x 5 min each with 2 mg/ml glycine in 1x PTW. Afterwards, the fish were fixed for 20 min in 4 % PFA in 1x PTW and washed 5x 5 min each with 1x PTW. The samples were then equilibrated by adding Hybridisation Mix (Hyb-Mix, pre-warmed to RT) until the fish sank to the bottom of the tube. The samples were then pre-hybridised in Hyb-Mix at 65°C for 2 h. 15 µl of Digoxigenin-labelled probe were mixed with 185 µl Hyb-Mix and denatured at 80°C for 10 min. Immediately after, hybridisation was performed overnight at 65°C. The next day, the samples were washed 2x 30 min each at 65°C with 50 % formamide/2x SSCT preheated to 65°C, then 15 min at 65°C with 2x SSCT preheated to 65°C and then 2x 30 min each at 65°C with 0.2x SSCT preheated to 65°C. Next the samples were washed 3x 5 min with 1x PTW and blocked at room temperature for 1 h with Blocking Buffer while rotating. After that, they were incubated overnight at 4°C with Anti-Digoxigenin-AP Fab fragments (dilution: 1:2000) in Blocking Buffer. The next day, they were washed 6x 10 min each with 1x PTW in a 6-well plate on the shaker, equilibrated 2x 5 min each with pre-staining buffer and 2x 5 min each with staining buffer. Then, the staining reaction was performed: the samples were incubated in 4.5 µl NBT (final: 337.5 µg/ml) and 3.5 µl BCIP (final: 175 µg/ml) per 1 ml staining buffer without shaking. The

incubation was performed in the dark until development of the blue colour was visible. The samples were over-stained, then destained with ethanol for 1 h at room temperature while shaking, washed 4x with 1x PTW and stored in 1x PTW/1 % PFA at 4°C until further processing by vibratome sectioning.

5.2.12 Vibratome sectioning

Vibratome sectioning was done with st.32 embryos after whole mount *in situ* hybridisation. The heads of stained embryos were transferred to 6-well plates, the medium was removed completely and the wells were filled with 4 % agarose in 1x PTW. The heads were positioned with the dorsal side facing the bottom of the well. Once the agarose had solidified, a small block of agarose including the specimen was cut out of the well with a scalpel and fixed upside down on the specimen holder using superglue. Then the specimen holder was fixed within the buffer tray and filled with H_2O. 30-40 µm sections were made and collected in a 24-well plate filled with 1x PTW. Finally, the sections were mounted on a glass slide with 60 % glycerol in PBS, covered with a coverslip, sealed with nail polish and imaged.

5.2.13 Cryosectioning

Fixed fish were washed 3x 10 min each with 1x PTW and cryoprotected in 30 % sucrose in 1x PTW at 4°C at least over night. To improve section quality the samples were then incubated in a 50:50 mixture of 30 % sucrose and Tissue Freezing Medium for at least 2 days at 4°C. Heads were mounted in mounting molds halfway filled with Tissue Freezing Medium, with the mouth facing down towards the mold. Samples were solidified in the cryostat and mounting molds were filled up with Tissue Freezing Medium and solidified again in the cryostat. 16 µm serial sections were obtained on a cryostat, collected on Superfrost Plus slides and dried at room temperature in the dark at 4°C.

5.2.14 Immunohistochemistry on cryosections

The sections were rehydrated in 1x PTW for 30 min at room temperature. All following incubation steps were carried out in a homemade non-transparent staining container with a lid. Furthermore, sections were covered with Parafilm® M during the incubation steps. After that a blocking step was performed for 1 h with 10 % normal goat serum in 1x PTW at room temperature. The blocking solution was removed by rinsing 2x 5 min each with 1x PTW. The respective

primary antibodies were applied diluted in 1 % normal goat serum overnight at 4°C. The next day the sections were washed 6x 10 min each with 1x PTW. Then the secondary antibodies were applied in 1 % normal goat serum together with DAPI (1:500 dilution in 1x PTW of 5 mg/ml stock) for 2 h at 37°C. Secondary antibodies were washed off 3x 10 min each with 1x PTW. 60 µl of 60 % glycerol in PBS was then added to mount the slides, after which the coverslip was lowered slowly and sealed with nail polish. The slides were then kept at 4°C until imaging.

5.2.15 BrdU immunohistochemistry on cryosections

All following incubation steps were carried out in a homemade non-transparent staining container with a lid. Furthermore, sections were covered with Parafilm® M during the incubation steps.
BrdU antibody immunostainings require an antigen retrieval step with HCl. For this, the sections were fixed in 4 % PFA (pH must be neutral) in 1x PTW for 30 min at room temperature after staining with all antibodies and DAPI except for BrdU. After that the sections were washed 3x 10 min each with 1x PTW. Antigen retrieval was performed by incubating the slides with 2 N HCl, 0.5 % Triton X-100 in 1x PBS for 60-90 min at 37°C. The solution was washed off 3x 10 min each with 1x PTW. Then, pH-recovery was performed using a 40 % saturated Borax solution diluted in 1x PTW for 15 min. After that the slides were washed 3x 10 min each with 1x PTW. Then a blocking step was performed for 1-2 h with 10 % normal goat serum in 1x PTW at room temperature. The blocking solution was removed by washing 2x 5 min each with 1x PTW. The primary anti-BrdU antibody was applied diluted 1:100 in 1 % normal goat serum overnight at 4°C. The next day the sections were washed 6x 10 min each with 1x PTW. Then the secondary antibody was applied diluted 1:500 in 1 % normal goat serum for at least 2 h at 37°C. After that the antibody was washed off 3x 10 min each with 1x PTW. 60 µl of 60 % glycerol in PBS was then added to mount the slides, after which the coverslip was lowered slowly and sealed with nail polish. The slides were then kept at 4°C until imaging.

5.2.16 Wholemount immunohistochemistry

After overnight fixation, fish were washed 5x with 1x PTW. Samples were transferred to 10 cm Petri dishes and washed 3x for 20 min each in 1x PTW on a horizontal shaker. To remove eye pigmentation, the fish were bleached

with bleaching solution for 1-2 h in a 6-well plate covered with aluminium foil on a horizontal shaker. Bleaching was stopped when eyes were of golden colour. Fish were rinsed 5x with 1x PTW, then washed 3x 10 min each with 1x PTW on a horizontal shaker. Retinae were dissected and lenses were removed using sharp tweezers and a stereomicroscope. Retinae were collected in cell strainers in a 6-well plate, followed by another bleaching step until the retinae were transparent. The bleaching progress was carefully monitored by regularly checking the retinae for loss of pigmentation using a stereomicroscope. When bleaching was complete, retinae were rinsed 5x with 1x PTW, then washed 3x 10 min each with 1x PTW on a horizontal shaker. For permeabilisation of the tissue, retinae were incubated in acetone at -20°C for 20 min in glass vials. After rinsing twice with 1x PTW in the glass vials, the retinae were again transferred to a 6-well plate and washed 2x 5 min each with 1x PTW on a horizontal shaker. Then, a blocking step was performed in 2 ml Eppendorf tubes with 500 µl-1 ml blocking solution on the rotating arm (not overhead) either for 1-2 h at room temperature or overnight at 4°C. Afterwards the retinae were incubated with the primary antibody (either 1:250 or 1:500) in 200 µl blocking solution on the thermoblock (covered with a lid) at 26°C, 350 rpm overnight. The primary antibody solution was removed by washing the samples several times thoroughly with 1x PTW in a 6-well plate on a horizontal shaker. Afterwards, retinae were incubated in 2 ml Eppendorf tubes with the secondary antibody (dilution 1:500) and DAPI (dilution 1:500) in 200 µl blocking solution on the thermoblock (covered with a lid) at 32°C, 350 rpm for 2-4 h covered with aluminium foil. The secondary antibody solution was removed by washing the samples several times with 1x PTW in a 6-well plate on a horizontal shaker, covered with aluminium foil. The retinae were stored in 1x PTW at 4°C until imaging.

5.2.17 Imaging

The colorimetric *in situ* hybridisations were imaged with the upright Zeiss Axio imager M1 (Plan-Apochromat lenses: 10x/0.45, 20x/0.8; DIC filter).
All immunohistochemistry (cryosections and whole mount) images were acquired with the inverted confocal laser scanning microscope Leica TCS Sp8 (ACS APO objective lenses: 10x/0.30 dry, 20x/0.75 multi-immersion, 40x/1.2 oil and 63x/1.30 glycerol; laser lines: 405 nm, 488 nm, 532 nm and 638 nm) equipped with several photomultiplier tubes (PMTs) and the Leica Application Suite Software. For imaging the whole mount retinae, they were mounted

in MaTek dishes in 1 % low melting agarose. They were mounted in a way that the most peripheral part of the retina was facing the bottom of the dish and the optic nerve was facing towards the person mounting. After the agarose solidified, the dishes were filled with 1x PTW and imaged.

5.2.18 Image processing, figure preparation and statistical analysis

Adjustment of brightness and contrast of acquired images was performed with Fiji image processing software (ImageJ 1.49b) [Schindelin et al., 2012] and/or Adobe® Photoshop® CS6 without emphasising, hiding or manipulating any parts of the raw images. Figure layout, orientation and cropping of images was done using Adobe® Illustrator® CS6. Statistical analysis and graphical representation of the data was performed using ggplot2 [Wickham, 2016] and RStudio [R Core Team, 2018] (Version 1.0.153 - ©2009-2017 RStudio, Inc.). Angular width of ArCoSs was determined using a custom macro in Fiji (Tsingos and Wittbrodt, unpublished).

5.2.19 PCR

PCRs were carried out as described in Table 5.24.

Table 5.24: PCR setup.

Component	Volume per 50 µl reaction	Final concentration
5x Q5 Reaction buffer	10 µl	1x
2.5 mM dNTPs	4 µl	200 µM
10 µM forward primer	1 µl	0.2 µM
10 µM reverse primer	1 µl	0.2 µM
template DNA	variable	< 1 µg
Q5 High-Fidelity DNA Polymerase	0.3 µl	0.012 U/µl
nuclease-free H_2O	ad 50 µl	

In case of plasmid DNA, 1 pg-1 ng were used as template per 50 µl reaction. In case of genomic DNA extracted with Fin-Clip buffer, the amount of template did not exceed 10 % of the total reaction volume.

The PCR conditions were as described by the manufacturer (NEB), specifically: 98°C 30 s, 30-35 cycles of 98°C 10 s, annealing for 20-45 s and 72°C 30 s per kilo base pair (kb) and a final extension of 2 min at 72°C. Annealing temperature was calculated using the NEB Tm calculator (http://tmcalculator.neb.com/#!/main).

PCR genotyping was carried out using 30 PCR cycles.

If needed, PCR was purified using the innuPREP DOUBLEpure Kit (Analytik Jena) according to the manufacturer's instructions. The DNA was eluted with 12-20 µl pre-warmed (50°C) nuclease-free H_2O.

5.2.20 Agarose gel electrophoresis

DNA samples were mixed with 6x DNA loading dye and loaded into the slots of 0.8-2 % agarose gels in 1x TAE-filled gel chambers. Electrophoresis was carried out with an electrical potential difference of 90-120 V. After electrophoresis, the agarose gel was stained in a aqueous TAE/ethidium bromide solution (EtBr Bath) for 10-15 min. The gels were photographed using a UV light-based (λ = 254 nm) gel documentation system.

5.2.21 Gel extraction

Respective DNA bands were identified and cut out of the agarose gel using a scalpel. The DNA was extracted using the innuPREP DOUBLEpure Kit (Analytik Jena) according to the manufacturer's instructions. The DNA was eluted with 12-20 µl pre-warmed (50°C) nuclease-free H_2O.

5.2.22 DNA restriction

0.5 µl of the desired restriction enzymes, 1x buffer (according to the restriction enzymes used) and approximately 4 µg of DNA were mixed and incubated at 37°C for a minimum of 1-2 h. Subsequently, the product of this restriction digest was analysed by gel electrophoresis. If needed, restriction digest was purified using the innuPREP DOUBLEpure Kit (Analytik Jena) according to the manufacturer's instructions. The DNA was eluted with 12-20 µl pre-warmed (50°C) nuclease-free H_2O. For test restriction digests, a maximum amount of 1.5 µg per Miniprep were digested using 0.2 µl of the desired restriction enzyme.

5.2.23 PCR genotyping of *rx1* and *rx2* TALEN mutants

PCR was setup as described in subsection 5.2.19, using max. 5 µl genomic DNA in Fin-Clip buffer as template. Genotyping primers for *rx1* were JW1549 and JW1550, and for *rx2* JW0942/JW0943. For genotyping of *rx1*, PCR was cleaned up using the innuPREP DOUBLEpure Kit (Analytik Jena) according to the manufacturer's instructions. The DNA was eluted with 12 µl pre-warmed (50°C) ddH_2O and directly subjected to restriction digest using BsrGI-HF (NEB) as described in Table 5.25.

Table 5.25: Restriction digest for genotyping *rx1*.

Component	Volume per 50 µl reaction
purified PCR product	9 µl
10x CutSmart®buffer (NEB)	5 µl
BsrGI-HF (NEB)	0.5 µl
nuclease-free H_2O	ad 50 µl

Restriction digest was incubated at 37°C for 1 h 20 min and analysed on a 1.5 % agarose gel. Due to absence of the BsrGI restriction site in the *rx1* TALEN mutant, expected band sizes were the following (see Table 5.26):

Table 5.26: Expected band sizes for genotyping *rx1*.

Genotype	expected band sizes [bp]
wild-type	220 + 90
rx1$^{+/-}$	306 + 220 + 90
rx1$^{-/-}$	306

For genotyping of *rx2*, PCR was directly subjected to restriction digest using AccI (NEB) without prior purification (see Table 5.27).

Table 5.27: Restriction digest for genotyping *rx2*.

Component	Volume per 25 µl reaction
PCR product	6 µl
10x CutSmart®buffer (NEB)	2.5 µl
AccI (NEB)	0.5 µl
nuclease-free H_2O	ad 25 µl

Restriction digest was incubated at 37°C for 1 h 10 min and analysed on a 1 % agarose gel. Due to absence of the AccI restriction site in the *rx2* TALEN mutant, expected band sizes were the following (see Table 5.28):

Table 5.28: Expected band sizes for genotyping *rx2*.

Genotype	expected band sizes [bp]
wild-type	668 + 191
rx2$^{+/-}$	857 + 668 + 191
rx2$^{-/-}$	857

5.2.24 Phosphorylation and dephosphorylation of DNA

Blunt cut vectors were dephosphorylated by use of Fast Alkaline Phosphatase (Roche). Up to 10 µg of plasmid DNA were mixed with Fast Digest Buffer and 1 µl enzyme. The mix was incubated at 37°C for 20 min and then heat-inactivated at 65°C for 15 min.

5.2.25 DNA ligation

For ligation the optimal ratio between vector and insert was calculated using EnzymeX 3 software and the following formula: amount of insert = insert size / vector size × 3 (molar ratio of insert / vector) × amount of vector to be used. The following reaction (see Table 5.29) was set up and incubated either for 1 h at room temperature or overnight at 18°C.

Table 5.29: DNA ligation reaction setup.

Component	Volume per 10 µl reaction	Composition
linearised vector		50 ng
insert		
T4 DNA ligase (5,U/µl)	1 µl	0.5 U
10x T4 DNA Ligase Buffer	1 µl	1x
nuclease-free H_2O	ad 10 µl	

5.2.26 Annealing of oligonucleotides

The following annealing reaction was set up (see Table 5.30).

Table 5.30: Annealing of oligonucleotides.

Component	Volume
top strand oligo (100 µM)	1 µl
bottom strand oligo (100 µM)	1 µl
nuclease-free H_2O	18 µl
Oligo Annealing Buffer	20 µl

The reaction was carried out in a PCR cycler using the following conditions: 95°C 5 min, ramp down to 70°C (0.1°C /s), hold 10 min, ramp down to 65°C (0.1°C /s), ramp down to 60°C (0.1°C /s), hold 10 min, ramp down to 10°C (0.1°C /s). The sample was diluted 1:33, yielding a final concentration of 0.075 pmol/µl. 1 µl was used to ligate into 25 ng of vector for 15 min at room temperature before transformation into chemically competent cells.

5.2.27 Golden Gate cloning

Restriction-ligation reactions (see also [Kirchmaier et al., 2013]) were set up according to Table 5.31.

Table 5.31: Golden Gate reaction setup.

Component	Volume per 20 µl reaction
Entry Vectors (EVs)/Insert	20 fmol each
Destination Vector digested with BsaI	20 fmol
10x FastDigest Buffer (Thermo Fisher Scientific)	1 µl
10x T4 DNA Ligase Buffer (Thermo Fisher Scientific)	1 µl
nuclease-free H_2O	ad 18.8 µl
mix well!	
Eco31I-FD (Thermo Fisher Scientific)	0.6 µl
T4 DNA Ligase 30 U/µl (Thermo Fisher Scientific)	0.6 µl

Destination Vector was pre-digested with BsaI and purified from the gel before setting up the reaction. 10x T4 DNA Ligase Buffer was stored in 10 µl aliquots at -20°C. A fresh aliquot was used for each reaction. Reactions were set up in PCR tubes and incubated using the following settings (either "common protocol" or "short protocol", see Table 5.32):

Table 5.32: Golden Gate protocol.

Protocol	Temperature	Time
common protocol		
	37 ℃	30 min
	16 ℃	20 min
repeat 9x		
	85 ℃	10 min
	50 ℃	10 min
short protocol		
	37 ℃	5 min
	16 ℃	2 min
repeat 9x		
	85 ℃	10 min
	20 ℃	5 min

Of the 20 µl assembly mix, 5 µl were used for transformation with 50 µl MachT1 chemically competent cells. The cells were plated onto LB-Kanamycin plates containing 50 µl X-Gal for blue-white selection.

5.2.28 Transformation of chemically competent cells

50 µl chemically competent cells were thawed on ice. 5-10 µl of ligation were added to 50 µl of cells, mixed carefully by stirring gently with the pipette tip and incubated shortly on ice. A heat shock was performed for 45 s at 42°C, the tube was snap-cooled on ice, then 300 µl of TB medium were added and the mix was incubated for 1 hour at 37°C while shaking at 164 rpm. The mix was plated onto LB plates pre-warmed to 37°C, containing the respective antibiotics. In case of blue-white selection 50 µl X-Gal were spread evenly onto LB-Kanamycin plates and pre-warmed to 37°before the mix was plated. After incubation overnight at 37°C, grown colonies were used for plasmid preparation.

5.2.29 Plasmid preparation

For small scale plasmid preparations (Miniprep) 4 ml of LB-medium with respective antibiotic were inoculated with single bacterial clones and incubated for at least 6 h at 37°C and 164 rpm. 2 ml of the culture were centrifuged for 2 min at 14000 rpm. The supernatant was discarded and the pellet was resuspended in 200 µl cold P1 buffer. 200 µl P2 buffer were added and the tubes were inverted several times. 200 µl cold P3 buffer were added and the tubes were inverted again several times. The tubes were centrifuged for 10 min at 14000 rpm at 4°C. The supernatant was transferred into a new tube, 500 µl Isopropanol were added, mixed thoroughly and centrifuged for 10 min at 14000 rpm at 4°C. The supernatant was discarded and 500 µl 70 % ethanol were added. After centrifugation for 5 min at 14000 rpm at 4°C, supernatant was discarded, the pellet was dried until it turned transparent and then was dissolved in 40 µl of H_2O.

For large scale plasmid preparations (Midiprep) 50 ml LB-medium with respective antibiotic were inoculated with single bacterial clones or 10 µl of bacterial culture of a positively identified colony and grown at 37°C and 164 rpm overnight. Purification of plasmid DNA was carried out using the Plasmid Midi Kit (Qiagen) according to manufacturer's instructions. The following changes were made: all centrifugation steps were performed at 4000 rpm increasing the

duration of the centrifugation steps accordingly. The centrifugation step after the addition of P3 was replaced by filtration of the solution using filter paper. The pellet was resuspended in 80 µl TE overnight at 4°C and stored at -20°C. For large scale plasmid preparations ("Big Mini") using the QIAprep Spin Miniprep Kit (Qiagen), 20 ml LB-medium with respective antibiotic were inoculated with single bacterial clones or 10 µl of bacterial culture of a positively identified colony and grown at 37°C and 164 rpm overnight. To pellet the culture, 2x 2 ml Eppendorf tubes were used per culture. 2 ml of the culture were centrifuged for 2 min at 8000 rpm at room temperature. The supernatant was discarded and another 2 ml of the culture were centrifuged at 8000 rpm at room temperature using the same tube. The supernatant was discarded and the pellets were completely resuspended in 250 µl Buffer P1. 250 µl Buffer P2 were added and mixed thoroughly by inverting 4-6 times (solution turns blue) and not longer than 5 min. 350 µl Buffer N3 was added and immediately mixed thoroughly by inverting 4-6 times (solution turns clear). The tubes were centrifuged for 10 min at 13000 rpm at room temperature. The supernatant of the first Eppendorf tube was applied to the spin column by pipetting (800 µl), followed by a centrifugation step for 1 min at 13000 rpm at room temperature. The flow-through was discarded and the supernatant of the second Eppendorf tube was applied to the same spin column by pipetting. The tube was centrifuged for 1 min at 13000 rpm at room temperature and the flow-through was discarded. The spin column was washed by adding 750 µl Buffer PE and centrifuging for 1 min at full speed at room temperature. The flow-through was discarded and the tube was again centrifuged for 1 min at full speed at room temperature to remove residual wash buffer. After no wash buffer was left on the column, it was placed into a clean 1.5 ml Eppendorf tube. 50 µl RNase free H_2O were added and incubated for 4 min. The tube was centrifuged for 1 min at 13000 rpm to elute the DNA.

5.2.30 DNA Sequencing

Plasmids and PCR fragments were sequenced by a commercial service (Eurofins Genomics).

5.2.31 Software for *in silico* cloning

Geneious® 8.1.9 software was used for *in silico* cloning and analysis of sequencing results. EnzymeX 3 software was used for calculating ligation reactions and

retrieving information on restriction enzymes.

5.2.32 Donor plasmids

Donor plasmids were generated by Golden Gate assembly subsection 5.2.27 into the pGGDestSC-ATG destination vector (addgene #49322).
#5152 (mCherry-FL-rx2, see also Table 5.2) was designed and cloned according to donor plasmid #3922 (eGFP-FL-rx2, see also Table 5.2) as described in [Gutierrez-Triana et al., 2018]. mCherry coding sequence was amplified using primers JW6689 and JW6690. Generation of #4974 (eGFP-FL-rx1, see also Table 5.2) is described in [Gutierrez-Triana et al., 2018]. Design of #4367 (*rx2 conditional*, see also Table 5.2) is described in [Stemmer, 2015]. For #5166 (H2B-EGFPwCR13-OPT-rx1, see also Table 5.2), the same homology flanks (HFs) were used as in #4974, the ocean pout cassette (OPT) was released from pDB770 (GBT-RP2) (gift from Darius Balciunas, Temple University, Philadelphia, USA) [Clark et al., 2011] and cloned by Thomas Thumberger into pGGEV4 of the Golden Gate system. For M820 (H2B-mRFP-OPT-rx2, see also Table 5.2), the same homology flanks were used as in #3922 and #5152.

5.2.33 sgRNA target site selection

sgRNAs were designed with CCTop as described in [Stemmer et al., 2015] and [Gutierrez-Triana et al., 2018]. Cloning of sgRNA templates and *in vitro* transcription was performed as described in [Stemmer et al., 2015].

5.2.34 *In vitro* transcription of Cas9 mRNA

The pCS2^{+}-Cas9 plasmid (#5197) was linearised using NotI and the mRNA was transcribed *in vitro* using the mMESSAGE mMACHINE™ Sp6 Transcription Kit (ThermoFisher Scientific, AM1340).

5.2.35 RT-PCR

Total RNA was isolated from 60 homozygous embryos (st..32) by lysis in TRIzol and chloroform extraction according to the manufacturer's protocol. RNA was precipitated using isopropanol and resuspended in nuclease-free H_2O. cDNA was reverse transcribed with RevertAid First Strand cDNA Synthesis Kit after

DNAse digestion and inactivation following the manufacturer's instructions. PCR was performed and PCR products were analysed on a 1.5 % agarose gel.

5.2.36 Southern Blot

In order to check for copy number insertions in the *eGFP-FL-rx2*, *eGFP-FL-rx1* (see also [Gutierrez-Triana et al., 2018] for description of the procedure) and *rx2 conditional* transgenic lines, genomic DNA was isolated either from GFP expressing embryos (*eGFP-FL-rx2*, *eGFP-FL-rx1*) or from adult males (*rx2 conditional*) expressing the construct.
30 embryos or were lysed in TEN-9 buffer plus Proteinase K (10 mM Tris pH 8, 1 mM EDTA, 100 mM NaCl, 1 mg/ml Proteinase K) at 60°C overnight. Testes and liver of adult males were dissected, frozen in liquid nitrogen, ground with a pestle and transferred to 2 ml Eppendorf tubes. Lysis was done using TEN-9 buffer supplemented with Proteinase K (1.25 µg/µl final concentration) and RNase A (0.03125 µg/µl final concentration) at 50°C and 400 rpm overnight. Embryonic DNA was ethanol precipitated, adult DNA was isopropanol precipitated, after removal of lipids and proteins by phenol-chloroform extraction. Total DNA was resuspended in 1x restriction enzyme buffer and digested overnight at 37°C with respective enzymes.
10 µg digested genomic DNA were loaded per lane on a 0.8 % agarose gel and size fractionated by electrophoresis. The gel was depurinated in Depurination solution for 30 min at room temperature, rinsed with H_2O, denatured in Denaturation solution for 30 min at room temperature and neutralised in Neutralisation buffer before it was transferred overnight at room temperature onto a Hybond membrane (Amersham). The membrane was washed with 50 mM NaPi for 5 min at room temperature, then crosslinked and pre-hybridised in Church hybridisation buffer at 65°C for at least 30 min. The probes were synthesised from the respective donor plasmid with primers JW1458 and JW1745 for GFP, and JW3840 and JW3566 for RFP, using the PCR DIG Probe Synthesis Kit (Roche, 11636090910) and the following PCR protocol: initial denaturation at 95°C for 2 min, 35 cycles of 95°C 30 s, 60°C 30 s (GFP) / 65°C 30 s (RFP), 72°C 40 s and final extension at 72°C 7 min. The probe was boiled in hybridisation buffer for 10 min at 95°C and the membrane was hybridised overnight at 65°C. The membrane was washed with preheated (65°C) Church washing buffer at 65°C for 10 min, then at room temperature for 10 min and with 1x DIG for 5 min at room temperature. The membrane was blocked in 1 % w/v blocking reagent (Roche) in 1x DIG1 solution at room temperature for at least 30 min.

The membrane was incubated with 1:10000 anti-Digoxigenin-AP Fab fragments (Roche) for 30 min at room temperature in 1 % w/v blocking reagent (Roche) in 1x DIG1 solution. Two washing steps with 1x DIG1 and 0.3 % Tween were performed for 20 min at room temperature, followed by a 5 min washing step in 1x DIG3 at room temperature. Detection was performed using 6 µl/ml CDP star (Roche).

Stripping Protocol for Southern Blots

Stripping protocol was carried out according to GE Amersham Hybond N^+ manual ("Hot SDS procedure"). In brief, boiling solution of 0.1 % SDS in 0.1x SSC was poured directly onto the blot and let cool down for approximately 10 min. The blot was briefly washed with 2x SSC. Afterwards, blocking, antibody incubation and detection steps were carried out as described above and removal of the probe was checked. Then, probe hybridisation step was carried out over night, followed by blocking, antibody incubation and detection steps as described above.

5.2.37 Western Blot

sodium dodecyl sulfate polyacrylamide gel electrophoresis (SDS-PAGE)

For characterisation of the anti-Rx2 antibody, Western Blot analysis was carried out. Hatchlings of either Cab strain, *rx1* TALEN or *rx2* TALEN strains were euthanised using 20x tricaine and heads were dissected in 1x PBS using forceps. Heads were pooled in 2 ml Eppendorf tubes and homogenised in 1x RIPA Buffer supplemented with protease inhibitors using micro pestles. Samples were incubated on ice for 10 min, then centrifuged at full speed for 5 min at 4°C. The supernatant was transferred to a fresh 1.5 ml Safe-Lock Eppendorf tube and 2.5x Laemmli Sample Buffer containing mercaptoethanol was added to a final concentration of 1x. Samples were boiled at 99°C for 10 min. Separating and stacking gel were prepared according to Table 5.33.

Table 5.33: SDS-PAGE.

Component	Final Concentration
Separating Gel	
30 % Acrylamide (29:1)	10 % Acrylamide

Component	Final Concentration
4x Separation Buffer, pH 8.8	1x Separation Buffer, pH 8.8
ddH_2O	
20 % APS	0.2 % APS
TEMED	0.1 %
Stacking Gel	
30 % Acrylamide (29:1)	4.5 % Acrylamide
4x Stack Buffer, pH 6.8	1x Stack Buffer, pH 6.8
ddH_2O	
20 % APS	0.2 % APS
TEMED	0.1 %

Separating gel was prepared first and 70 % ethanol was added on top to ensure an even surface. After polymerisation, the stacking gel was poured on top of the separating gel. After polymerisation, 30-40 µl per sample, as well as 10 µl PageRuler Prestained Protein Ladder for reference were loaded. Empty wells were loaded with 20 µl of a 1:1 mixture of 2.5x Laemmli Sample Buffer containing 2-mercaptoethanol and 1x PBS. Gel was run in 1x SDS Running Buffer at 60 V for approximately 3 h at room temperature. Progress was checked by regularly monitoring the Protein Ladder.

Western Blot

After electrophoresis was complete, the stacking gel and the last few mm of the separating gel containing only glycine and no protein were cut off. The gel was then incubated in 1x Blotting Buffer for at least 5 min at room temperature. After activating the PVDF membrane with 100 % methanol for 20-30 s, it was incubated, together with the Whatman papers, in 1x Blotting Buffer. Using flat-tipped forceps, the semi-dry blot was mounted by putting 3 Whatman papers, the PVDF membrane, the SDS-PAGE and 3 Whatman papers in this order. Air bubbles were removed by carefully rolling a plastic pipette onto the stack. The following formula was used to calculate the electric current needed for blotting: surface area x 2 mA/cm^2. Blotting of 1 gel was done at 75 mA (2 gels: 150 mA) for 1 h at room temperature.
The blot was disassembled and the membrane was incubated with the proteins

facing upwards in 4 % Blocking Solution for 1 h at room temperature on a tilting shaker. After that, the solution was replaced by 3 % Blocking Solution containing primary antibody (1:1000) and the membrane was incubated overnight at 4°C on a tilting shaker, covered with aluminium foil. The antibody-containing solution was removed and the membrane was briefly rinsed two times with TBS-T, followed by 6 washing steps on a tilting shaker, 5 min each with TBS-T at room temperature. The membrane was then incubated in 3 % Blocking Solution containing the secondary antibody (1:10000) for 1 h at room temperature on a tilting shaker, covered with aluminium foil. The antibody-containing solution was removed and the membrane was briefly rinsed two times with TBS-T, followed by 6 washing steps on a tilting shaker, 5 min each with TBS-T at room temperature.
The SuperSignal West Femto Trial Kit (Thermo Fisher Scientific) was used for detection of the signal. Excess buffer was removed from the membrane followed by a 2 min incubation in a mix of equal parts Stable Peroxide Buffer and Luminol/Enhancer. Pictures were acquired using a Blot Documentation System from Intas, either in single capture or in sequential mode. Detection times of 5 s, 10 s, 20 s, 1 min and 5 min were used.

Q5® site-directed mutagenesis

Q5® site-directed mutagenesis was done to introduce the 10 bp TALEN deletion in the *rx1* and *rx2* homeobox, respectively *in vitro*, using plasmid #4831 (see Table 5.34) and primers JW6028 and JW6029, as well as plasmid #4832 (see Table 5.34) and primers JW6026 and JW6027, respectively.

Table 5.34: Plasmids used for Q5 site-directed mutagenesis.

Number	Alias
4831	pCS2+ containing full-length *rx2* cDNA
4832	pCS2+ containing full-length *rx1* cDNA

25 µl Q5 PCR reaction was setup using 5 ng plasmid template. Annealing temperatures were calculated using the NEBase Changer tool (http://nebasechanger.neb.com/; JW6026/JW6027: 68°C; JW6028/JW6029: 64°C). PCR was run for 25 cycles and purified using the innuPREP DOUBLEpure Kit (Analytik Jena) and eluted in 25 µl nuclease-free H_2O. Kinase,

Ligase, DpnI (KLD) treatment was done according to the following scheme (see Table 5.35).

Table 5.35: Q5 site-directed mutagenesis.

Component	Volume
purified PCR product	1 µl
nuclease-free H_2O	9.5 µl
10x CutSmart Buffer (NEB)	1.5 µl
ATP 10 mM	1.5 µl
PNK (Thermo Fisher Scientific)	0.5 µl
T4 DNA Ligase 5 U/µl	0.5 µl
DpnI (NEB)	0.5 µl

Reaction was incubated for at least 10 min at room temperature before 5 µl were transformed into chemically competent cells.

TNT reaction

In order to produce Rx1 and Rx2 wild-type (wt) proteins, as well as Rx1 and Rx2 proteins whose coding sequences lack 10 bp of the homeobox, therefore mimicking the TALEN-mutation, the TNT® Quick Coupled Transcription/-Translation System (SP6 promoter) (Promega) was used. Circular plasmids were used as templates, and are listed in Table 5.36:

Table 5.36: Plasmids used in TNT reaction. "Number" indicates internal lab plasmid stock number.

Number	Alias
4831	pCS2+ containing full-length *rx2* cDNA
4831-mut	pCS2+ containing *rx2* cDNA with 10 bp deletion in homeobox
4832	pCS2+ containing full-length *rx1* cDNA
4832-mut	pCS2+ containing *rx1* cDNA with 10 bp deletion in homeobox

For the TNT reaction, following components were mixed (see Table 5.37).

Table 5.37: TNT reaction setup.

Component	Volume
TNT® Quick Master Mix	20 µl
Methionine, 1 mM	0.5 µl
plasmid DNA template	500 µg
nuclease-free H_2O	ad 25 µl

The mix was incubated at 30°C for 90 min. 1 µl of the mix was added to 9 µl 1x SDS Running Buffer and 10 µl 2x Laemmli Sample Buffer containing 2-mercaptoethanol. Samples were run on a 10 % SDS-PAGE, at 60 V for 3 h, then blotted onto a PVDF-membrane at 120 mA for 1 h at room temperature.

5.2.38 RNA Sequencing

Optic vesicle dissection

For RNA Sequencing analysis, optic vesicles of medaka embryos st..18 and st..20 (Iwamatsu, 2004) were dissected. The embryos were collected the day before and were kept either at room temperature or at 26°C overnight. In order to perforate the chorion, they were rolled on sandpaper (1000 grit) until the hairs on the chorion were not visible anymore. Embryos at appropriate stages (st..16-18) were treated with hatching enzyme for approximately 1 h at 28°C. In the meantime the solutions for the following steps were prepared using TipOne®RPT filter tips (sterile). Cell lysis buffer and final buffer were prepared according to [Picelli et al., 2014] (see Table 5.38).

Table 5.38: Buffers for RNA Sequencing of optic vesicles.

Solution	Ingredient	Composition
cell lysis buffer	Triton X-100	0.2 %
	RiboLock	
mix RiboLock and 0.2 % Triton X-100 in a 1:20 ratio		

Solution	Ingredient	Composition
final buffer	cell lysis buffer	
	oligo-dT_{30}VN (100 µM)	10 µM
	dNTPs	10 µM
mix cell lysis buffer, oligo-dT_{30}VN and dNTPs in a 2:1:1 ratio		

The final buffer was then distributed to 0.2 ml thin-walled PCR tubes (Eppendorf), 16 µl per PCR tube and put on ice. This particular amount of final buffer per PCR tube was used according to the recommended ratio of liquid of sample to final buffer 1:8 (vol) by [Picelli et al., 2014]. This takes into account that approximately 1-2 µl of liquid is brought in with the transfer of the optic vesicle to the PCR tube. After the chorion of the embryos was dissolved by hatching enzyme (the hatching process was monitored by regular assessment under the stereomicroscope), embryos were transferred to glass Petri dishes filled with filtered 1x ERM (0.2 µm Whatman filter). A needle (BD Microlance, 0.3 mm × 13 mm) attached to a 1 ml syringe served as dissection tool. Dissection was carried out at the microinjection setup. Glass capillaries to transfer the dissected optic vesicles were pulled using the needle puller P-97 from Sutter Instrument Co USA with the following settings: heat 505; pull 25; vel 250; time 10. The fine tip of the capillary was cut off using a razor blade to create an opening that fits the dissected optic vesicles. The capillary was inserted into the micromanipulator and connected to the transplantation air-stream system controlled by a 1 ml syringe that allows to control volume uptake and release. The dissection itself was carried out in a glass Petri dish filled with filtered 1x ERM. A construction of several glass Petri dishes was used: the glass Petri dish containing the embryos in filtered 1x ERM was placed onto the lid of a glass Petri dish to lift the whole plane of dissection. Then, the embryos of most appropriate stages were chosen and transferred to the glass Petri dish filled with filtered 1x ERM using cell saver tips. First, the yolk was removed, then the membrane on the right side of the embryo was cut off, followed by cutting off the membrane on the left side of the embryo. The right optic vesicle was cut off first, then the left optic vesicle was cut off. Then, right and left optic vesicles were individually transferred into individual PCR tubes containing the final buffer (transferring as little liquid as possible); the right optic vesicle was transferred first, followed by the left optic vesicle. PCR tubes containing an optic vesicle

were immediately put back on ice. Each sample of optic vesicles was shortly centrifuged and placed at -80°C for storage within 5 min after dissection.

Preparing samples for genotyping

The rest of the embryo (everything except the optic vesicles) was used for genotyping and was transferred using cell saver tips to a PCR tube containing 25 µl Fin-Clip buffer/Proteinase K mix. The samples were centrifuged shortly and incubated at 60°C in the PCR cycler (lid temperature 65°C) for 3 h (followed by incubation at room temperature overnight). The next day, samples were shortly centrifuged and 60 µl H_2O were added, followed by an incubation step at 95°C to inactivate the Proteinase K. Samples were centrifuged for 1 min at full speed and the supernatant containing the genomic DNA was transferred to a fresh 1.5 ml Eppendorf tube. The concentration of the extracted DNA was measured using a spectrophotometer (the concentration was always around 10-20 ng/µl). The extracted DNA was either stored at 4°C or directly used for PCR genotyping. For genotyping protocol refer to subsection 5.2.23.

RNA preparation and RNA Sequencing

For RNA preparation, the protocol by [Picelli et al., 2014] was followed except for the following changes:
4.3 µl of the optic vesicle lysate was used.
Post cDNA amplification, the samples were diluted to 0.1 ng/µl and 5 µl of this was used for the tagmentation. Tagmentation was for 10 min, 12 cycles were used.
Sequencing was performed on the NextSeq 500 system, high output mode, 75 base single end plus barcode read (dual index 16 bases (8+8)).
Sequencing depth was about 10-20 million reads.

References

[Abouzeid et al., 2012] Abouzeid, H., Youssef, M. a., Bayoumi, N., ElShakankiri, N., Marzouk, I., Hauser, P., and Schorderet, D. F. (2012). RAX and anophthalmia in humans: evidence of brain anomalies. *Molecular Vision*, 18:1449–56.

[Agathocleous and Harris, 2009] Agathocleous, M. and Harris, W. A. (2009). From Progenitors to Differentiated Cells in the Vertebrate Retina. *Annual Review of Cell and Developmental Biology*, 25:45–69.

[Ahmad et al., 2000] Ahmad, I., Tang, L., and Pham, H. (2000). Identification of neural progenitors in the adult mammalian eye. *Biochemical and Biophysical Research Communications*, 270(2):517–521.

[Akamatsu et al., 2005] Akamatsu, W., Fujihara, H., Mitsuhashi, T., Yano, M., Shibata, S., Hayakawa, Y., Okano, H. J., Sakakibara, S.-i., Takano, H., Takano, T., Takahashi, T., Noda, T., and Okano, H. (2005). The RNA-binding protein HuD regulates neuronal cell identity and maturation. *Proceedings of the National Academy of Sciences*, 102(12):4625–4630.

[Amato et al., 2004] Amato, M. a., Arnault, E., and Perron, M. (2004). Retinal stem cells in vertebrates: parallels and divergences. *The International Journal of Developmental Biology*, 48(8-9):993–1001.

[Amini et al., 2018] Amini, R., Rocha-Martins, M., and Norden, C. (2018). Neuronal migration and lamination in the vertebrate retina. *Frontiers in Neuroscience*, 11:doi: 10.3389/fnins.2017.00742.

[Andreazzoli et al., 1999] Andreazzoli, M., Gestri, G., Angeloni, D., Menna, E., and Barsacchi, G. (1999). Role of Xrx1 in Xenopus eye and anterior brain development. *Development*, 126(11):2451–2460.

[Andreazzoli et al., 2003] Andreazzoli, M., Gestri, G., Cremisi, F., Casarosa, S., Dawid, I. B., and Barsacchi, G. (2003). Xrx1 controls proliferation and neurogenesis in Xenopus anterior neural plate. *Development*, 130(21):5143–5154.

[Bailey et al., 2004] Bailey, T. J., El-Hodiri, H., Zhang, L., Shah, R., Mathers, P. H., and Jamrich, M. (2004). Regulation of vertebrate eye development by

Rx genes. *The International Journal of Developmental Biology*, 48(8-9):761–70.

[Baye and Link, 2008] Baye, L. M. and Link, B. A. (2008). Nuclear migration during retinal development. *Brain Research*, Feb 4(1192):29–36.

[Bejarano-Escobar et al., 2015] Bejarano-Escobar, R., Álvarez Hernán, G., Morona, R., González, A., Martín-Partido, G., and Francisco-Morcillo, J. (2015). Expression and function of the LIM-homeodomain transcription factor Islet-1 in the developing and mature vertebrate retina. *Experimental Eye Research*, 138:22–31.

[Bélanger et al., 2017] Bélanger, M. C., Robert, B., and Cayouette, M. (2017). Msx1-Positive Progenitors in the Retinal Ciliary Margin Give Rise to Both Neural and Non-neural Progenies in Mammals. *Developmental Cell*, 40(2):137–150.

[Bert et al., 2016] Bert, B., Chmielewska, J., Bergmann, S., Busch, M., Driever, W., Finger-Baier, K., Höß ler, J., Köhler, A., Leich, N., Misgeld, T., Nöldner, T., Reiher, A., Schartl, M., Seebach-Sproedt, A., Thumberger, T., Schönfelder, G., and Grune, B. (2016). Considerations for a European animal welfare standard to evaluate adverse phenotypes in teleost fish. *EMBO Journal*, 35(11):1151–1154.

[Bhatia et al., 2009] Bhatia, B., Singhal, S., Lawrence, J. M., Khaw, P. T., and Limb, G. A. (2009). Distribution of Müller stem cells within the neural retina: Evidence for the existence of a ciliary margin-like zone in the adult human eye. *Experimental Eye Research*, 89(3):373–382.

[Bhaya et al., 2011] Bhaya, D., Davison, M., and Barrangou, R. (2011). CRISPR-Cas systems in bacteria and archaea: versatile small RNAs for adaptive defense and regulation. *Annual Review of Genetics*, 45(1):273–297.

[Boch et al., 2009] Boch, J., Scholze, H., Schornack, S., Landgraf, A., Hahn, S., Kay, S., Lahaye, T., Nickstadt, A., and Bonas, U. (2009). Breaking the code of DNA binding specificity of TAL-type III effectors. *Science*, 326(5959):1509–12.

[Borday et al., 2012] Borday, C., Cabochette, P., Parain, K., Mazurier, N., Janssens, S., Tran, H. T., Sekkali, B., Bronchain, O., Vleminckx, K., Locker, M., and Perron, M. (2012). Antagonistic cross-regulation between Wnt and

Hedgehog signalling pathways controls post-embryonic retinal proliferation. *Development*, 139(19):3499–3509.

[Boulton and Dayhaw-Barker, 2001] Boulton, M. and Dayhaw-Barker, P. (2001). The role of the retinal pigment epithelium: Topographical variation and ageing changes. *Eye*, 15(3):384–389.

[Brown et al., 2010] Brown, K. E., Keller, P. J., Ramialison, M., Rembold, M., Stelzer, E. H., Loosli, F., and Wittbrodt, J. (2010). Nlcam modulates midline convergence during anterior neural plate morphogenesis. *Developmental Biology*, 339(1):14–25.

[Carl and Wittbrodt, 1999] Carl, M. and Wittbrodt, J. (1999). Graded interference with FGF signalling reveals its dorsoventral asymmetry at the mid-hindbrain boundary. *Development*, 126(24):5659–5667.

[Casarosa et al., 2003] Casarosa, S., Amato, M. a., Andreazzoli, M., Gestri, G., Barsacchi, G., and Cremisi, F. (2003). Xrx1 controls proliferation and multipotency of retinal progenitors. *Molecular and Cellular Neuroscience*, 22(1):25–36.

[Caussinus et al., 2012] Caussinus, E., Kanca, O., and Affolter, M. (2012). Fluorescent fusion protein knockout mediated by anti-GFP nanobody. *Nature Structural and Molecular Biology*, 19(1):117–122.

[Centanin et al., 2014] Centanin, L., Ander, J.-J., Hoeckendorf, B., Lust, K., Kellner, T., Kraemer, I., Urbany, C., Hasel, E., Harris, W. A., Simons, B. D., and Wittbrodt, J. (2014). Exclusive multipotency and preferential asymmetric divisions in post-embryonic neural stem cells of the fish retina. *Development*, 141(18):3472–82.

[Centanin et al., 2011] Centanin, L., Hoeckendorf, B., and Wittbrodt, J. (2011). Fate restriction and multipotency in retinal stem cells. *Cell Stem Cell*, 9(6):553–562.

[Centanin and Wittbrodt, 2014] Centanin, L. and Wittbrodt, J. (2014). Retinal neurogenesis. *Development*, 141(2):241–4.

[Cepko et al., 1996] Cepko, C. L., Austin, C. P., Yang, X., Alexiades, M., and Ezzeddine, D. (1996). Cell fate determination in the vertebrate retina. *Proceedings of the National Academy of Sciences USA*, 93(2):589–595.

[Cerveny et al., 2010] Cerveny, K. L., Cavodeassi, F., Turner, K. J., de Jong-Curtain, T. a., Heath, J. K., and Wilson, S. W. (2010). The zebrafish flotte lotte mutant reveals that the local retinal environment promotes the differentiation of proliferating precursors emerging from their stem cell niche. *Development*, 137(13):2107–2115.

[Cerveny et al., 2012] Cerveny, K. L., Varga, M., and Wilson, S. W. (2012). Continued growth and circuit building in the anamniote visual system. *Developmental Neurobiology*, 72(3):328–345.

[Chassaing et al., 2014] Chassaing, N., Causse, A., Vigouroux, A., Delahaye, A., Alessandri, J. L., Boespflug-Tanguy, O., Boute-Benejean, O., Dollfus, H., Duban-Bedu, B., Gilbert-Dussardier, B., Giuliano, F., Gonzales, M., Holder-Espinasse, M., Isidor, B., Jacquemont, M.-L., Lacombe, D., Martin-Coignard, D., Mathieu-Dramard, M., Odent, S., Picone, O., Pinson, L., Quelin, C., Sigaudy, S., Toutain, A., Thauvin-Robinet, C., Kaplan, J., and Calvas, P. (2014). Molecular findings and clinical data in a cohort of 150 patients with anophthalmia/microphthalmia. *Clinical Genetics*, 86(4):326–334.

[Chow and Lang, 2001] Chow, R. L. and Lang, R. A. (2001). Early eye development in vertebrates. *Annual Review of Cell and Developmental Biology*, 17:255–96.

[Chuang et al., 1999] Chuang, C. J., Mathers, P. H., and Raymond, P. A. (1999). Expression of three Rx homeobox genes in embryonic and adult zebrafish. *Mechanisms of Development*, 84(1-2):195–198.

[Chuang and Raymond, 2001] Chuang, C. J. and Raymond, P. A. (2001). Zebrafish genes rx1 and rx2 help define the region of forebrain that gives rise to retina. *Developmental Biology*, 231(1):13–30.

[Clark et al., 2011] Clark, K. J., Balciunas, D., Pogoda, H. M., Ding, Y., Westcot, S. E., Bedell, V. M., Greenwood, T. M., Urban, M. D., Skuster, K. J., Petzold, A. M., Ni, J., Nielsen, A. L., Patowary, A., Scaria, V., Sivasubbu, S., Xu, X., Hammerschmidt, M., and Ekker, S. C. (2011). In vivo protein trapping produces a functional expression codex of the vertebrate proteome. *Nature Methods*, 8(6):506–515.

[Coles et al., 2004] Coles, B. L. K., Angénieux, B., Inoue, T., Del Rio-Tsonis, K., Spence, J. R., McInnes, R. R., Arsenijevic, Y., and van der Kooy, D.

(2004). Facile isolation and the characterization of human retinal stem cells. *Proceedings of the National Academy of Sciences*, 101(44):15772–15777.

[Cong et al., 2013] Cong, L., Ran, F. A., Cox, D., Lin, S., Barretto, R., Habib, N., Hsu, P. D., Wu, X., Jiang, W., Marraffini, L. A., and Zhang, F. (2013). Multiplex genome engineering using CRISPR/Cas systems. *Science*, 339(6121):819–823.

[Daniel et al., 2018] Daniel, K., Icha, J., Horenburg, C., Müller, D., Norden, C., and Mansfeld, J. (2018). Conditional control of fluorescent protein degradation by an auxin-dependent nanobody. *Nature Communications*, 9(1):doi: 10.1038/s41467–018–05855–5.

[Danno et al., 2008] Danno, H., Michiue, T., Hitachi, K., Yukita, A., Ishiura, S., and Asashima, M. (2008). Molecular links among the causative genes for ocular malformation: Otx2 and Sox2 coregulate Rax expression. *Proceedings of the National Academy of Sciences*, 105(14):5408–5413.

[Deng et al., 2012] Deng, D., Yan, C., Pan, X., Mahfouz, M., Wang, J., Zhu, J.-K., Shi, Y., and Yan, N. (2012). Structural basis for sequence-specific recognition of DNA by TAL effectors. *Science*, 335(6069):720–723.

[Deschet et al., 1999] Deschet, K., Bourrat, F., Ristoratore, F., Chourrout, D., and Joly, J.-S. (1999). Expression of the medaka (Oryzias latipes) Ol-Rx3 paired-like gene in two diencephalic derivatives, the eye and the hypothalamus. *Mechanisms of Development*, 83(1-2):179–182.

[Eckert et al., 2017] Eckert, P., Schütz, L., Wittbrodt, J., and Heermann, S. (2017). Optic fissure margin morphogenesis sets the stage for consecutive optic fissure fusion, pioneered by a distinct subset of margin cells using a hyaloid vessel as scaffold. *bioRxiv*, 141275:doi: https://doi.org/10.1101/141275.

[El Yakoubi et al., 2012] El Yakoubi, W., Borday, C., Hamdache, J., Parain, K., Tran, H. T., Vleminckx, K., Perron, M., and Locker, M. (2012). Hes4 controls proliferative properties of neural stem cells during retinal ontogenesis. *Stem Cells*, 30(12):2784–2795.

[Esteve and Bovolenta, 2006] Esteve, P. and Bovolenta, P. (2006). Secreted inducers in vertebrate eye development: More functions for old morphogens. *Current Opinion in Neurobiology*, 16(1):13–19.

[Fischer et al., 2002] Fischer, A., Dierks, B., and Reh, T. (2002). Exogenous growth factors induce the production of ganglion cells at the retinal margin. *Development*, 129(9):2283–2291.

[Fischer et al., 2013] Fischer, A. J., Bosse, J. L., and El-Hodiri, H. M. (2013). The ciliary marginal zone (CMZ) in development and regeneration of the vertebrate eye. *Experimental Eye Research*, Nov(116):199–204.

[Fischer et al., 2001] Fischer, A. J., Hendrickson, A., and Reh, T. A. (2001). Immunocytochemical characterization of cysts in the peripheral retina and pars plana of the adult primate. *Investigative Ophthalmology and Visual Science*, 42(13):3256–3263.

[Fischer and Reh, 2000] Fischer, A. J. and Reh, T. A. (2000). Identification of a proliferating marginal zone of retinal progenitors in postnatal chickens. *Developmental Biology*, 220(2):197–210.

[Fischer et al., 2008] Fischer, A. J., Ritchey, E. R., Scott, M. A., and Wynne, A. (2008). Bullwhip neurons in the retina regulate the size and shape of the eye. *Developmental Biology*, 317(1):196–212.

[Fish et al., 2014] Fish, M. B., Nakayama, T., Fisher, M., Hirsch, N., Cox, A., Reeder, R., Carruthers, S., Hall, A., Stemple, D. L., and Grainger, R. M. (2014). Xenopus mutant reveals necessity of rax for specifying the eye field which otherwise forms tissue with telencephalic and diencephalic character. *Developmental Biology*, 395(2):317–330.

[Fukui et al., 1993] Fukui, A., Nakamura, T., Sugino, K., Takio, K., Uchiyama, H., Asashima, M., and Sugino, H. (1993). Isolation and Characterization of Xenopus Follistatin and Activins. *Developmental Biology*, 159(1):131–139.

[Furukawa et al., 1997] Furukawa, T., Kozak, C. a., and Cepko, C. L. (1997). Rax, a novel paired-type homeobox gene, shows expression in the anterior neural fold and developing retina. *Proceedings of the National Academy of Sciences*, 94(7):3088–3093.

[Furutani-Seiki and Wittbrodt, 2004] Furutani-Seiki, M. and Wittbrodt, J. (2004). Medaka and zebrafish, an evolutionary twin study. *Mechanisms of Development*, 121(7-8):629–637.

[Gerkema et al., 2013] Gerkema, M. P., Davies, W. I. L., Foster, R. G., Menaker, M., and Hut, R. A. (2013). The nocturnal bottleneck and the

evolution of activity patterns in mammals. *Proceedings of the Royal Society B: Biological Sciences*, 280(1765):doi: 10.1098/rspb.2013.0508.

[Giannaccini et al., 2013] Giannaccini, M., Giudetti, G., Biasci, D., Mariotti, S., Martini, D., Barsacchi, G., and Andreazzoli, M. (2013). Brief report: Rx1 defines retinal precursor identity by repressing alternative fates through the activation of TLE2 and Hes4. *Stem Cells*, 31(12):2842–2847.

[Giudetti et al., 2014] Giudetti, G., Giannaccini, M., Biasci, D., Mariotti, S., Degl'innocenti, A., Perrotta, M., Barsacchi, G., and Andreazzoli, M. (2014). Characterization of the Rx1-dependent transcriptome during early retinal development. *Developmental Dynamics*, 243(10):1352–1361.

[Gonzalez-Rodriguez et al., 2010] Gonzalez-Rodriguez, J., Pelcastre, E. L., Tovilla-Canales, J. L., Garcia-Ortiz, J. E., Amato-Almanza, M., Villanueva-Mendoza, C., Espinosa-Mattar, Z., and Zenteno, J. C. (2010). Mutational screening of CHX10, GDF6, OTX2, RAX and SOX2 genes in 50 unrelated microphthalmia-anophthalmia-coloboma (MAC) spectrum cases. *British Journal of Ophthalmology*, 94(8):1100–1104.

[Gutierrez-Triana et al., 2016] Gutierrez-Triana, J. A., Mateo, J. L., Ibberson, D., Ryu, S., and Wittbrodt, J. (2016). iDamIDseq and iDEAR: an improved method and computational pipeline to profile chromatin-binding proteins. *Development*, 143(22):4272–4278.

[Gutierrez-Triana et al., 2018] Gutierrez-Triana, J. A., Tavhelidse, T., Thumberger, T., Thomas, I., Wittbrodt, B., Kellner, T., Anlas, K., Tsingos, E., and Wittbrodt, J. (2018). Efficient single-copy HDR by 5 ' modified long dsDNA donors. *eLife*, Aug 29(7):doi: 10.7554/eLife.39468.

[Gutschner et al., 2016] Gutschner, T., Haemmerle, M., Genovese, G., Draetta, G. F., and Chin, L. (2016). Post-translational Regulation of Cas9 during G1 Enhances Homology-Directed Repair. *Cell Reports*, 14(6):1555–1566.

[Hall et al., 2012] Hall, M. I., Kamilar, J. M., and Christopher Kirk, E. (2012). Eye shape and the nocturnal bottleneck of mammals. *Proceedings of the Royal Society B: Biological Sciences*, 279(1749):4962–4968.

[Harris and Perron, 1998] Harris, W. A. and Perron, M. (1998). Molecular recapitulation: the growth of the vertebrate retina. *The International Journal of Developmental Biology*, 42(3):299–304.

[Heermann et al., 2015] Heermann, S., Schütz, L., Lemke, S., Krieglstein, K., and Wittbrodt, J. (2015). Eye morphogenesis driven by epithelial flow into the optic cup facilitated by modulation of bone morphogenetic protein. *eLife*, Feb 24(4):doi: 10.7554/eLife.05216.

[Heesy and Hall, 2010] Heesy, C. P. and Hall, M. I. (2010). The nocturnal bottleneck and the evolution of mammalian vision. *Brain, Behavior and Evolution*, 75(3):195–203.

[Horvath and Barrangou, 2010] Horvath, P. and Barrangou, R. (2010). CRISPR/Cas, the immune system of bacteria and archaea. *Science*, 327(5962):167–170.

[Hsu et al., 1998] Hsu, D. R., Economides, A. N., Wang, X., Eimon, P. M., and Harland, R. M. (1998). The Xenopus dorsalizing factor Gremlin identifies a novel family of secreted proteins that antagonize BMP activities. *Molecular Cell*, 1(5):673–683.

[Hsu et al., 2013] Hsu, P. D., Scott, D. A., Weinstein, J. A., Ran, F. A., Konermann, S., Agarwala, V., Li, Y., Fine, E. J., Wu, X., Shalem, O., Cradick, T. J., Marraffini, L. A., Bao, G., and Zhang, F. (2013). DNA targeting specificity of RNA-guided Cas9 nucleases. *Nature Biotechnology*, 31(9):827–832.

[Hustedt and Durocher, 2017] Hustedt, N. and Durocher, D. (2017). The control of DNA repair by the cell cycle. *Nature Cell Biology*, 19(1):1–9.

[Iemura et al., 1998] Iemura, S.-i., Yamamoto, T. S., Takagi, C., Uchiyama, H., Natsume, T., Shimasaki, S., Sugino, H., and Ueno, N. (1998). Direct binding of follistatin to a complex of bone-morphogenetic protein and its receptor inhibits ventral and epidermal cell fates in early Xenopus embryo. *Proceedings of the National Academy of Sciences*, 95(16):9337–9342.

[Inoue and Wittbrodt, 2011] Inoue, D. and Wittbrodt, J. (2011). One for All-A Highly Efficient and Versatile Method for Fluorescent Immunostaining in Fish Embryos. *PLoS ONE*, 6(5):doi: 10.1371/journal.pone.0019713.

[Irie et al., 2015] Irie, S., Sanuki, R., Muranishi, Y., Kato, K., Chaya, T., and Furukawa, T. (2015). Rax Homeoprotein Regulates Photoreceptor Cell Maturation and Survival in Association with Crx in the Postnatal Mouse Retina. *Molecular and Cellular Biology*, 35(15):2583–2596.

[Iwamatsu, 2004] Iwamatsu, T. (2004). Stages of normal development in the medaka Oryzias latipes. *Mechanisms of Development*, 121(7-8):605–18.

[Jinek et al., 2012] Jinek, M., Chylinski, K., Fonfara, I., Hauer, M., Doudna, J. A., and Charpentier, E. (2012). A programmable dual-RNA-guided DNA endonuclease in adaptive bacterial immunity. *Science*, 337(6096):816–821.

[Johns, 1977] Johns, P. R. (1977). Growth of the adult goldfish eye. III. Source of the new retinal cells. *Journal of Comparative Neurology*, 176(3):343–57.

[Joung and Sander, 2013] Joung, J. K. and Sander, J. D. (2013). TALENs: A widely applicable technology for targeted genome editing. *Nature Reviews Molecular Cell Biology*, 14(1):49–55.

[Kay and Bonas, 2009] Kay, S. and Bonas, U. (2009). How Xanthomonas type III effectors manipulate the host plant. *Current Opinion in Microbiology*, 12(1):37–43.

[Kelly et al., 2016] Kelly, L. E., Martinez-De Luna, R. I., and El-Hodiri, H. M. (2016). Autoregulation of retinal homeobox (rax) gene promoter activity through a highly conserved genomic element. *Genesis*, 54(11):562–567.

[Kennedy et al., 2004] Kennedy, B. N., Stearns, G. W., Smyth, V. A., Ramamurthy, V., Van Eeden, F., Ankoudinova, I., Raible, D., Hurley, J. B., and Brockerhoff, S. E. (2004). Zebrafish rx3 and mab21l2 are required during eye morphogenesis. *Developmental Biology*, 270(2):336–349.

[Kim et al., 1996a] Kim, C.-H., Ueshima, E., Muraoka, O., Tanaka, H., Yeo, S.-Y., Huh, T.-L., and Miki, N. (1996a). Zebrafish elav/HuC homologue as a very early neuronal marker. *Neuroscience Letters*, 216(2):109–112.

[Kim et al., 1996b] Kim, Y.-G., Cha, J., and Chandrasegaran, S. (1996b). Hybrid restriction enzymes: zinc finger fusions to Fok I cleavage domain. *Proceedings of the National Academy of Sciences USA*, 93(3):1156–60.

[Kimmel et al., 1995] Kimmel, C. B., Ballard, W. W., Kimmel, S. R., Ullmann, B., and Schilling, T. F. (1995). Stages of embryonic development of the zebrafish. *Developmental Dynamics*, 203(3):253–310.

[Kimura et al., 2000] Kimura, A., Singh, D., Wawrousek, E. F., Kikuchi, M., Nakamura, M., and Shinohara, T. (2000). Both PCE-1/RX and OTX/CRX interactions are necessary for photoreceptor-specific gene expression. *The Journal of Biological Chemistry*, 275(2):1152–1160.

[Kirchmaier et al., 2013] Kirchmaier, S., Lust, K., and Wittbrodt, J. (2013). Golden GATEway Cloning - A Combinatorial Approach to Generate Fusion and Recombination Constructs. *PloS one*, 8(10):doi: 10.1371/journal.pone.0076117.

[Kiyama et al., 2012] Kiyama, T., Li, H., Gupta, M., Lin, Y.-P., Chuang, a. Z., Otteson, D. C., and Wang, S. W. (2012). Distinct Neurogenic Potential in the Retinal Margin and the Pars Plana of Mammalian Eye. *Journal of Neuroscience*, 32(37):12797–12807.

[Knickmeyer et al., 2018] Knickmeyer, M. D., Mateo, J. L., Eckert, P., Roussa, E., Rahhal, B., Zuniga, A., Krieglstein, K., Wittbrodt, J., and Heermann, S. (2018). TGFb-facilitated optic fissure fusion and the role of bone morphogenetic protein antagonism. *Open Biology*, 8(3):doi: 10.1098/rsob.170134.

[Köster et al., 1997] Köster, R., Stick, R., Loosli, F., and Wittbrodt, J. (1997). Medaka spalt acts as a target gene of hedgehog signaling. *Development (Cambridge, England)*, 124(16):3147–3156.

[Kuwahara et al., 2015] Kuwahara, A., Ozone, C., Nakano, T., Saito, K., Eiraku, M., and Sasai, Y. (2015). Generation of a ciliary margin-like stem cell niche from self-organizing human retinal tissue. *Nat Commun*, 6(6286):doi: 10.1038/ncomms7286.

[Lagutin et al., 2003] Lagutin, O. V., Zhu, Changqi, C., Kobayashi, D., Topczewski, J., Shimamura, K., Puelles, L., Russell, H. R., McKinnon, P. J., Solnica-Krezel, L., and Oliver, G. (2003). Six3 repression of Wnt signaling in the anterior neuroectoderm is essential for vertebrate forebrain development. *Genes and Development*, 17(3):368–79.

[Lequeux et al., 2008] Lequeux, L., Rio, M., Vigouroux, a., Titeux, M., Etchevers, H., Malecaze, F., Chassaing, N., and Calvas, P. (2008). Confirmation of RAX gene involvement in human anophthalmia. *Clinical Genetics*, 74(4):392–395.

[Livesey and Cepko, 2001] Livesey, F. J. and Cepko, C. L. (2001). Vertebrate neural cell-fate determination: lessons from the retina. *Nature Reviews Neuroscience*, 2(2):109–18.

[London et al., 2009] London, N. J. S., Kessler, P., Williams, B., Pauer, G. J., Hagstrom, S. a., and Traboulsi, E. I. (2009). Sequence alterations in RX

in patients with microphthalmia, anophthalmia, and coloboma. *Molecular Vision*, 15:162–7.

[Loosli et al., 1998] Loosli, F., Köster, R. W., Carl, M., Krone, A., and Wittbrodt, J. (1998). Six3, a medaka homologue of the Drosophila homeobox gene sine oculis is expressed in the anterior embryonic shield and the developing eye. *Mechanisms of Development*, 74(1-2):159–164.

[Loosli et al., 2003] Loosli, F., Staub, W., Finger-Baier, K. C., Ober, E. A., Verkade, H., Wittbrodt, J., and Baier, H. (2003). Loss of eyes in zebrafish caused by mutation of chokh/rx3. *EMBO reports*, 4(9):894–9.

[Loosli et al., 2001] Loosli, F., Winkler, S., Burgtorf, C., Wurmbach, E., Ansorge, W., Henrich, T., Grabher, C., Arendt, D., Carl, M., Krone, a., Grzebisz, E., and Wittbrodt, J. (2001). Medaka eyeless is the key factor linking retinal determination and eye growth. *Development (Cambridge, England)*, 128(20):4035–44.

[Loosli et al., 1999] Loosli, F., Winkler, S., and Wittbrodt, J. (1999). Six3 overexpression initiates the formation of ectopic retina Six3 overexpression initiates the formation of ectopic retina. *Genes and Development*, 13(6):649–654.

[Mali et al., 2013] Mali, P., Esvelt, K. M., and Church, G. M. (2013). Cas9 as a versatile tool for engineering biology. *Nature Methods*, 10(10):957–963.

[Marcucci et al., 2016] Marcucci, F., Murcia-Belmonte, V., Wang, Q., Coca, Y., Ferreiro-Galve, S., Kuwajima, T., Khalid, S., Ross, M. E., Mason, C., and Herrera, E. (2016). The Ciliary Margin Zone of the Mammalian Retina Generates Retinal Ganglion Cells. *Cell Reports*, 17(12):3153–3164.

[Martín-Partido and Francisco-Morcillo, 2015] Martín-Partido, G. and Francisco-Morcillo, J. (2015). The role of Islet-1 in cell specification, differentiation, and maintenance of phenotypes in the vertebrate neural retina. *Neural Regeneration Research*, 10(12):1951–1952.

[Martinez-de Luna et al., 2010] Martinez-de Luna, R. I., Moose, H. E., Kelly, L. E., Nekkalapudi, S., and El-Hodiri, H. M. (2010). Regulation of retinal homeobox gene transcription by cooperative activity among cis-elements. *Gene*, 467(1-2):13–24.

[Martinez-Morales et al., 2017] Martinez-Morales, J.-R., Cavodeassi, F., and Bovolenta, P. (2017). Coordinated Morphogenetic Mechanisms Shape the Vertebrate Eye. *Frontiers in Neuroscience*, 11(721):doi: 10.3389/fnins.2017.00721.

[Martinez-Morales et al., 2005] Martinez-Morales, J. R., Del Bene, F., Nica, G., Hammerschmidt, M., Bovolenta, P., and Wittbrodt, J. (2005). Differentiation of the vertebrate retina is coordinated by an FGF signaling center. *Developmental Cell*, 8(4):565–574.

[Martinez-Morales et al., 2009] Martinez-Morales, J. R., Rembold, M., Greger, K., Simpson, J. C., Brown, K. E., Quiring, R., Pepperkok, R., Martin-Bermudo, M. D., Himmelbauer, H., and Wittbrodt, J. (2009). Ojoplano-Mediated Basal Constriction Is Essential for Optic Cup Morphogenesis. *Development (Cambridge, England)*, 136(13):2165–75.

[Martinez-Morales and Wittbrodt, 2009] Martinez-Morales, J. R. and Wittbrodt, J. (2009). Shaping the vertebrate eye. *Current Opinion in Genetics and Development*, 19(5):511–517.

[Martínez-Navarrete et al., 2008] Martínez-Navarrete, G. C., Angulo, A., Martín-Nieto, J., and Cuenca, N. (2008). Gradual morphogenesis of retinal neurons in the peripheral retinal margin of adult monkeys and humans. *The Journal of Comparative Neurology*, 511(4):557–80.

[Maruyama et al., 2015] Maruyama, T., Dougan, S. K., Truttmann, M., Bilate, A. M., Ingram, J. R., and Ploegh, H. L. (2015). Increasing the efficiency of precise genome editing with CRISPR-Cas9 by inhibition of nonhomologous end joining. *Nature Biotechnology*, 33(5):538–542.

[Masai et al., 2000] Masai, I., Stemple, D. L., Okamoto, H., and Wilson, S. W. (2000). Midline signals regulate retinal neurogenesis in zebrafish. *Neuron*, 27(2):251–263.

[Mathers et al., 1997] Mathers, P. H., Grinberg, A., Mahon, K. A., and Jamrich, M. (1997). The Rx homeobox gene is essential for vertebrate eye development. *Nature*, 387(6633):603–607.

[Miller et al., 2007] Miller, J. C., Holmes, M. C., Wang, J., Guschin, D. Y., Lee, Y.-L., Rupniewski, I., Beausejour, C. M., Waite, A. J., Wang, N. S., Kim, K. A., Gregory, P. D., Pabo, C. O., and Rebar, E. J. (2007). An

improved zinc-finger nuclease architecture for highly specific genome editing. *Nature Biotechnology*, 25(7):778–785.

[Miller et al., 2011] Miller, J. C., Tan, S., Qiao, G., Barlow, K. A., Wang, J., Xia, D. F., Meng, X., Paschon, D. E., Leung, E., Hinkley, S. J., Dulay, G. P., Hua, K. L., Ankoudinova, I., Cost, G. J., Urnov, F. D., Zhang, H. S., Holmes, M. C., Zhang, L., Gregory, P. D., and Rebar, E. J. (2011). A TALE nuclease architecture for efficient genome editing. *Nature Biotechnology*, 29(2):143–150.

[Mladenov and Iliakis, 2011] Mladenov, E. and Iliakis, G. (2011). Induction and repair of DNA double strand breaks: The increasing spectrum of non-homologous end joining pathways. *Mutation Research*, 711(1-2):61–72.

[Moscou and Bogdanove, 2009] Moscou, M. J. and Bogdanove, A. J. (2009). A simple cipher governs DNA recognition by TAL effectors. *Science*, 326(5959):1501.

[Moshiri et al., 2005] Moshiri, A., McGuire, C. R., and Reh, T. A. (2005). Sonic hedgehog regulates proliferation of the retinal ciliary marginal zone in posthatch chicks. *Developmental Dynamics*, 233(1):66–75.

[Moshiri and Reh, 2004] Moshiri, A. and Reh, T. A. (2004). Persistent Progenitors at the Retinal Margin of ptc+/- Mice. *The Journal of Neuroscience*, 24(1):229–237.

[Muranishi et al., 2012] Muranishi, Y., Terada, K., and Furukawa, T. (2012). An essential role for Rax in retina and neuroendocrine system development. *Development Growth and Differentiation*, 54(3):341–348.

[Muranishi et al., 2011] Muranishi, Y., Terada, K., Inoue, T., Katoh, K., Tsujii, T., Sanuki, R., Kurokawa, D., Aizawa, S., Tamaki, Y., and Furukawa, T. (2011). An essential role for RAX homeoprotein and NOTCH-HES signaling in Otx2 expression in embryonic retinal photoreceptor cell fate determination. *Journal of Neuroscience*, 31(46):16792–16807.

[Nasonkin et al., 2013] Nasonkin, I. O., Merbs, S. L., Lazo, K., Oliver, V. F., Brooks, M., Patel, K., Enke, R. A., Nellissery, J., Jamrich, M., Le, Y. Z., Bharti, K., Fariss, R. N., Rachel, R. A., Zack, D. J., Rodriguez-Boulan, E. J., and Swaroop, A. (2013). Conditional knockdown of DNA methyltransferase 1 reveals a key role of retinal pigment epithelium integrity in photoreceptor outer segment morphogenesis. *Development*, 140(6):1330–1341.

[Nelson et al., 2008] Nelson, S. M., Frey, R. A., Wardwell, S. L., and Stenkamp, D. L. (2008). The developmental sequence of gene expression within the rod photoreceptor lineage in embryonic zebrafish. *Developmental Dynamics*, 237(10):2903–2917.

[Nelson et al., 2009] Nelson, S. M., Park, L., and Stenkamp, D. L. (2009). Retinal homeobox 1 is required for retinal neurogenesis and photoreceptor differentiation in embryonic zebrafish. *Developmental Biology*, 328(1):24–39.

[Neumann and Nuesslein-Volhard, 2000] Neumann, C. J. and Nuesslein-Volhard, C. (2000). Patterning of the zebrafish retina by a wave of sonic Hedgehog activity. *Science*, 289(5487):2137–2139.

[Nieuwkoop and Faber, 1994] Nieuwkoop, P. D. and Faber, J. (1994). *Normal Table of Xenopus laevis (Daudin).* Garland Publishing Inc, New York.

[Ohnuma et al., 2002] Ohnuma, S.-i., Hopper, S., Wang, K. C., Philpott, A., and Harris, W. A. (2002). Co-ordinating retinal histogenesis: early cell cycle exit enhances early cell fate determination in the Xenopus retina. *Development*, 129(10):2435–46.

[Onichtchouk et al., 1999] Onichtchouk, D., Chen, Y. G., Dosch, R., Gawantka, V., Delius, H., Massagué, J., and Niehrs, C. (1999). Silencing of TGF-β signalling by the pseudoreceptor BAMBI. *Nature*, 401(6752):480–485.

[Onwochei et al., 2000] Onwochei, B. C., Simon, J. W., Bateman, J. B., Couture, K. C., and Mir, E. (2000). Ocular Colobomata. *Survey of Ophthalmology*, 45(3):175–194.

[Orquera and de Souza, 2017] Orquera, D. P. and de Souza, F. S. (2017). Evolution of the Rax family of developmental transcription factors in vertebrates. *Mechanisms of Development*, 144(Pt B):163–170.

[Pan et al., 2010] Pan, Y., Martinez-De Luna, R. I., Lou, C. H., Nekkalapudi, S., Kelly, L. E., Sater, A. K., and El-Hodiri, H. M. (2010). Regulation of photoreceptor gene expression by the retinal homeobox (Rx) gene product. *Developmental Biology*, 339(2):494–506.

[Pan et al., 2006] Pan, Y., Nekkalapudi, S., Kelly, L. E., and El-Hodiri, H. M. (2006). The Rx-like homeobox gene (Rx-L) is necessary for normal photoreceptor development. *Investigative Ophthalmology and Visual Science*, 47(10):4245–4253.

[Parain et al., 2012] Parain, K., Mazurier, N., Bronchain, O., Borday, C., Cabochette, P., Chesneau, A., Colozza, G., Yakoubi, W. E., Hamdache, J., Locker, M., Gilchrist, M. J., Pollet, N., and Perron, M. (2012). A large scale screen for neural stem cell markers in Xenopus retina. *Developmental Neurobiology*, 72(4):491–506.

[Perron and Harris, 2000] Perron, M. and Harris, W. A. (2000). Retinal stem cells in vertebrates. *Bioessays*, 22(8):685–688.

[Perron et al., 1998] Perron, M., Kanekar, S., Vetter, M. L., and Harris, W. A. (1998). The genetic sequence of retinal development in the ciliary margin of the Xenopus eye. *Developmental biology*, 199(2):185–200.

[Piccolo et al., 1999] Piccolo, S., Agius, E., Leyns, L., Bhattacharyya, S., Grunz, H., Bouwmeester, T., and De Robertis, E. M. (1999). The head inducer Cerberus is a multifunctional antagonist of Nodal, BMP and Wnt signals. *Nature*, 397(6721):707–710.

[Picelli et al., 2014] Picelli, S., Faridani, O. R., Björklund, A. s. K., Winberg, G., Sagasser, S., and Sandberg, R. (2014). Full-length RNA-seq from single cells using Smart-seq2. *Nature Protocols*, 9(1):171–181.

[R Core Team, 2018] R Core Team (2018). *R: A Language and Environment for Statistical Computing*. R Foundation for Statistical Computing, Vienna, Austria.

[Rasmussen et al., 2001] Rasmussen, J. T., Deardorff, M. A., Tan, C., Rao, M. S., Klein, P. S., and Vetter, M. L. (2001). Regulation of eye development by frizzled signaling in Xenopus. *Proceedings of the National Academy of Sciences of the United States of America*, 98(7):3861–3866.

[Raymond et al., 2006] Raymond, P. a., Barthel, L. K., Bernardos, R. L., and Perkowski, J. J. (2006). Molecular characterization of retinal stem cells and their niches in adult zebrafish. *BMC Developmental Biology*, 6(36).

[Reinhardt, 2014] Reinhardt, R. (2014). *Cell intrinsic control of stem cell features in the retina*. PhD thesis, Ruprecht-Karls-Universität Heidelberg.

[Reinhardt et al., 2015] Reinhardt, R., Centanin, L., Tavhelidse, T., Inoue, D., Wittbrodt, B., Concordet, J.-P., Martinez-Morales, J. R., and Wittbrodt, J. (2015). Sox2, Tlx, Gli3, and Her9 converge on Rx2 to define retinal stem cells in vivo. *The EMBO Journal*, 34(11):1572–1588.

[Rembold et al., 2006] Rembold, M., Loosli, F., Adams, R. J., and Wittbrodt, J. (2006). Individual Cell Migration Serves as the Driving Force for Optic Vesicle Evagination. *Science*, 313(5790):1130–1134.

[Rinaldi et al., 2017] Rinaldi, F. C., Doyle, L. A., Stoddard, B. L., and Bogdanove, A. J. (2017). The effect of increasing numbers of repeats on TAL effector DNA binding specificity. *Nucleic Acids Research*, 45(11):6960–6970.

[Rodgers, 2017] Rodgers, H. M. (2017). *The role of rx in embryonic retinogenesis: determining genetic influences on optic vesicle formation and photoreceptor cell fate*. PhD thesis, School of Medicine at West Virginia University.

[Rohner et al., 2013] Rohner, N., Jarosz, D. F., Kowalko, J. E., Yoshizawa, M., Jeffery, W. R., Borowsky, R. L., Lindquist, S., and Tabin, C. J. (2013). Cryptic Variation in Morphological Evolution: HSP90 as a Capacitor for Loss of Eyes in Cavefish. *Science*, 342(6164):1372–1375.

[Rojas-Muñoz et al., 2005] Rojas-Muñoz, A., Dahm, R., and Nüsslein-Volhard, C. (2005). chokh/rx3 specifies the retinal pigment epithelium fate independently of eye morphogenesis. *Developmental Biology*, 288(2):348–62.

[Sampath et al., 1998] Sampath, K., Rubinstein, A. L., Cheng, A. M. S., Liang, J. O., Fekany, K., Solnica-Krezel, L., Korzh, V., Halpern, M. E., and Wright, C. V. (1998). Induction of the zebrafish ventral brain and floorplate requires cyclops/nodal signalling. *Nature*, 395(6698):185–9.

[San Filippo et al., 2008] San Filippo, J., Sung, P., and Klein, H. (2008). Mechanism of eukaryotic homologous recombination. *Annual Review of Biochemistry*, 77:229–57.

[Sasai et al., 1995] Sasai, Y., Lu, B., Steinbeisser, H., and De Robertis, E. M. (1995). Regulation of neural induction by the Chd and Bmp-4 antagonistic patterning signals in Xenopus. *Nature*, 376:333–336.

[Schindelin et al., 2012] Schindelin, J., Arganda-Carreras, I., Frise, E., Kaynig, V., Longair, M., Pietzsch, T., Preibisch, S., Rueden, C., Saalfeld, S., Schmid, B., Tinevez, J. Y., White, D. J., Hartenstein, V., Eliceiri, K., Tomancak, P., and Cardona, A. (2012). Fiji: An open-source platform for biological-image analysis. *Nature Methods*, 9(7):676–682.

[Shi et al., 2017] Shi, D., Tavhelidse, T., Thumberger, T., Wittbrodt, J., and Greb, T. (2017). Bifacial stem cell niches in fish and plants. *Current Opinion in Genetics and Development*, Aug(45):28–33.

[Sidhaye and Norden, 2017] Sidhaye, J. and Norden, C. (2017). Concerted action of neuroepithelial basal shrinkage and active epithelial migration ensures efficient optic cup morphogenesis. *eLife*, Apr 4(6):doi: 10.7554/eLife.22689.

[Sinn and Wittbrodt, 2013] Sinn, R. and Wittbrodt, J. (2013). An eye on eye development. *Mechanisms of Development*, 130(6-8):347–358.

[Sivasubbu et al., 2006] Sivasubbu, S., Balciunas, D., Davidson, A. E., Pickart, M. a., Hermanson, S. B., Wangensteen, K. J., Wolbrink, D. C., and Ekker, S. C. (2006). Gene-breaking transposon mutagenesis reveals an essential role for histone H2afza in zebrafish larval development. *Mechanisms of Development*, 123(7):513–529.

[Smith and Harland, 1992] Smith, W. C. and Harland, R. M. (1992). Expression Cloning of noggin , a New Dorsalizing Factor Localized to the Spemann Organizer in Xenopus Embryos. *Cell*, 70:829–840.

[Stemmer, 2015] Stemmer, M. (2015). *Studying neuronal differentiation in the teleost model systems medaka and cavefish including the establishment of a CRISPR/Cas9 mediated knock-in approach.* PhD thesis, Ruprecht-Karls-Universität Heidelberg.

[Stemmer et al., 2015] Stemmer, M., Thumberger, T., del Sol Keyer, M., Wittbrodt, J., and Mateo, J. L. (2015). CCTop: An Intuitive, Flexible and Reliable CRISPR/Cas9 Target Prediction Tool. *Plos One*, 10(4):doi: 10.1371/journal.pone.0124633.

[Stern, 2006] Stern, C. D. (2006). Neural induction: 10 years on since the 'default model'. *Current Opinion in Cell Biology*, 18(6):692–697.

[Stigloher et al., 2006] Stigloher, C., Ninkovic, J., Laplante, M., Geling, A., Tannhäuser, B., Topp, S., Kikuta, H., Becker, T. S., Houart, C., and Bally-Cuif, L. (2006). Segregation of telencephalic and eye-field identities inside the zebrafish forebrain territory is controlled by Rx3. *Development*, 133(15):2925–2935.

[Straznicky and Gaze, 1971] Straznicky, K. and Gaze, R. M. (1971). The growth of the retina in Xenopus laevis: an autoradiographic study. *Journal of Embryology and Experimental Morphology*, 26(1):67 – 79.

[Sun and Zhao, 2013] Sun, N. and Zhao, H. (2013). Transcription activator-like effector nucleases (TALENs): a highly efficient and versatile tool for genome editing. *Biotechnology and Bioengineering*, 110(7):1811–21.

[Tang et al., 2017] Tang, X., Gao, J., Jia, X., Zhao, W., Zhang, Y., Pan, W., and He, J. (2017). Bipotent progenitors as embryonic origin of retinal stem cells. *The Journal of Cell Biology*, 216(6):1833–1847.

[Terada et al., 2006] Terada, K., Kitayama, A., Kanamoto, T., Ueno, N., and Furukawa, T. (2006). Nucleosome regulator Xhmgb3 is required for cell proliferation of the eye and brain as a downstream target of Xenopus rax/Rx1. *Developmental Biology*, 291(2):398–412.

[Terns and Terns, 2011] Terns, M. P. and Terns, R. M. (2011). CRISPR-based adaptive immune systems. *Current Opinion in Microbiology*, 14(3):321–327.

[Terns and Terns, 2014] Terns, R. M. and Terns, M. P. (2014). CRISPR-based technologies: Prokaryotic defense weapons repurposed. *Trends in Genetics*, 30(3):111–118.

[Tropepe et al., 2000] Tropepe, V., Coles, B. L. K., Chiasson, B. J., Horsford, J. D., Elia, A. J., McInnes, R. R., and Van der Kooy, D. (2000). Retinal stem cells in the adult mammalian eye. *Science*, 287(5460):2032–2036.

[Tsingos et al., 2018] Tsingos, E., Höckendorf, B., Sütterlin, T., Kirchmaier, S., Grabe, N., Centanin, L., and Wittbrodt, J. (2018). Retinal stem cells modulate proliferative parameters to coordinate post-embryonic morphogenesis in the eye of fish. *bioRxiv*, 437269:doi: https://doi.org/10.1101/437269.

[Tucker et al., 2001] Tucker, P., Laemle, L., Munson, A., Kanekar, S., Oliver, E. R., Brown, N., Schlecht, H., Vetter, M., and Glaser, T. (2001). The eyeless mouse mutation (ey1) removes an alternative start codon from the Rx/rax homeobox gene. *Genesis*, 31(1):43–53.

[Urnov et al., 2010] Urnov, F. D., Rebar, E. J., Holmes, M. C., Zhang, H. S., and Gregory, P. D. (2010). Genome editing with engineered zinc finger nucleases. *Nature Reviews Genetics*, 11(9):636–646.

[Voronina et al., 2004] Voronina, V. A., Kozhemyakina, E. A., O'Kernick, C. M., Kahn, N. D., Wenger, S. L., Linberg, J. V., Schneider, A. S., and Mathers, P. H. (2004). Mutations in the human RAX homeobox gene in a patient with anophthalmia and sclerocornea. *Human Molecular Genetics*, 13(3):315–322.

[Voronina et al., 2005] Voronina, V. A., Kozlov, S., Mathers, P. H., and Lewandoski, M. (2005). Conditional alleles for activation and inactivation of the mouse Rx homeobox gene. *Genesis*, 41(4):160–164.

[Walls, 1942] Walls, G. L. (1942). *The vertebrate eye and its adaptive radiation*. Cranbrook Institute of Science, Bloomfield Hills.

[Wan et al., 2016] Wan, Y., Almeida, a. D., Rulands, S., Chalour, N., Muresan, L., Wu, Y., Simons, B. D., He, J., and Harris, W. a. (2016). The ciliary marginal zone of the zebrafish retina: clonal and time-lapse analysis of a continuously growing tissue. *Development*, 143(7):1099–1107.

[Wang et al., 2017] Wang, L., Yang, L., Guo, Y., Du, W., Yin, Y., Zhang, T., and Lu, H. (2017). Enhancing Targeted Genomic DNA Editing in Chicken Cells Using the CRISPR/Cas9 System. *PLoS One*, 12(1):doi: 10.1371/journal.pone.0169768.

[Wang et al., 2004] Wang, Q.-l., Chen, S., Esumi, N., Swain, P. K., Haines, H. S., Peng, G., Melia, B. M., McIntosh, I., Heckenlively, J. R., Jacobson, S. G., Stone, E. M., Swaroop, A., and Zack, D. J. (2004). QRX, a novel homeobox gene, modulates photoreceptor gene expression. *Human Molecular Genetics*, 13(10):1025–40.

[Weinhardt et al., 2018] Weinhardt, V., Shkarin, R., Wernet, T., Wittbrodt, J., Baumbach, T., and Loosli, F. (2018). Quantitative morphometric analysis of adult teleost fish by X-ray computed tomography. *Scientific Reports*, 8(1):doi: 10.1038/s41598–018–34848–z.

[Wetts et al., 1989] Wetts, R., Serbedzija, G. N., and Fraser, S. E. (1989). Cell lineage analysis reveals multipotent precursors in the ciliary margin of the frog retina. *Developmental Biology*, 136(1):254–263.

[Wickham, 2016] Wickham, H. (2016). *ggplot2: Elegant Graphics for Data Analysis*. Springer-Verlag New York.

[Wiedenheft et al., 2012] Wiedenheft, B., Sternberg, S. H., and Doudna, J. A. (2012). RNA-guided genetic silencing systems in bacteria and archaea. *Nature*, 482(7385):331–338.

[Wilson and Hemmati-Brivanlou, 1995] Wilson, P. A. and Hemmati-Brivanlou, A. (1995). Induction of epidermis and inhibition of neural fate by Bmp-4. *Nature*, 376(6538):331–333.

[Wilson et al., 2000] Wilson, S. I., Graziano, E., Harland, R., Jessell, T. M., and Edlund, T. (2000). An early requirement for FGF signalling in the acquisition of neural cell fate in the chick embryo. *Current Biology*, 10(8):421–429.

[Wilson and Houart, 2004] Wilson, S. W. and Houart, C. (2004). Early steps in the development of the forebrain. *Developmental Cell*, 6(2):167–181.

[Winkler et al., 1991] Winkler, C., Vielkind, J. R., and Schartl, M. (1991). Transient expression of foreign DNA during embryonic and larval development of the medaka fish (Oryzias latipes). *MGG Molecular & General Genetics*, 226(1-2):129–140.

[Winkler et al., 2000] Winkler, S., Loosli, F., Henrich, T., Wakamatsu, Y., and Wittbrodt, J. (2000). The conditional medaka mutation eyeless uncouples patterning and morphogenesis of the eye. *Development*, 127(9):1911–1919.

[Wright et al., 2014] Wright, D. a., Li, T., Yang, B., and Spalding, M. H. (2014). TALEN-mediated genome editing: prospects and perspectives. *Biochemical Journal*, 462(1):15–24.

[Wu et al., 2009] Wu, H. Y., Perron, M., and Hollemann, T. (2009). The role of Xenopus Rx-L in photoreceptor cell determination. *Developmental Biology*, 327(2):352–365.

[Xue and Harris, 2012] Xue, X. Y. and Harris, W. a. (2012). Using myc genes to search for stem cells in the ciliary margin of the Xenopus retina. *Developmental Neurobiology*, 72(4):475–490.

[Yin et al., 2014] Yin, J., Morrissey, M. E., Shine, L., Kennedy, C., Higgins, D. G., and Kennedy, B. N. (2014). Genes and signaling networks regulated during zebrafish optic vesicle morphogenesis. *BMC Genomics*, 15:doi: 10.1186/1471–2164–15–825.

[Zimmerman et al., 1996] Zimmerman, L. B., De Jesús-Escobar, J. M., and Harland, R. M. (1996). The Spemann organizer signal noggin binds and inactivates bone morphogenetic protein 4. *Cell*, 86(4):599–606.

Publications

Gutierrez-Triana, J.A.*, **Tavhelidse, T.***, Thumberger, T.*, Thomas, I., Wittbrodt, B., Kellner, T., Anlas, K., Tsingos, E. and Wittbrodt, J.(2018). Efficient single-copy HDR by 5' modified long dsDNA donors. *Elife* Aug 29, 7; doi: 10.7554/eLife.39468.

Shi, D.*, **Tavhelidse, T.***, Thumberger, T., Wittbrodt, J. and Greb, T. (2017). Bifacial stem cell niches in fish and plants. *Current Opinion in Genetics & Development* 45:28-33.

Reinhardt, R., Centanin, L., **Tavhelidse, T.**, Inoue, D., Wittbrodt, B., Concordet, J.P., Martinez-Morales, J.R. and Wittbrodt, J. (2015). Sox2, Tlx, Gli3, and Her9 converge on Rx2 to define retinal stem cells *in vivo*. *The EMBO Journal* 34(11):1572-88.

Acknowledgments

Jochen, thank you for everything! Thank you for giving me the opportunity to work in your lab, first during my lab rotations, then during my Master's thesis and now for my PhD thesis. Thank you for all your support during all these years and the years to come. You are not only the best PI I could ever ask for, you also are incredibly human and empathic at the same time. Thank you!
Thanks also to Jun.-Prof. Dr. Steffen Lemke for being not only my second reviewer, but also for all the input, feedback and suggestions during my TAC meetings. Thank you also for being such a positive person, always excited about science.
Dr. Lázaro Centanin, thank you for your enthusiastic input, feedback and suggestions during my TAC meetings, but also thank you for the time we were working together on the Rx-project, which actually started all of this.
Thank you, Prof. Dr. Jan Lohmann and Prof. Dr. Marc Freichel for agreeing to be part of my committee.
A big thank you also goes to Frederike and Ute - thank you for the small and the long (!) conversations we've had, especially for THE conversation we had the other day! Thank you for the small breaks that make me forget the daily routine for a little while and just thank you for being so refreshingly human! Frederike, thank you for the unforgettable time we've spent Down Under (Down Unda at the docta drinking some wata).
Beate, I can not thank you enough for all your work, all the effort you have put into our project! Thank you for being so supportive and kind! Thank you also for the birthday muffins and the super delicious mousse au chocolat (top secret recipe). I really appreciate your support - science- and food-wise, as well as your mental support!
Thomas! Thank you for making this time unforgettable! Thank you for all the projects we were and are still collaborating on, thank you for having always time for "ich hab' eine Frage" despite actually never having time and there is always more than just one question, thank you for connecting me with Illustrator via countless tutorials, thank you for endless science-related and non-science-related discussions and rants, thank you for the paper-writing-madness-way-after-midnight including Pizza from Mamma Leone. Thank you for (finally) proofreading my thesis, thanks for all the valuable input! Thank you for all your support and being so extremely helpful and caring!

Arturooooooooo, thank you for the whiskey and rum tastings to celebrate the last Friday of the week, even though I was tasting it only sometimes and every time I did, decided that I still don't like it so much. Thank you for your positivity, your laugh, you clapping your hands to get stuff done. Thank you for asking me why the heck your(!) timer is beeping ("warum?"), thank you for endless science discussions late in the evenings, thank you for THE discussion we had the other evening where you encouraged me to change projects. Thank you for caring about me and my scientific future! Thank you for the collaboration on the modified story, it was an unforgettable time having you in the lab! You are still missed here and will always be!
Tanja, thank you for being so supportive and helpful all the time - may it be science, food, health or creativity-related. Thank you for the great job you are doing for all of us in the lab!
Robert, thank you for starting this project, providing the basis for this thesis! Also thank you for your supervision during my lab rotations and my Master's thesis and of course thank you also for all the Glitzerkätzchen-time.
Lea, thank you for all the conversations we've had, all the jokes we've shared and of course for our special feeding deal ;-).
Juan, thank you for all your endless help and support with the transcriptome data! I really appreciate it!
Colin, thank you so much (!!!) for all your time to help with the layout of this thesis! It didn't matter whether you were working in the lab or from home, or enjoying your free time, whether it was on the weekend or late at night, I could always ask you for help - and you were always willing to help and solved any issue! I really appreciate this a lot!
Lucie, thank you for proofreading my thesis (kind of last-minute), I really appreciate it!
A big shout-out to the Breakfast Club - thank you for all the fun times we've shared not only over having breakfast.
Thank you for your friendship, Silvi! I still remember how we first met when I joined the lab in 2012 for my first lab rotation still listening to gangster hip-hop (at least that is what you thought). Thank you for all the fun times, all the (deep) conversations we've had, thank you for always being there for me, it really means a lot!
Isa, thank you for studying Biology in the first place - otherwise we probably wouldn't have met! Thank you for being such a smart and great student and now Hiwi, thank you for meeting up in Australia (still feels surreal) thank you for all the cat-talk, thank you for all the inspiring conversations we've had,

thank you for caring so much! Thank you for taping my leg, thank you for caring about my shoulder pain and my flexibility - thank you for introducing me to yoga! Thanks for being such a wonderful person and friend!
Natalia, thank you for being such a smart and hard-working student! Thank you for all your help during this project!
Kerim, thank you for being such a smart and special (;-)) student! Thank you for all your help and the conversations we've had, often not having the same opinion or at least heavily discussing! I really enjoyed that time!
Narges, thank you for being such a kind and caring person! I love remembering the time we've spent together in the lab.
Ceschina, thank you for the time we've spent together here at COS, thank you for still keeping in touch! Un grande abbracio e un bacio!
Manuel, thank you for starting the conditional project!
Let's see where it will finally lead us: on to new adventures! #postdoclife
Ravi, thank you for all your help on the measurements of the mutants!
Sheermann, thank you for all the input for our current working hypothesis!
A BIG thank you to all present and past lab members of the Wittbrodt, Centanin and Lemke labs! You all have shaped and contributed to this incredibly supportive environment!
Of course shout-out to my friends (Liter Squad-VayCay)! Thank you for being great friends, we always had an awesome time, especially spending legendary holidays in Hamburg, Trier, Croatia, Portugal... you name it. It always was and always will be a welcomed break from the lab routine.
Thanks also to my basketball team for the well-needed breaks from work - let's go Ladytigers!
Thank you Doro, Arno, Lena and my godson David for being such amazing friends and extended family! Thank you for always being there and being so incredibly understanding!

♡ ♡ ♡ A HUGE thanks goes to my family! Thank you for all your unconditional love, support, help and understanding! Thank you for always being there for me! Thank you from the bottom of my heart! This all would never ever have been possible without your support! LIEBE.
Thank you, Paddel, for everything! All the above mentioned of course also applies to you - because you ARE family! Thank you for giving me your heart and having mine, unconditionally! Thanks for all your support and understanding! Thank you for the "life" in "work-life-balance"!
My heart aches remembering my beloved grandparents Oma and Babu, who

accompanied me on this journey but got out one stop earlier. I miss you. ♡ ♡ ♡

Many people accompanied and supported me on this way, which has finally reached another intersection. Thank you for everything and I am looking forward to what will come.

Declaration

Herewith I declare that I prepared the PhD Thesis "The role of *rx* genes in establishment and maintenance of the medaka ciliary marginal zone" on my own and with no other sources and aids than quoted.

Heidelberg, 2018

List of Figures

List of Tables